Journal of Pathology and Translational Medicine

# JPTM

Journal of Pathology and Translational Medicine

September 2016
Vol. 50 / No. 5
jpatholtm.org
pISSN: 2383-7837
eISSN: 2383-7845

ISSN 2383-7837

## *CD99 Is Strongly Expressed in Basal Cells of the Normal Adult Epidermis and Some Subpopulations of Appendages: Comparison with Developing Fetal Skin*

Vol. 50, No. 5, pp 327-403, September 2016

# Journal of Pathology and Translational Medicine

**Volume 50 • Number 5 • September 2016 (bimonthly)**
Published since 1967
Printed on 11 September 2016 Published on 15 September 2016

J Pathol Transl Med
pISSN: 2383-7837
eISSN: 2383-7845


## Aims & Scope

*The Journal of Pathology and Translational Medicine* is an open venue for the rapid publication of major achievements in various fields of pathology, cytopathology, and biomedical and translational research. The Journal aims to share new insights into the molecular and cellular mechanisms of human diseases and to report major advances in both experimental and clinical medicine, with a particular emphasis on translational research. The investigations of human cells and tissues using high-dimensional biology techniques such as genomics and proteomics will be given a high priority. Articles on stem cell biology are also welcome. The categories of manuscript include original articles, review and perspective articles, case studies, brief case reports, and letters to the editor.

## Subscription Information


To subscribe to this journal, please contact the Korean Society of Pathologists/the Korean Society for Cytopathology. Full text PDF files are also available at the official website (http://jpatholtm.org). *Journal of Pathology and Translational Medicine* is indexed by PubMed, PubMed Central, Scopus, KoreaMed, KoMCI, WRPIM and CrossRef. Circulation number per issue is 700.




## Contact the Korean Society of Pathologists/the Korean Society for Cytopathology


**Publishers:** Min Cheol Lee, MD, So Young Jin, MD
**Editors-in-Chief:** Soon Won Hong, MD, Chong Jai Kim, MD
**Published by** the Korean Society of Pathologists/the Korean Society for Cytopathology

**Editorial Office**
Room 1209 Gwanghwamun Officia, 92 Saemunan-ro, Jongno-gu,
Seoul 03186, Korea/#406 Lilla Swami Bldg, 68 Dongsan-ro,
Seocho-gu, Seoul 06784, Korea
Tel: +82-2-795-3094/+82-2-593-6943
Fax: +82-2-790-6635/+82-2-593-6944
E-mail: office@jpatholtm.org

**Printed by** iMiS Compnay Co., Ltd.
Jungang Bldg. 18-8 Wonhyo-ro 89-gil, Yongsan-gu, Seoul 04314, Korea
Tel: +82-2-717-5511 Fax: +82-2-717-5515 E-mail: ml@smileml.com

**Manuscript Editing by** InfoLumi Co.
210-202, 421 Pangyo-ro, Bundang-gu, Seongnam 13522, Korea
Tel: +82-70-8839-8800 E-mail: infolumi.chang@gmail.com


Front cover image: CD99 expression in normal adult epidermis and hair follicles (Fig. 1). p363.




This journal was supported by the Korean Federation of Science and Technology Societies Grant funded by the Korean Government.

Journal of Pathology and Translational Medicine

J Pathol Transl Med
pISSN: 2383-7837
eISSN: 2383-7845

Volume 50, Number 5, September 2016

# CONTENTS

## ORIGINAL ARTICLES



## CASE REPORTS



CONTENTS CONTINUED

**Instructions for Authors** for *Journal of Pathology and Translational Medicine* are available at http://jpatholtm.org/authors/authors.php

*Journal of Pathology and Translational Medicine 2016; 50: 327-336*
*http://dx.doi.org/10.4132/jptm.2016.06.22*

■ ORGINAL ARTICLE ■

# Clinicopathologic Correlations of E-cadherin and Prrx-1 Expression Loss in Hepatocellular Carcinoma

Kijong Yi · Hyunsung Kim
Yumin Chung · Hyein Ahn
Jongmin Sim · Young Chan Wi
Ju Yeon Pyo · Young-Soo Song
Seung Sam Paik · Young-Ha Oh

Department of Pathology, Hanyang University College of Medicine, Seoul, Korea

**Received:** January 25, 2016
**Revised:** June 16, 2016
**Accepted:** June 21, 2016

**Corresponding Author**
Young-Ha Oh, MD
Department of Pathology, Hanyang University College of Medicine, 222-1 Wangsimni-ro, Seongdong-gu, Seoul 04763, Korea
Tel: +82-31-560-2498
Fax: +82-31-560-2339
E-mail: yhoh@hanyang.ac.kr

**Background:** Developing predictive markers for hepatocellular carcinoma (HCC) is important, because many patients experience recurrence and metastasis. Epithelial to mesenchymal transition (EMT) is a developmental process that plays an important role during embryogenesis and also during cancer metastasis. Paired-related homeobox protein 1 (Prrx-1) is an EMT inducer that has recently been introduced, and its prognostic significance in HCC is largely unknown. **Methods:** Tissue microarray was constructed using surgically resected primary HCCs from 244 cases. Immunohistochemical staining of E-cadherin and Prrx-1 was performed. The correlation between E-cadherin loss and Prrx-1 expression, as well as other clinicopathologic factors, was evaluated. **Results:** E-cadherin expression was decreased in 96 cases (39.4%). Loss of E-cadherin correlated with a higher recurrence rate ($p < .001$) but was not correlated with patient's survival. Thirty-two cases (13.3%) showed at least focal nuclear Prrx-1 immunoreactivity while all non-neoplastic livers ($n = 22$) were negative. Prrx-1 expression was not associated with E-cadherin loss, survival or recurrence rates, pathologic factors, or the Ki-67 labeling index. Twenty tumors that were positive for E-cadherin and Prrx-1 had significantly higher nuclear grades than the rest of the cohort ($p = .037$). In Cox proportional hazard models, E-cadherin loss and large vessel invasion were independent prognostic factors for shorter disease-free survival. Cirrhosis and high Ki-67 index (> 40%) were independent prognostic factors for shorter overall survival. **Conclusions:** Prrx-1 was expressed in small portions of HCCs but not in normal livers. Additional studies with a large number of Prrx-1-positive cases are required to confirm the results of this study.

**Key Words:** Liver; Neoplasms; Epithelial-mesenchymal transition; Prrx-1 protein

Hepatocellular carcinoma (HCC) is one of the most lethal and relatively prevalent cancers worldwide, as well as in Korea. The Korean National Cancer Information Center estimates that over 2.2 per hundred thousand persons were killed by HCC in 2013, which is the second most common cause of death by cancer in Korea.[1] Although surgical resection is effective in cases of the incipient disease, even in early stages, a considerable number of patients experience recurrence and metastasis leading to a poor prognosis.[2] Therefore, it is important to develop markers that indicate poor prognosis, and to provide stratified follow-up guidelines for clinicians.

Epithelial tumor metastasis can be described by a developmental program called epithelial to mesenchymal transition (EMT), which plays crucial roles in embryonic development, including mesoderm formation and migration of neural crest cells.[3] During metastasis, the tumor cells lose their epithelial property, gain migratory activity, disseminate through the blood stream, and finally, establish metastatic foci in distant organs.[3]

Paired-related homeobox protein 1 (Prrx-1; PRX-1) is a transcription factor that has recently been found to induce EMT in embryogenesis, as well as in several cancers, including breast, pancreas, colon, and thyroid cancer.[4-7] However, it has been inconsistently reported on whether its upregulation or downregulation is associated with poor prognosis. In colorectal and thyroid cancers, overexpression of Prrx-1 was associated with poor prognosis or worse histologic type.[4,7] In comparison, in breast cancers and HCCs, downregulation of Prrx-1 was associated with poor prognosis.[5,8]

In this study, we used tissue microarray (TMA) to determine if the loss of E-cadherin is a prognostic marker for predicting early recurrence and poor survival rate. We surgically obtained 244 cases of human HCC tissues in the Hanyang University Medical Center, Seoul and Guri hospitals. We examined Prrx-1 expression in HCC using immunohistochemistry, and investigated the relationship between its expression and loss of E-cadherin. We also worked to determine if expression of Prrx-1 could

pISSN 2383-7837
eISSN 2383-7845

be a prognostic marker to predict metastasis or poor survival rate, because it induces EMT and its significance is currently unknown. We also investigated the relationship between clinicopathologic factors such as tumor size, vascular invasion, histologic grade, and the Ki-67 index to explore the clinical significances of E-cadherin and Prrx-1.

## MATERIALS AND METHODS

### Patients and specimens

A total of 244 patients who underwent surgical resection for HCC from 1991 to 2013 at Hanyang University Medical Center, Seoul and Guri hospitals were selected as subjects for this study. Medical records were reviewed to identify baseline clinical information, clinical course, underlying etiology, and liver function status at the diagnosis. Histological review was performed to determine stage, grade (Edmondson and Steiner's grading system), vascular invasion, size of tumor, and multiplicity. This study was conducted under review of the Institutional Review Board (IRB) of Hanyang University Guri Hospital (Code, 2015-11-012).

### TMA, immunohistochemistry, and interpretation

Representative tissue blocks were selected for TMA construction after histological review. For each case, a 2-mm single core was punched from the tumor but not from normal tissue. All immunostainings were performed using the automated system, Leica Bond III (Leica Biosystems, Nusslock, Germany) and Bond Polymer Refine Detection Kit (Leica Biosystems). E-cadherin antibody (mouse monoclonal, NCL-L-E-Cad, Novocastra, Newcastle upon Tyne, UK) was diluted at 1:25. Prrx-1 antibody (rabbit polyclonal, NBP2-13816, Novus Biologicals, Littleton, CO, USA) was diluted at 1:20. Ki-67 antibody (mouse monoclonal, NCL-L-Ki67-MM1, Novocastra) was diluted at

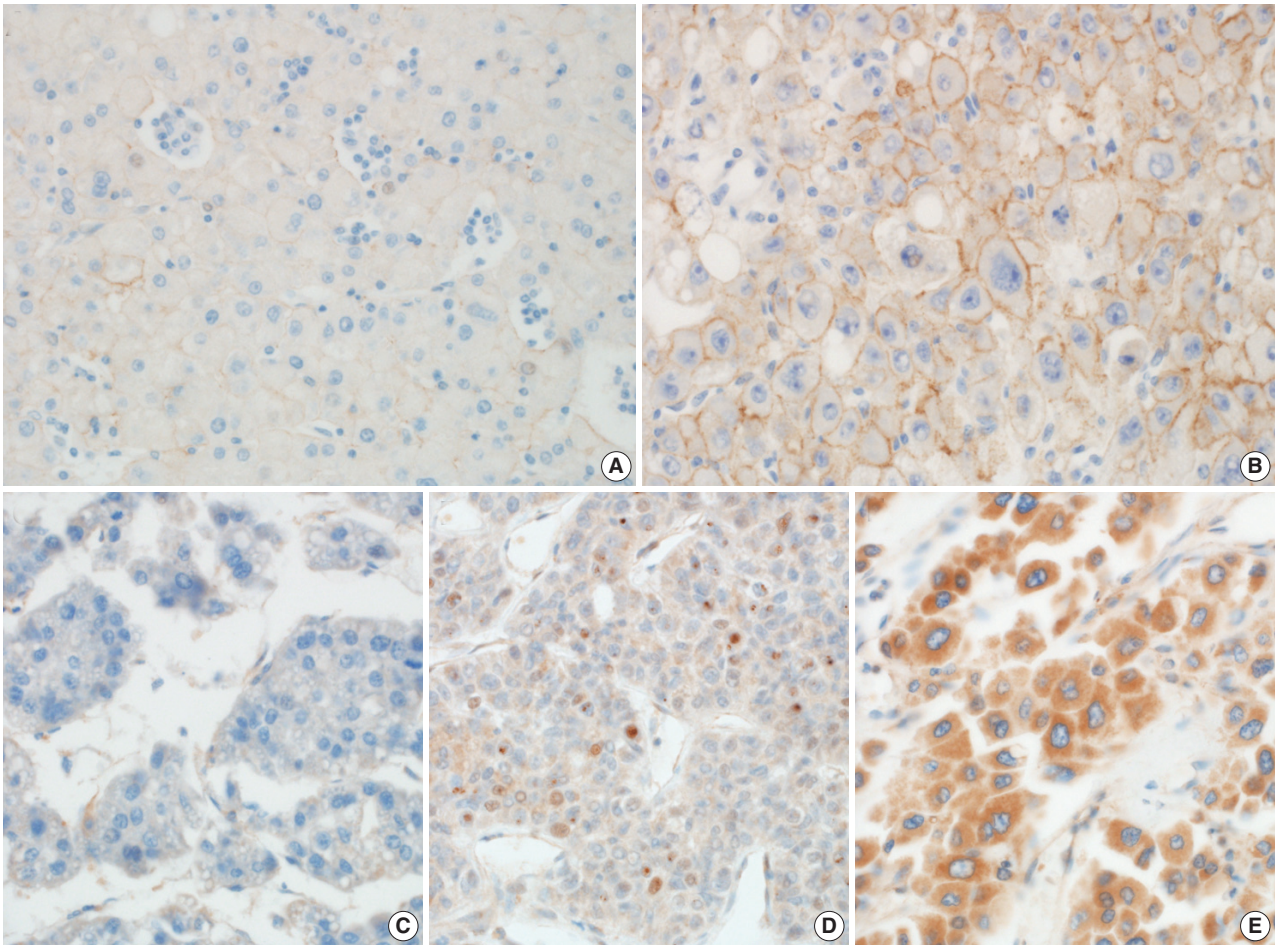


**Fig. 1.** Immunohistochemical staining of E-cadherin and paired-related homeobox protein 1 (Prrx-1) in hepatocellular carcinomas. Representative photos of immunohistochemical staining in hepatocellular carcinomas. (A) E-cadherin decreased. (B) E-cadherin maintained. (C) Prrx-1 negative. (D) Prrx-1 positive. (E) Prrx-1 negative, but cytoplasmic positive.


http://dx.doi.org/10.4132/jptm.2016.06.22

1:200. TMA sections (4-μm-thick) were de-waxed, and the antigen was retrieved with Bond Epitope Retrieval Solution 2 (Leica Biosystems), then incubated with primary antibodies for 60 minutes.

Two pathologists assessed E-cadherin staining into two categories as described previously;[9] negative or faint membranous stained and moderate to strong membranous stained. The average E-cadherin stainability of HCC cells in each core was evaluated. Prrx-1 staining was evaluated by its nuclear positivity as previously described.[4] Cytoplasmic stained cases without nuclear positivity for Prrx-1 were interpreted as negative because they were considered to be nonspecific cytoplasmic antibody entrapping. Representative images of immunohistochemical staining are presented in Fig. 1. To determine whether the immunoexpression of Prrx-1 in HCCs was upregulated or lost, comparing to normal or cirrhotic liver, we performed Prrx-1 immunostain to two whole block sections and one TMA section that contained 20 cores of normal liver tissue block obtained that were obtained from liver resections from traumatic liver laceration, or metastatic colon cancer. We stained one whole section from each of the three Prrx-1–positive HCCs and three Prrx-1–negative HCCs, to determine if the single TMA core was representative of the entire tumor's Prrx-1 expression status. The cases were randomly selected from the cohort and all sections included adjacent cirrhotic liver. Ki-67 immunostain was performed on TMA sections. The Ki-67 labeling index was calculated by a free image analyzing software, TMARKER v2.21625.[10]

### Statistical analysis

We investigated the relationship between the loss of E-cadherin and clinicopathologic factors as well as survival time and recurrence. Expression of Prrx-1 was evaluated with the same method. Concordance of loss of E-cadherin and Prrx-1 expression was analyzed. We also correlated the expression with other markers to investigate whether those markers reflect aggressive pathologic features. The association between immunohistochemical stain results and clinicopathologic parameters was analyzed using the chi-square test, Fisher exact test, and Mann-Whitney U test. Recurrence and survival rate was calculated by the Kaplan-Meier method, and the comparisons were made using the log-rank test. The Cox proportional hazard regression model was adopted to determine the prognostic impact of immunohistochemical results and other clinicopathologic parameters. For the Cox regression, high Ki-67 was defined as Ki-67 index over 40, by considering the cutoff values of previous studies.[11,12] For all calculations, differences at $p < .05$ were considered statistically significant. All statistical calculations were performed using the R software ver. 3.1.0 (R Core Team 2014).

## RESULTS

### Clinicopathological characteristics

The clinicopathologic features are summarized in Table 1. The median age of the 244 patients was 56 years (range, 24 to 87 years). One hundred eighty-three patients were male (75%), and 61 were female (25%). One hundred seventy-one patients had hepatitis B virus (HBV, 70.1%), and 16 had hepatitis C virus (HCV, 6.6%). Two patients had both HCV and HBV coinfection (0.8%). Twenty-five patients had no viral hepatitis but had a history of chronic alcohol intake without any apparent vi-

**Table 1.** Clinicopathologic characteristics of HCC patients (n=244)

| Parameter | No. (%) |
|---|---|
| Age (yr)[a] | 56 (24–87) |
| Sex (male:female) | 183:61 (3:1) |
| Etiological factor | |
| HBV | 171 (70.1) |
| HCV | 16 (6.6) |
| HBV+HCV | 2 (0.8) |
| Alcohol | 25 (10.2) |
| Unknown | 30 (12.3) |
| Underlying disease | |
| Chronic hepatitis | 44 (18) |
| Cirrhosis | 200 (82) |
| Child-Pugh class | |
| A | 230 (94.3) |
| B | 14 (5.7) |
| AJCC stage | |
| I | 132 (54.1) |
| II | 79 (32.4) |
| III | 33 (13.5) |
| Tumor size (cm)[a] | 3.5 (0.6–19.5) |
| Multiplicity (solitary/multiple) | |
| Solitary | 201 (82.4) |
| Multiple | 43 (17.6) |
| Histologic grade | |
| 1, 2 | 109 (44.7) |
| 3, 4 | 135 (55.3) |
| Small vessel invasion | 94 (38.5) |
| Large vessel invasion | 24 (9.8) |
| Recurrence rate (%) | |
| 1 Year | 35.0 |
| 5 Years | 65.3 |
| Survival rate (%) | |
| 1 Year | 87.4 |
| 5 Years | 55.6 |

HCC, hepatocellular carcinoma; HBV, hepatitis B virus; HCV, hepatitis C virus; AJCC, American Joint Committee on Cancer.
[a]Median (range).

ral etiology (10.2%). Thirty patients had neither viral hepatitis nor history of chronic alcoholic intake (12.3%). Cirrhosis was detected in 200 patients (82%). Child-Pugh classes were stage B in 14 patients (5.7%), while the others are stage A (94.3%). Regarding pathologic stage, 132 patients were stage I (54.1%), 79 were II (33.4%), eight were IIIA (3.3%), 24 were IIIB (9.8%), and one was IIIC (0.4%). Median tumor size was 3.5 cm (range, 0.6 to 19.5 cm). Two hundred one cases presented as a solitary tumor (82.4%) while the others presented as multiple tumors. Portal vein, hepatic vein, or their major branch involvement was detected in 45 patients (18.4%).

One hundred and six patients died during follow-up. Median survival time was 70.8 months (range, 1.3 to 287.7 months) and 5-year survival rate was 55.6%. In addition, 35% of cases showed a tumor recurrence within 1 year, and 65.3% underwent recurrence within 5 years. The Kaplan-Meier method showed a significant difference in overall survival and disease-free survival between stages I and II (p = .006, and p < .001, respectively). However, those between stage II and stage III were not statistically significant (p = .450 and p = .106, respectively). Additionally, 3.9% of stage I patients experienced tumor recurrence within 1 year (n = 19), compared with 20.6% of stage II (n

**Table 2.** Association between E-cadherin and Prrx-1 expression and clinicopathologic parameters in HCC patients (n = 244)

| Parameter | E-cadherin | | p-value | Prrx-1 | | p-value |
|---|---|---|---|---|---|---|
| | Decreased (n = 96) | Maintained (n = 148) | | Positive (n = 32) | Negative (n = 212) | |
| Age (yr)[a] | 57 (31–77) | 55 (24–87) | .135[b] | 60 (24–74) | 55.5 (28–87) | .161[b] |
| Sex (male:female) | 74:22 (3.4:1) | 109:39 (2.8:1) | .650[c] | 24:8 (3:1) | 159:53 (3:1) | >.990[c] |
| Etiology (%) | | | .090[d] | | | |
| HBV | 59 (61.5) | 112 (75.7) | | 20 (62.5) | 151 (71.2) | .501[d] |
| HCV | 10 (10.4) | 6 (4.1) | | 2 (6.2) | 14 (6.6) | |
| HBV + HCV | 1 (1) | 1 (0.7) | | 0 | 2 (0.8) | |
| Alcohol | 13 (13.5) | 12 (8.1) | | 3 (9.4) | 22 (10.8) | |
| Unknown | 13 (13.5) | 17 (11.5) | | 7 (21.9) | 23 (10.8) | |
| Underlying disease (%) | | | .048[c] | | | .893[d] |
| Chronic hepatitis | 11 (11.5) | 33 (22.3) | | 5 (18.4) | 39 (15.6) | |
| Cirrhosis | 85 (88.5) | 115 (77.7) | | 27 (81.6) | 173 (81.6) | |
| Child-Pugh class | | | .996[c] | | | >.990[d] |
| A | 91 (94.8) | 139 (93.9) | | 30 (93.8) | 200 (94.3) | |
| B | 5 (5.2) | 9 (6.1) | | 2 (5.7) | 12 (5.7) | |
| AJCC stage | | | .707[c] | | | .399[d] |
| I | 50 (52.1) | 82 (55.4) | | 20 (62.5) | 112 (52.8) | |
| II | 34 (35.4) | 45 (30.4) | | 7 (21.9) | 72 (34.0) | |
| III | 12 (12.5) | 21 (14.2) | | 5 (15.6) | 28 (13.2) | |
| Multiplicity | | | .406[c] | | | .571[c] |
| Single | 82 (85.4) | 119 (80.4) | | 28 (87.5) | 173 (81.6) | |
| Multiple | 14 (14.6) | 29 (19.6) | | 4 (12.5) | 39 (18.4) | |
| Tumor size[a] | 3.3 (0.6–19.5) | 3.5 (0.7–17) | .877[b] | 3.15 (1.2–15) | 3.5 (0.6–19.5) | |
| Histologic grade | | | .224[c] | | | .286[c] |
| 1, 2 | 48 (50) | 61 (41.2) | | 11 (34.4) | 98 (46.2) | |
| 3, 4 | 48 (50) | 87 (58.8) | | 21 (65.6) | 114 (53.8) | |
| Large vessel invasion | 11 (11.5) | 13 (8.8) | .642[c] | 4 (12.5) | 20 (9.4) | .533[d] |
| Small vessel invasion | 41 (42.7) | 53 (35.8) | .344[c] | 13 (40.6) | 81 (38.2) | .946[c] |
| Prrx-1 positivity | 12 (12.5) | 20 (13.5) | .972[c] | 12 (37.5) | 84 (39.6) | .972[c] |
| Ki-67 index[e] | 21 (9–37.5) | 22 (10–41) | .754[b] | 21 (9–35.5) | 22 (9.5–40.5) | .533[b] |
| Recurrence rate (%) | | | < .001[f] | | | .947[f] |
| 1 Year | 45.8 | 28.5 | | 43.1 | 34.2 | |
| 5 Years | 78.1 | 57.1 | | 71.2 | 64.8 | |
| Survival rate (%) | | | .459[f] | | | .409[f] |
| 1 Year | 88.3 | 86.8 | | 77.5 | 88.9 | |
| 5 Years | 55.2 | 55.6 | | 66.3 | 55.1 | |

Values are presented as number (%) unless otherwise indicated.
Prrx-1, paired-related homeobox protein 1; HCC, hepatocellular carcinoma; HBV, hepatitis B virus; HCV, hepatitis C virus; AJCC, American Joint Committee on Cancer.
[a]Median (range); [b]Mann-Whitney U test; [c]Chi-square test; [d]Fisher exact test; [e]Median (first quantile–third quantile); [f]Log-rank test.


http://dx.doi.org/10.4132/jptm.2016.06.22

= 19), and 29.8% of stage III (n = 11).

### E-cadherin and Prrx-1 immunohistochemical staining results

E-cadherin expression was decreased in 96 cases (39.3%), whereas others showed moderate to strong membranous immunoreactivity. Thirty-two cases (13.3%) showed at least focal nuclear Prrx-1 immunoreactivity. Loss of E-cadherin and Prrx-1 expression was not concordant (p = .972 on the chi-square test). One hundred twenty cases showed minimally weak cytoplasmic stainability (49.2%). Cytoplasmic staining of Prrx-1 was not correlated with loss of E-cadherin expression (p = .217 on the chi-square test).

All normal livers, including two whole section and one TMA section, of which there were twenty cases, were negative for Prrx-1 staining. All Prrx-1 stainings with whole sections of three Prrx-1–positive HCCs and three Prrx-1–negative HCCs showed consistent results with the TMA stainings. All adjacent cirrhotic livers from the six sections were negative for Prrx-1.

### HCC biomarker relationships

We examined the correlation between Prrx-1 and E-cadherin immunohistochemical staining results and various clinicopathological factors. HCCs with decreased E-cadherin tend to occur more frequently in the background of cirrhosis, compared to E-cadherin maintained HCCs (88.5% vs 77.7%, p = .048 on the chi-square test). Both large vessel (portal vein, hepatic vein, or their major branches) invasion and small vessel invasion were more frequent in the E-cadherin reduced group compared with the maintained group; however, they were not statistically significant (large vessel invasion: 11.5% vs 8.8%, p = .642 on chi-square test; small vessel invasion: 42.7% vs 35.8%, p = .344 on chi-square test). Hepatitis B, hepatitis C, history of chronic alcohol intake, age, sex, pathologic stage, multiplicity of the tumor, tumor size, and histologic grade were not significantly associated with E-cadherin expression (Table 2).

None of the factors were statistically significantly correlated with Prrx-1 expression and clinicopathological factors, although both large vessel invasion and small vessel invasion were more frequent in Prrx-1–positive HCCs (large vessel invasion: 12.5% vs 9.4%, p = .533; small vessel invasion: 40.6% vs 38.2%, p = .946) (Table 2). Prrx-1–positive HCCs showed more frequent p53 overexpression (25% vs 13.7%, p = .114 on chi-square test), although this result was not statistically significant.

Survival analysis indicated that E-cadherin decreased HCCs that were identified in earlier recurrences than in E-cadherin

**Table 3.** Association between E-cadherin and Prrx-1 expression as a combinational marker and clinicopathologic parameters in HCC patients (n = 244)

| Parameter | E-cadherin positive | | E-cadherin negative | |
|---|---|---|---|---|
| | Prrx-1 positive (n = 20) | Prrx-1 negative (n = 128) | Prrx-1 positive (n = 12) | Prrx-1 negative (n = 84) |
| AJCC stage | | | | |
| I | 11 (55) | 73 (57) | 9 (75) | 41 (48.8) |
| II | 6 (30) | 40 (31.2) | 1 (8.3) | 33 (39.3) |
| III | 3 (15) | 15 (11.7) | 2 (16.7) | 10 (11.9) |
| Multiplicity | | | | |
| Single | 18 (90) | 101 (78.9) | 10 (83.3) | 72 (85.7) |
| Multiple | 2 (10) | 27 (21.1) | 2 (16.7) | 12 (14.3) |
| Histologic grade[a] | | | | |
| 1, 2 | 4 (20) | 57 (44.5) | 7 (58.3) | 41 (48.8) |
| 3, 4 | 16 (80) | 71 (55.5) | 5 (41.7) | 43 (51.2) |
| Large vessel invasion | 18 (90) | 117 (91.4) | 10 (83.3) | 75 (89.3) |
| Small vessel invasion | 10 (50) | 85 (66.4) | 9 (75) | 46 (54.8) |
| Ki-67 index[b] | 26 (7.5–43.5) | 21 (10–40.5) | 21 (12.5–39) | 21 (9–34.5) |
| Recurrence rate (%) | | | | |
| 1 Year | 60.1 | 73 | 51.1 | 54.6 |
| 5 Years | 54.1 | 43 | 15.3 | 23.2 |
| Survival rate (%) | | | | |
| 1 Year | 73.9 | 88.8 | 83.3 | 89 |
| 5 Years | 54.6 | 56.9 | 83.3 | 51.7 |

Values are presented as number (%) unless otherwise indicated.
Prrx-1, paired-related homeobox protein 1; HCC, hepatocellular carcinoma; AJCC, American Joint Committee on Cancer.
[a]Comparing both E-cadherin and Prxx-1 positive-group (the first column) to the others, the former showed significantly higher histologic grade (p = .037 on chi-squared test); [b]Median (first quantile–third quantile).

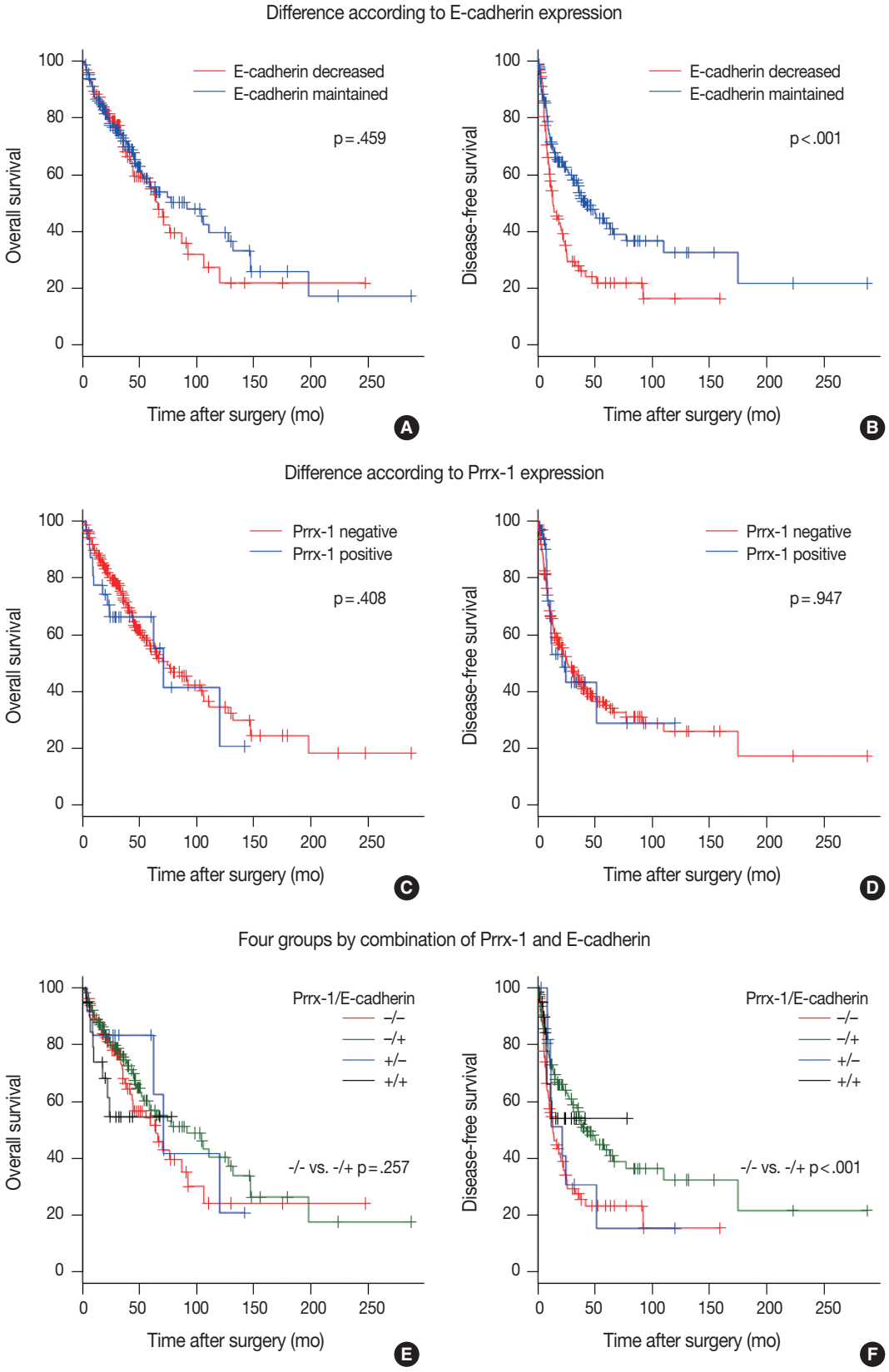


**Fig. 2.** Kaplan-Meier curves for overall survival (A, C, E) and disease-free survival (B, D, F) in hepatocellular carcinomas according to American Joint Committee on Cancer stage, E-cadherin and paired-related homeobox protein 1 (Prrx-1) expression (log-rank test).


http://dx.doi.org/10.4132/jptm.2016.06.22

maintained HCCs (mean, 1.08 years vs 3.51 years; p < .001 on the log-rank test) (Fig. 2B). Within one year, 41 cases (45.8%) of E-cadherin decreased HCCs experienced recurrence, while 40 cases of E-cadherin (28.5%) maintained HCCs did not. The overall survival rate was not significantly different on the log-rank test (p = .459) (Fig. 2A). We also examined the correlation between patient's survival/recurrence and Prrx-1 expression. Although 1-year recurrence rate (43.1% vs 34.2%) and 5-year recurrence rate (71.2% vs 64.8%) were higher in Prrx-1 that expressed HCCs than in Prrx-1–negative HCCs, the difference was not statistically significant on the log-rank test (p = .947) (Fig. 2D). Overall survival was also not significantly different (p = .408) (Fig. 2C).

We categorized HCCs into four groups, depending on the E-cadherin and Prrx-1 expression. The clinicopathologic parameters, recurrence rate, and survival rate were compared between Prrx-1–positive and Prrx-1–negative groups, and among E-cadherin–positive cases, in addition to the same comparison among E-cadherin–negative cases. Each of the four groups were also compared with the other three groups. The E-cadherin–positive and Prrx-1–positive group (n = 20) showed significantly higher nuclear grades than the rest of the group (n = 224) (nuclear grade 3 or 4 proportion: 80% vs 53.1%, p = .037 on chi-squared test). Other parameters in the various group comparison were not significantly different (Table 3, Fig. 2E and F).

## Cox proportional hazard regression model

Factors that may affect the prognosis of HCC were filtered

| | Univariate analysis | | | Multivariate analysis | | | |
|---|---|---|---|---|---|---|---|
| | Hazard ratio | 95% CI | p-value | Hazard ratio | 95% CI | p-value | Hazard ratio (95% CI) |
| AJCC stage | | | | | | | |
| I vs. II | 2.612 | 1.860–3.668 | **<.001** | 1.823 | 0.932–3.568 | .079 | |
| I vs. III | 2.659 | 1.713–4.126 | **<.001** | 1.263 | 0.475–3.356 | .640 | |
| Cirrhosis[a] | 1.583 | 0.984–2.547 | .058 | | | | |
| Child-Pugh class (B) | 1.026 | 0.502–2.099 | .944 | | | | |
| Grade (3, 4) | 0.927 | 0.622–1.381 | .710 | | | | |
| Multiplicity | 1.678 | 1.124–2.505 | **.011** | 1.329 | 0.798–2.215 | .275 | |
| Small vessel invasion | 2.442 | 1.737–3.433 | **<.001** | 1.206 | 0.658–2.21 | .545 | |
| Large vessel invasion | 4.512 | 2.780–7.322 | **<.001** | 3.633 | 1.444–9.139 | **.006** | |
| E-cadherin loss | 1.830 | 1.305–2.566 | **<.001** | 1.786 | 1.263–2.525 | **.001** | |
| Prrx-1 positivity | 1.018 | 0.603–1.717 | .948 | | | | |
| Ki-67 index (≥40) | 1.400 | 0.959–2.045 | .082 | | | | |

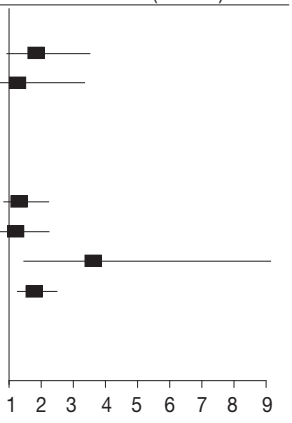


**Fig. 3.** Cox proportional hazard regression model for disease-free survival. CI, confidence interval; AJCC, American Joint Committee on Cancer; Prrx-1, paired-related homeobox protein 1. [a]Cirrhosis vs chronic hepatitis.

| | Univariate analysis | | | Multivariate analysis | | | |
|---|---|---|---|---|---|---|---|
| | Hazard ratio | 95% CI | p-value | Hazard ratio | 95% CI | p-value | Hazard ratio (95% CI) |
| AJCC stage | | | | | | | |
| I vs. II | 1.774 | 1.169–2.693 | **.007** | 1.266 | 0.616–2.602 | .521 | |
| I vs. III | 2.465 | 1.373–4.424 | **.003** | 0.616 | 0.153–2.481 | .496 | |
| Cirrhosis[a] | 2.406 | 1.315–4.403 | **.004** | 2.389 | 1.303–4.379 | **.005** | |
| Child-Pugh class (B) | 1.784 | 0.953–3.342 | .071 | | | | |
| Grade (3, 4) | 1.230 | 0.784–1.93 | .367 | | | | |
| Multiplicity | 1.084 | 0.651–1.804 | .756 | | | | |
| Small vessel invasion | 2.206 | 1.495–3.255 | **<.001** | 1.572 | 0.752–3.287 | .230 | |
| Large vessel invasion | 2.988 | 1.687–5.290 | **<.001** | 3.379 | 0.853–13.381 | .083 | |
| E-cadherin loss | 1.159 | 0.784–1.714 | .458 | | | | |
| Prrx-1 positivity | 1.278 | 0.713–2.292 | .410 | | | | |
| Ki-67 index (≥40) | 1.669 | 1.103–2.526 | **.015** | 1.583 | 1.045–2.399 | **.030** | |

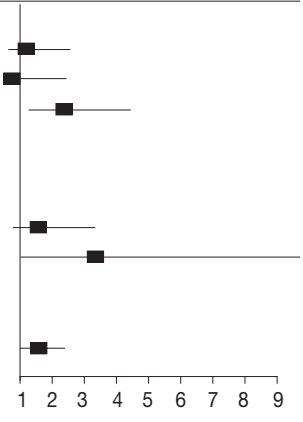


**Fig. 4.** Cox proportional hazard regression model for overall survival. CI, confidence interval; AJCC, American Joint Committee on Cancer; Prrx-1, paired-related homeobox protein 1. [a]Cirrhosis vs chronic hepatitis.

for the multivariate Cox proportional hazard regression model ($p < .05$ in univariate Cox proportional hazard regression model). The disease-free and overall survival were separately processed and are in Figs. 3 and 4, respectively. The stage, multiplicity, small and large vessel invasion, and decrease of E-cadherin were selected for factors in disease-free survival. Among them, the large vessel invasion ($p = .006$) and loss of E-cadherin ($p = .001$) were independent risk factors. The stage, cirrhosis, small and large vessel invasion, and high Ki-67 labeling index were selected for overall survival. Cirrhosis ($p = .005$) and high Ki-67 labeling index ($p = .030$) were independent risk factors for overall survival.

## DISCUSSION

EMT has an important role in cancer progression because it influences tumor cell migration, allows local tissue invasion, and into the blood vessel, which is a necessary step in cancer metastasis.[3] In colorectal cancer, tumor budding is one of the most important prognostic factors and reflects aggressive biologic behavior. The tumor budding is also explained as an EMT process, consistently with its morphologic change to fibroblast-like appearance.[13] E-cadherin is a type of cadherins, which is a type 1 transmembrane protein, that plays an important role in cell adhesion. Loss of the E-cadherin is a hallmark of EMT and it is related to poor prognosis in various human cancers.[14] In addition, several studies based on immunohistochemical staining of E-cadherin have reported the prognostic significance of HCC.[15-17]

Loss of E-cadherin is clearly associated with hematogenous tumor spread, lymph node metastasis, and local recurrence in various types of cancer, including breast cancer, colorectal cancer, and liver cancer.[18-20] For HCC, Chen *et al*.[18] performed a meta-analysis to access the prognostic value of E-cadherin in HCC, and revealed that loss of E-cadherin was strongly associated with poor overall survival, recurrence-free survival, metastasis, vascular invasion, higher grade, and advanced TNM stage.[18] As mentioned earlier, several other EMT inducers were evaluated as prognostic markers. SNAI1, an EMT inducer, was expressed in an invasive portion of HCC and was associated with the higher grade. Twist-1, another EMT inducer, was found to be associated with distant metastasis in HCC.[21]

As previously mentioned, either upregulation or downregulation of Prrx-1 has been reported to be associated with poor prognosis, depending on the type of cancer. In colorectal cancer, overexpression of *PRRX1* mRNA was involved in metastasis and poor prognosis.[7] In thyroid cancer, 57.7% of anaplastic thyroid carcinomas and two of five hobnail variants of papillary carcinoma, which are very aggressive and associated with high mortality rate, were positive for Prrx-1 on immunohistochemical staining, while all conventional papillary carcinomas were negative.[4] In comparison, Ocana *et al*.[5] found that loss of Prrx-1 contributes to metastatic colonization and poor prognosis in breast cancer. They performed an experiment with a xenograft model, using human breast cancer cells that expressed both Prrx-1 and Twist1. A knockdown of both Prrx-1 and Twist1 increased lung metastasis but not in a setting of only one knockdown. This indicated that downregulation of Prrx-1 is necessary to develop metastatic nodules and gain proliferative activity.[5] Similarly, Hirata *et al*.[8] studied mRNA expression level of Prrx-1 in HCC and found that the Prrx-1 downregulated group showed a poorer prognosis than the upregulated group. However, this study showed that normal livers did not express Prrx-1 protein immunohistochemically, and evokes a question that the decreased level of the *PRRX1* mRNA has biological implications, as only a few (in our case, 13%) of the HCCs showed nuclear immunoreactivity on Prrx-1.

Ki-67 is a marker that reflects proliferative activity, which increases during carcinogenesis. Poorly differentiated HCCs show a higher index of Ki-67 than in well- to moderately-differentiated HCCs.[22] In general, the proliferating activity decreases when tumor cells undergo EMT.[23] We expected that loss of E-cadherin and expression of Prrx-1 would inversely correlate with the Ki-67 index. However, there was no significant difference, which was likely due to the limitation of a small number of Prrx-1–positive cases and many other biological confounding variables that effect on the proliferation.

Through this study, we attempted to elucidate whether Prrx-1–positive or Prrx-1–negative HCCs are associated with poor prognosis. As EMT is a dynamic process and its timely regulation is necessary to metastasis, it is necessary to develop new markers to know whether the tumor will re-gain proliferative and epithelial property after hematogenous spread, when we observe E-cadherin loss in the resected primary tumor. However, we only validated E-cadherin as a useful prognostic factor to predict recurrence, and Prrx-1 was not correlated with patient's prognosis and recurrence. Our experiment had some limitations, which were attributable, in part to the role of Prrx-1 on the prognosis of HCCs. The design of the present experiment did not implicate the complex mechanism of EMT–reverse EMT process during cancer metastasis. Cross-sectional studies using immunohistochemical staining on paraffin block have a limitation to dealing dynamic processes. Especially, as Prrx-1 is a transcription

 http://dx.doi.org/10.4132/jptm.2016.06.22

factor, two assumptions are required for this immunohistochemical study: (1) the expression of Prrx-1 should be consistent through the time until E-cadherin molecules disappear in the cell membrane, and (2) the functional expression range and threshold should be consistent with detection range and interpretation cutoff. However, many cellular signals work in a stochastic manner and show oscillatory responses, which give an uncertainty to our assumption.[24,25] Prrx-1 overexpression was observed in 15.1% of HCCs in this study by immunohistochemistry. It is quite a small percentage comparing with 45.2% (28/62), which is the fraction of high-*PRRX1* mRNA that expressed HCCs in the experiment by Hirata *et al*.[8] We believe that this also gives an uncertainty to our second assumption.

In summary, Prrx-1 was expressed in small portion (13.3%) of HCCs but not in non-neoplastic livers. We validated that E-cadherin loss had the prognostic value to predict recurrence in HCCs. Prrx-1 was not correlated with EMT nor prognosis nor recurrence by immunohistochemical staining study. Further study with a larger series of HCCs is required to elucidate the significance of Prrx-1 in HCCs.

## Conflicts of Interest

No potential conflict of interest relevant to this article was reported.

## REFERENCES


1. Jung KW, Won YJ, Kong HJ, Oh CM, Seo HG, Lee JS. Cancer statistics in Korea: incidence, mortality, survival and prevalence in 2010. Cancer Res Treat 2013; 45: 1-14.
2. Tung-Ping Poon R, Fan ST, Wong J. Risk factors, prevention, and management of postoperative recurrence after resection of hepatocellular carcinoma. Ann Surg 2000; 232: 10-24.
3. Thiery JP, Acloque H, Huang RY, Nieto MA. Epithelial-mesenchymal transitions in development and disease. Cell 2009; 139: 871-90.
4. Hardin H, Guo Z, Shan W, *et al*. The roles of the epithelial-mesenchymal transition marker PRRX1 and miR-146b-5p in papillary thyroid carcinoma progression. Am J Pathol 2014; 184: 2342-54.
5. Ocana OH, Corcoles R, Fabra A, *et al*. Metastatic colonization requires the repression of the epithelial-mesenchymal transition inducer Prrx1. Cancer Cell 2012; 22: 709-24.
6. Reichert M, Takano S, von Burstin J, *et al*. The Prrx1 homeodomain transcription factor plays a central role in pancreatic regeneration and carcinogenesis. Genes Dev 2013; 27: 288-300.
7. Takahashi Y, Sawada G, Kurashige J, *et al*. Paired related homoeobox 1, a new EMT inducer, is involved in metastasis and poor prognosis in colorectal cancer. Br J Cancer 2013; 109: 307-11.
8. Hirata H, Sugimachi K, Takahashi Y, *et al*. Downregulation of PRRX1 confers cancer stem cell-like properties and predicts poor prognosis in hepatocellular carcinoma. Ann Surg Oncol 2015; 22 Suppl 3: S1402-9.
9. Woo HY, Min AL, Choi JY, Bae SH, Yoon SK, Jung CK. Clinicopathologic significance of the expression of Snail in hepatocellular carcinoma. Korean J Hepatol 2011; 17: 12-8.
10. Schuffler PJ, Fuchs TJ, Ong CS, Wild PJ, Rupp NJ, Buhmann JM. TMARKER: A free software toolkit for histopathological cell counting and staining estimation. J Pathol Inform 2013; 4(Suppl): S2.
11. Nakanishi K, Sakamoto M, Yamasaki S, Todo S, Hirohashi S. Akt phosphorylation is a risk factor for early disease recurrence and poor prognosis in hepatocellular carcinoma. Cancer 2005; 103: 307-12.
12. Ito Y, Matsuura N, Sakon M, *et al*. Both cell proliferation and apoptosis significantly predict shortened disease-free survival in hepatocellular carcinoma. Br J Cancer 1999; 81: 747-51.
13. Prall F. Tumour budding in colorectal carcinoma. Histopathology 2007; 50: 151-62.
14. Peinado H, Olmeda D, Cano A. Snail, Zeb and bHLH factors in tumour progression: an alliance against the epithelial phenotype? Nat Rev Cancer 2007; 7: 415-28.
15. Cho SB, Lee KH, Lee JH, *et al*. Expression of E- and N-cadherin and clinicopathology in hepatocellular carcinoma. Pathol Int 2008; 58: 635-42.
16. Zhang L, Huang G, Li X, *et al*. Hypoxia induces epithelial-mesenchymal transition via activation of SNAI1 by hypoxia-inducible factor -1alpha in hepatocellular carcinoma. BMC Cancer 2013; 13: 108.
17. Kwon GY, Yoo BC, Koh KC, Cho JW, Park WS, Park CK. Promoter methylation of E-cadherin in hepatocellular carcinomas and dysplastic nodules. J Korean Med Sci 2005; 20: 242-7.
18. Chen J, Zhao J, Ma R, Lin H, Liang X, Cai X. Prognostic significance of E-cadherin expression in hepatocellular carcinoma: a meta-analysis. PLoS One 2014; 9: e103952.
19. Aoki S, Shimamura T, Shibata T, *et al*. Prognostic significance of dysadherin expression in advanced colorectal carcinoma. Br J Cancer 2003; 88: 726-32.
20. Asgeirsson KS, Jonasson JG, Tryggvadóttir L, *et al*. Altered expression of E-cadherin in breast cancer. patterns, mechanisms and clinical significance. Eur J Cancer 2000; 36: 1098-106.
21. Zhao XL, Sun T, Che N, *et al*. Promotion of hepatocellular carcinoma metastasis through matrix metalloproteinase activation by epithelial-mesenchymal transition regulator Twist1. J Cell Mol Med

2011; 15: 691-700.
22. Tannapfel A, Geissler F, Köckerling F, Katalinic A, Hauss J, Wittekind C. Apoptosis and proliferation in relation to histopathological variables and prognosis in hepatocellular carcinoma. J Pathol 1999; 187: 439-45.
23. Tsai JH, Donaher JL, Murphy DA, Chau S, Yang J. Spatiotemporal regulation of epithelial-mesenchymal transition is essential for squamous cell carcinoma metastasis. Cancer Cell 2012; 22: 725-36.
24. Ferrell JE Jr, Machleder EM. The biochemical basis of an all-or-none cell fate switch in *Xenopus* oocytes. Science 1998; 280: 895-8.
25. Batchelor E, Loewer A, Lahav G. The ups and downs of p53: understanding protein dynamics in single cells. Nat Rev Cancer 2009; 9: 371-7.


http://dx.doi.org/10.4132/jptm.2016.06.22

*Journal of Pathology and Translational Medicine 2016; 50: 337-344*
*http://dx.doi.org/10.4132/jptm.2016.05.20*

■ORIGINAL ARTICLE■

# SIRT7, H3K18ac, and ELK4 Immunohistochemical Expression in Hepatocellular Carcinoma

Hye Seung Lee · Wonkyung Jung
Eunjung Lee[1] · Hyeyoon Chang
Jin Hyuk Choi · Han Gyeom Kim
Aeree Kim · Baek-hui Kim

Department of Pathology, Korea University Guro Hospital, Seoul; [1]Department of Pathology, Korea University Anam Hospital, Seoul, Korea

**Received:** March 16, 2016
**Revised:** May 18, 2016
**Accepted:** May 19, 2016

**Corresponding Author**
Baek-hui Kim, MD, PhD
Department of Pathology, Korea University Guro Hospital, Korea University School of Medicine, 148 Gurodong-ro, Guro-gu, Seoul 08308, Korea
Tel: +82-2-2626-1472
Fax: +82-2-2626-1486
E-mail: maelstrom@naver.com

**Background:** SIRT7 is one of the histone deacetylases and is NAD-dependent. It forms a complex with ETS-like transcription factor 4 (ELK4), which deacetylates H3K18ac and works as a transcriptional suppressor. Overexpression of SIRT7 and deacetylation of H3K18ac have been shown to be associated with aggressive clinical behavior in some cancers, including hepatocellular carcinoma (HCC). The present study investigated the immunohistochemical expression of SIRT7, H3K18ac, and ELK4 in hepatocellular carcinoma. **Methods:** A total of 278 HCC patients were enrolled in this study. Tissue microarray blocks were made from existing paraffin-embedded blocks. Immunohistochemical expressions of SIRT7, H3K18ac and ELK4 were scored and analyzed. **Results:** High SIRT7 ($p = .034$), high H3K18ac ($p = .001$), and low ELK4 ($p = .021$) groups were associated with poor outcomes. Age < 65 years ($p = .028$), tumor size ≥ 5 cm ($p = .001$), presence of vascular emboli ($p = .003$), involvement of surgical margin ($p = .001$), and high American Joint Committee on Cancer stage (III&V) ($p < .001$) were correlated with worse prognoses. In multivariate analysis, H3K18ac ($p = .001$) and ELK4 ($p = .015$) were the significant independent prognostic factors. **Conclusions:** High SIRT7 expression with poor overall survival implies that deacetylation of H3K18ac contributes to progression of HCC. High H3K18ac expression with poor prognosis is predicted due to a compensation mechanism. In addition, high ELK4 expression with good prognosis suggests another role of ELK4 as a tumor suppressor beyond SIRT7's helper. In conclusion, we could assume that the H3K18ac deacetylation pathway is influenced by many other factors.

**Key Words:** Carcinoma, hepatocellular; ELK4; Sirtuin 7 protein; H3K18ac; Immunohistochemistry

Hepatocellular carcinoma (HCC) is the sixth most prevalent neoplasm and is the second most common cause of cancer-related death worldwide.[1] Due to its invasiveness and metastatic potential, demonstration of the pathogenesis of HCC is essential. In addition to environmental factors, a variety of genetic or epigenetic alterations including histone modification are the cause of HCC.[2,3] Histone modification involves post-translational modification of N-terminal tails of histone proteins by acetylation, methylation, phosphorylation, ubiquitylation, sumoylation, adenosine diphosphate ribosylation, biotinylation, and so on.[4] Histone deacetylases (HDACs) are critical regulators of gene expression that promote formation of heterochromatin by deacetylating histone and non-histone proteins. Therefore, aberrant regulation of HDACs contributes to malignant transformation and progression in a wide variety of human cancers, such as HCC, gastric cancer, lung cancer, and other cancers.

Seven sirtuin family members (SIRT1-7) belong to the HDAC, and are highly conserved from bacteria to mammals.[5,6] They are also NAD-dependent, regulating a wide range of cellular processes, including aging, DNA repair, cell cycle, metabolism, and stress response.[6,7] Currently, SIRT1, 2, 3, 6, and 7 are known to be involved with HCC.[8-12] Among them, SIRT7 has been reported to be proportionally upregulated in pre-neoplastic nodules to overt human HCC tissues.[12] In addition, down-regulated H3K18ac has been observed in human HCC samples.[13] SIRT7 specifically deacetylates H3K18ac and contributes to the maintenance of tumor integrity by reducing the transcription of genes at specific loci, including tumor suppressor genes.[12,14] SIRT7 requires cofactors such as ETS-like transcription factor 4 (ELK4). ELK4 belongs to the ternary complex factor subfamily in ETS domain transcription factors.[15] About 60% of the SIRT7-binding sites contain an ELK4-binding motif, and the SIRT7-ELK4 complex induces deacetylation of H3K18ac. Gene-based studies have been performed on SIRT7, but there has been no research on SIRT7 with its deacetylation indicated by immunohistochemical (IHC) study in HCC. Therefore, in the present study we ex-

pISSN 2383-7837
eISSN 2383-7845

amined the IHC expression of ELK4, SIRT7, and H3K18ac in paraffin-embedded HCC samples.

## MATERIALS AND METHODS

### Case selection and review

A total of 278 HCC patients, who underwent curative surgery at Korea University Guro Hospital between 2000 and 2013 were enrolled in this study. All hematoxylin and eosin–stained slides were reviewed. To classify the pathologic staging, the American Joint Committee on Cancer (AJCC) staging system (seventh edition) was applied.[16] Tumor differentiation was graded according to the Edmondson-Steiner grading system.[17] Tumor necrosis was evaluated by gross photo and microscopic examination. The results were categorized as 'present' when necrosis was detected, even in minor amounts. Missing data were excluded, and clinicopathologic data including sex, age and TNM stage were obtained from patients' medical records. This study was approved by the Institutional Review Board of Korea University Guro Hospital (KUGH14140-001).

### Tissue microarray construction and immunohistochemistry

Representative tumor areas in all patients (n = 278), and non-tumor areas in 52 patients were obtained and embedded on par-

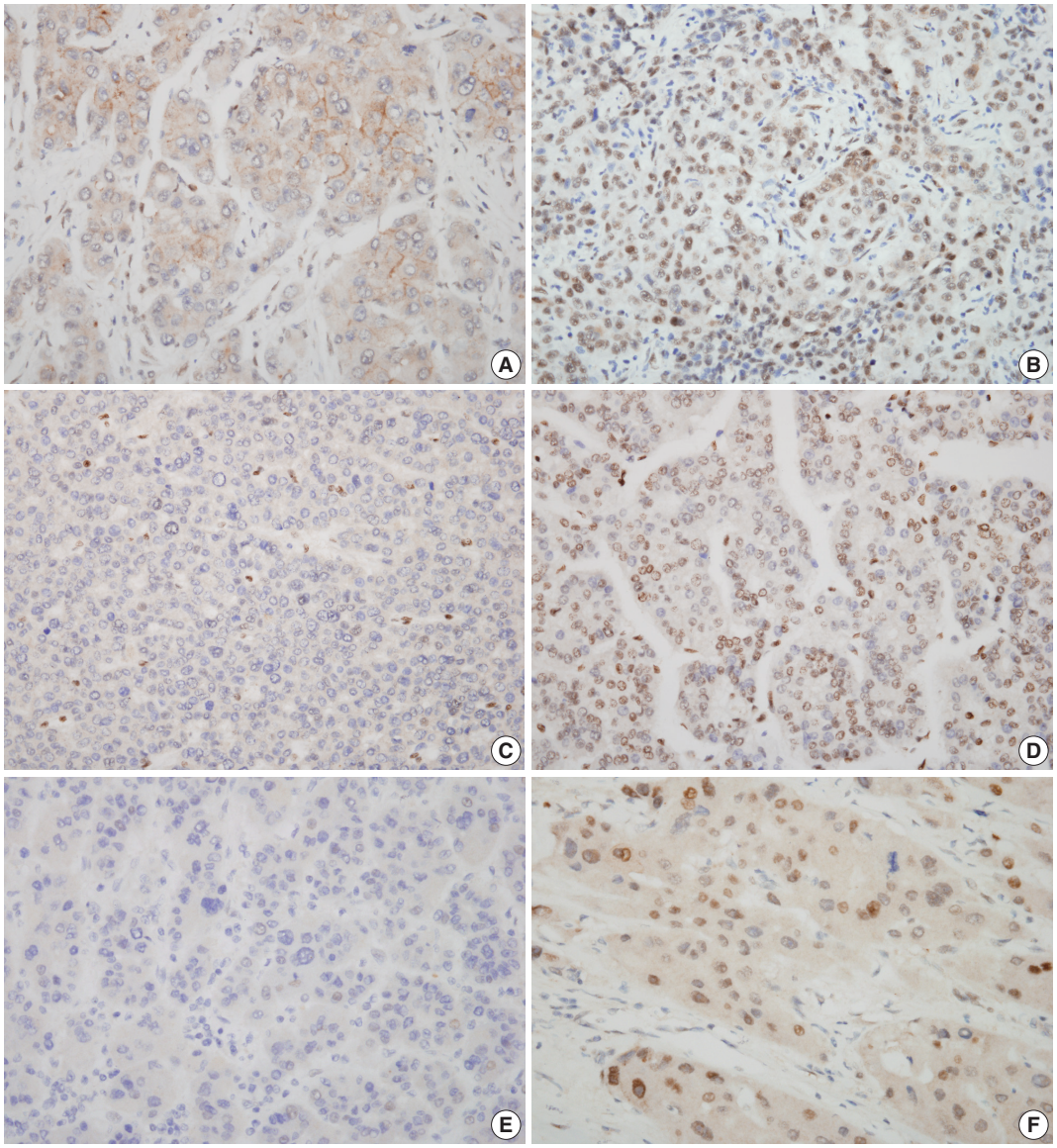


**Fig. 1.** Characteristic nuclear staining of tumor cells by immunohistochemistry. Low SIRT7 expression (A), high SIRT7 expression (B), low H3K18ac expression (C), high H3K18ac expression (D), low ELK4 expression (E), and high ELK4 expression (F) are seen.


http://dx.doi.org/10.4132/jptm.2016.05.20

affin blocks. Tissue cores 2.0 mm in diameter were collected from paraffin-embedded donor blocks and embedded in tissue microarray (TMA) blocks. IHC staining was performed on 4 μm TMA section slides using Bond-Max auto-stainer (Leica, Wetzlar, Germany). After incubation with primary antibodies, Bond Polymer Refine Detection kit (Leica) was used for chromogenic reaction. The following primary antibodies were used in this study; ELK4 (1:50, rabbit polyclonal, Novus, Littleton, CO, USA), SIRT7 (1:100, rabbit polyclonal, Abcam, Cambridge, MA, USA), and H3K18ac (1:1000, rabbit polyclonal, Abcam).

### IHC assessment

Nuclear staining patterns of tumor cells for ELK4, SIRT7, and H3K18ac were analyzed (Fig. 1). More than 10% of stained tumor cells were categorized as positive. Scoring of intensity was done according to the following scale: 0, no or equivocal; 1, weak; 2, moderate; and 3, strong staining. Cases showing moderate (score 2) or strong (score 3) staining in more than 10% were regarded as "high expression." Cases with no or weak staining were regarded as "low expression." This assessment was performed by two pathologists blind to all clinicopathologic data and outcome variables. Due to tissue loss in microarray cores, three samples of SIRT7 (n = 275) and two of H3K18ac (n = 276) were excluded. None of the ELK4 (n = 278) samples were excluded.

### Statistical analysis

To examine univariate overall survival, the log-rank test with the Kaplan-Meier survival curve was used. The Cox's proportional hazards regression model was used for univariate and multivariate analyses of overall and disease-free survival. Overall survival rate was calculated from the date of surgery to the date of the latest follow-up or death. The disease-free survival rate was also calculated from the date of surgery to the date of recurrence on follow-up images or pathologic confirmation. For comparing means, the independent t test was used. Pearson's correlation coefficient was applied to the correlation between IHC expression and the clinicopathologic data. The p-value less than .05 was con-

**Table 1.** Correlation between immunohistochemical markers and clinicopathologic data

| Characteristic | No. (%) | Immunohistochemistry expression | | | | | | | | |
|---|---|---|---|---|---|---|---|---|---|---|
| | | SIRT7 (n = 275) | | | H3K18Ac (n = 276) | | | ELK4 (n = 278) | | |
| | | Low (n = 224, 81%) | High (n = 51, 19%) | p-value | Low (n = 133, 48%) | High (n = 143, 52%) | p-value | Low (n = 222, 76%) | High (n = 66, 24%) | p-value |
| Age (yr) | | | | | | | | | | |
| < 65 | 214 (77) | 176 | 37 | .721 | 80 | 115 | .184 | 80 | 115 | .184 |
| ≥ 65 | 64 (23) | 50 | 12 | | 35 | 28 | | 35 | 28 | |
| Sex | | | | | | | | | | |
| Female | 47 (16.9) | 36 | 9 | .448 | 16 | 31 | .021* | 16 | 31 | .033* |
| Male | 231 (83) | 190 | 40 | | 117 | 112 | | 117 | 112 | |
| Edmondson-Steiner grade | | | | | | | | | | |
| I–II | 178 (64) | 154 | 23 | .002* | 107 | 76 | < .001* | 135 | 43 | .828 |
| III–IV | 100 (36) | 72 | 26 | | 26 | 67 | | 77 | 23 | |
| Tumor size (cm) | | | | | | | | | | |
| < 5 | 214 (77) | 176 | 37 | .721 | 103 | 111 | .972 | 163 | 51 | .948 |
| ≥ 5 | 64 (23) | 50 | 12 | | 30 | 32 | | 49 | 15 | |
| AJCC stage | | | | | | | | | | |
| I–II | 244 (87.8) | 199 | 42 | .653 | 119 | 123 | .384 | 183 | 61 | .188 |
| III–IV | 34 (12.2) | 27 | 7 | | 14 | 20 | | 29 | 5 | |
| Vascular emboli | | | | | | | | | | |
| Absent | 183 (65.8) | 153 | 29 | .255 | 98 | 85 | .012* | 148 | 35 | .056 |
| Present | 95 (34.2) | 73 | 20 | | 35 | 58 | | 64 | 29 | |
| Margin | | | | | | | | | | |
| Negative | 263 (94.6) | 214 | 46 | .821 | 125 | 136 | .683 | 199 | 64 | .727 |
| Positive | 15 (5.4) | 12 | 3 | | 8 | 7 | | 13 | 2 | |
| Tumor necrosis | | | | | | | | | | |
| Absent | 158 (61.7) | 131 | 25 | .261 | 80 | 77 | .133 | 113 | 45 | .211 |
| Present | 98 (38.3) | 76 | 21 | | 40 | 57 | | 77 | 21 | |

ELK4, ETS-like transcription factor 4; AJCC, American Joint Committee on Cancer.
*Statistically significant (p < .05).

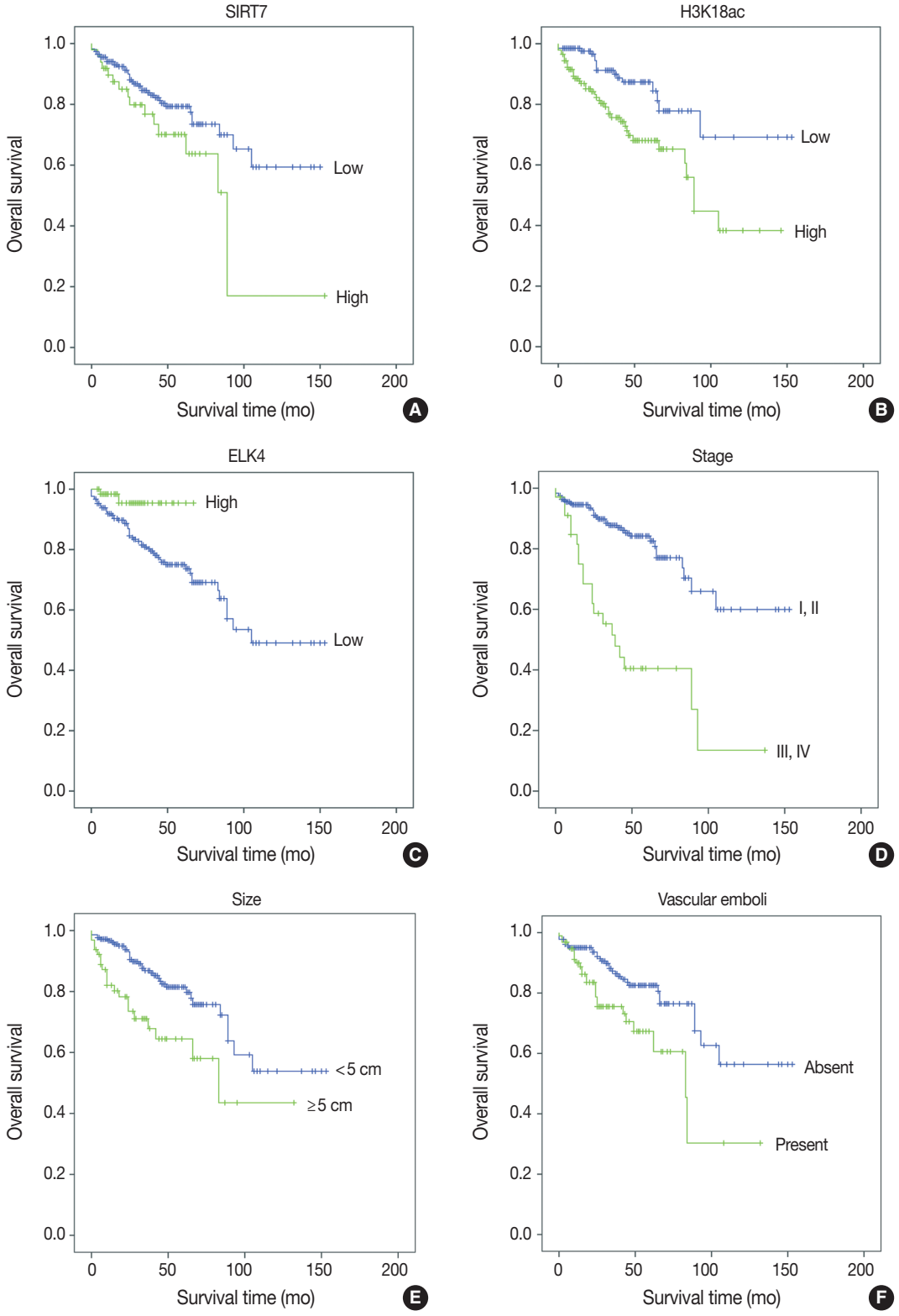


**Fig. 2.** Kaplan-Meier survival curves of immunohistochemical (IHC) markers and clinicopathologic data. With IHC markers (A–C), high SIRT7 expression (A) and high H3K18ac expression (B) were associated with poor prognosis ($p = .034$ and $p = .001$, respectively). However, high ETS-like transcription factor 4 (ELK4) expression was associated with good prognosis ($p = .021$) (C). With clinicopathologic factors (D–F), high American Joint Committee on Cancer stage (III, IV) ($p < .001$) (D), large tumor size (maximal diameter ≥ 5 cm) ($p = .001$) (E), and the presence of vascular emboli (F) were associated with poor overall survival ($p = .003$).


http://dx.doi.org/10.4132/jptm.2016.05.20

sidered to be statistically significant. All statistical analyses were performed using the SPSS ver. 20 (IBM Corp., Armonk, NY, USA).

## RESULTS

### Patient characteristics

In the present study, there were 231 (83%) male and 47 (17%) female HCC patients between 26–84 years of age (median ± standard deviation, 57 ± 10.2 years) who underwent curative operation. The median postoperational follow-up period was 34 months. A total of 56 patients (20%) died during the follow-up period. Among all patients, 149 (54%) were in AJCC stage I, 95 (34%) were in stage II, nine (3%) were in stage III, and 25 (9%) were in stage IV.

### Expressions of SIRT7, H3K18ac, and ELK4 in non-tumor and tumor cells

The results of all three antibodies showed significant nuclear expression patterns (Fig. 1). In non-tumor hepatocytes of 52 patients, high SIRT7, H3K18ac, and ELK4 expressions were observed in seven (13%), four (8%), and one (2%) patients, respectively; however, in tumor cells, 51 (19%), 143 (52%), and 66 (24%) patients showed high expressions for SIRT7, H3K18ac, and ELK4, respectively (Table 1). Interestingly, H3K18ac showed significantly high expression in tumor cells (mean value, 1.08 and 1.71, respectively; $p < .001$). In addition, SIRT7 was higher in tumor cells (mean value, 1.06 and 1.08, respectively; $p = .858$) and ELK4 was higher in non-tumor hepatocytes (mean value, 0.96 and 0.87, respectively; $p = .120$). However, these results were not significant.

### Analyses of overall and disease-free survival

Univariate analyses of overall survival rate using the Kaplan-Meier method showed that high expression in both SIRT7 and H3K18ac were associated with poor overall survival rate ($p = .034$ and $p = .001$, respectively) (Fig. 2A, B); however, high expression in ELK4 was associated with good overall survival ($p = .021$) (Fig. 2C). High AJCC stage ($p < .001$) (Fig. 2D), large tumor size (≥5 cm) ($p = .001$) (Fig. 2E), and the presence of vascular emboli ($p = .003$) (Fig. 2F) were associated with poor overall survival rate. Additionally, younger age (<65 years) ($p = .028$) and positive surgical margin ($p = .001$) were correlated with poor outcomes. Analyses using Cox's proportional hazards are shown

**Table 2.** Univariate and multivariate analyses of overall survival using Cox's proportional hazards model

| Variable | Univariate analysis | | Multivariate analysis | |
|---|---|---|---|---|
| | HR (95% CI) | p-value | HR (95% CI) | p-value |
| High SIRT7 expression | 1.853 (1.036–3.313) | .038* | 1.323 (0.720–2.430) | .368 |
| High H3K18Ac expression | 2.569 (1.438–4.592) | .001* | 2.731 (1.469–5.076) | .001* |
| High ELK4 expression | 0.219 (0.053–0.907) | .036* | 0.162 (0.037–0.704) | .015* |
| Tumor size (≥5 cm) | 2.427 (1.400–4.207) | .002* | 2.044 (1.104–3.787) | .023* |
| Vascular emboli | 2.176 (1.273–3.720) | .004* | 1.287 (0.707–2.343) | .409 |
| Margin positive | 3.371 (1.582–7.183) | .002* | 2.943 (1.300–6.661) | .010* |
| AJCC stage III–IV | 4.302 (2.489–7.438) | <.001* | 3.007 (1.650–5.483) | <.001* |

HR, hazard ratio; CI, confidence interval; ELK4, ETS-like transcription factor 4; AJCC, American Joint Committee on Cancer.
*Statistically significant ($p < .05$).

**Table 3.** Univariate and multivariate analysis using Cox's proportional hazards analysis of disease-free survival

| Variable | Univariate analysis | | Multivariate analysis | |
|---|---|---|---|---|
| | HR (95% CI) | p-value | HR (95% CI) | p-value |
| High SIRT7 expression | 1.573 (1.013–2.444) | .044* | 1.440 (0.912–2.276) | .118 |
| High H3K18Ac expression | 1.229 (0.844–1.789) | .283 | 1.022 (0.680–1.537) | .915 |
| High ELK4 expression | 0.922 (0.566–1.502) | .744 | 0.901 (0.545–1.490) | .685 |
| Tumor size (≥5 cm) | 1.393 (0.903–2.150) | .134 | 1.110 (0.697–1.769) | .660 |
| Vascular emboli | 1.465 (1.001–2.144) | .049* | 1.192 (0.790–1.800) | .402 |
| Margin positive | 1.200 (0.558–2.580) | .640 | 0.903 (0.403–2.025) | .805 |
| AJCC stage III–IV | 2.128 (1.310–3.458) | .002* | 1.898 (1.101–3.273) | .021* |
| Edmondson-steiner's grade | 1.513 (1.040–2.202) | .030* | 1.270 (0.839–1.923) | .258 |

HR, hazard ratio; CI, confidence interval; ELK4, ETS-like transcription factor 4; AJCC, American Joint Committee on Cancer.
*Statistically significant ($p < .05$).

**Table 4.** Bivariate analysis of SIRT7, H3K18ac, and ELK4 (n=275)

| | | SIRT7 | H3K18ac | ELK4 |
|---|---|---|---|---|
| SIRT7 | Correlation coefficient | 1.000 | 0.165 | –0.054 |
| | p-value | | .006* | .372 |
| H3K18ac | Correlation coefficient | 0.165 | 1.000 | –0.035 |
| | p-value | .006* | | .560 |
| ELK4 | Correlation coefficient | –0.054 | –0.035 | 1.000 |
| | p-value | .372 | .560 | |

ELK4, ETS-like transcription factor 4.
*Statistically significant ($p < .05$).

in Table 2.

In multivariate analyses (Table 2), high expression in H3K18ac was determined to be a poor prognostic factor ($p = .001$), whereas high expression in ELK4 was indicated as a good prognostic factor ($p = .015$). However, high SIRT7 expression was unremarkable ($p = .368$). Tumor size ≥5 cm, positive margin, and advanced stage (III–IV) ($p = .024$, $p = .012$, and $p < .001$, respectively) were related independently as poor prognostic factors. Finally, the presence of vascular emboli was not significant ($p = .409$).

Disease-free survival rate analyses were performed using the Cox's proportional hazard model. High SIRT7 expression, presence of vascular emboli, AJCC stage III-IV and Edmondson-Steiner grade III–IV were associated with worse prognosis (Table 3). However, only AJCC stage was shown to be an independent factor in the multivariate analysis ($p = .021$).

### Analyses of correlation

SIRT7 and H3K18ac showed a positive correlation ($p = .006$) (Table 4); however, ELK4 did not show a significant correlation with the other two markers. Tumor size showed a positive association with AJCC stage ($p < .001$), vascular tumor emboli ($p = .001$), and necrosis ($p < .001$). Additionally, tumor necrosis was positively associated with presence of vascular emboli ($p = .012$) as well as AJCC stage III and IV ($p = .005$). Edmondson-Steiner grade III and IV showed positive correlation with the existence of vascular emboli ($p = .000$) and high AJCC stage ($p = .010$). Elder patients (≥65 years) had positive association with positive surgical margin ($p = .029$).

Table 1 summarizes the correlation between IHC markers and clinicopathologic data. Edmondson-Steiner grade III and IV had a correlation with high SIRT7 and high H3K18ac expression ($p = .002$ and $p < .001$, respectively). A high T stage or presence of vascular emboli were associated with high H3K18ac expression ($p = .027$ and $p = .012$, respectively). In addition, high H3K18ac expression showed a significant correlation with females ($p = .033$) and high ELK4 expression with males ($p = .021$).

## DISCUSSION

The objective of the present study was to analyze H3K18ac, which is deacetylated by SIRT7 linked with ELK4, by IHC expression in HCC samples. We hypothesized that high IHC expression of SIRT7 would be associated with high ELK4 and low H3K18ac expression, and these results would lead to a poor overall survival rate. On the contrary to the hypothesis, this study found that SIRT7 expression had a weak positive correlation with H3K18ac, but no correlation with ELK4 (Table 4). In addition, high H3K18ac expression was unexpectedly associated with poor prognosis, whereas high ELK4 expression was associated with better prognosis in the overall survival analyses (Table 2). Lastly, high SIRT7 expression associated with poor prognosis was in accordance with our major hypothesis.

There is no definite explanation of the unexpected positive correlation of SIRT7 and H3K18ac, but there are several possible mechanisms. First, other pathways may exist. For example, SIRT2 and SIRT6 can also deacetylate H3K18ac in addition to SIRT7.[18,19] Conversely, SIRT7 also deacetyl-ates p53 in addition to H3K18ac.[20] Although the prognostic direction of H3K18ac was unexpected, it seems to have significance, which is shown in the univariate and multivariate overall survival analyses. In addition, correlation analyses revealed a positive association with poor Edmondson-Steiner grade, high T stage and presence of vascular emboli (Tables 1, 2). Putting these evidences together, we can suggest that there are other important mechanisms beyond the deacetylation of H3K18ac by SIRT7. The weak correlation coefficient value may be a reflection of this (Table 4).

Second, the method of approach was different. In previous studies, experiments were performed with cell-lines and were focused on the specific gene foci.[12,14] In the present study, we used surgical specimens and examined overall protein expressions by the IHC approach. Some authors have argued that gene-specific expression of histone acetylation can run contrary to the overall state of modification. This phenomenon could have resulted from compensation and made a difference in the overall expres-


http://dx.doi.org/10.4132/jptm.2016.05.20

sion of acetylation seen in the IHC study.[21-23] Further evaluation of the relationship of SIRT7 and H3K18ac in HCC is needed.[19] Because previous HCC studies of H3K18ac were focused on tumor suppressor genes, the roles of H3K18ac in proto-oncogene or global H3K18ac expression in HCC progression have not been sufficiently investigated. However, several studies have shown the correlation of H3K18ac with poor prognosis in other malignancies, such as pancreatic adenocarcinoma or esophageal cancer.[23,24] Moreover, in some malignant tumors, especially in HCCs, global acetylation of H3K18 could be more associated with genes related to tumor progression or proliferation than tumor suppression.[25-27]

High SIRT7 expression in this study was associated with poor overall survival rate and high tumor grade but did not show a statistical correlation with H3K18ac and ELK4 expression. Most studies on SIRT7 in HCC have focused on the HDAC activity of SIRT7 in relation to tumor suppressor genes.[12,14] Recent studies have revealed other mechanisms of SIRT7 in human cells. They have reported that SIRT7 can regulate protein folding in mitochondria, and a decrease in SIRT7 could result in stem cell senescence.[28] Another study also reported that SIRT7 can interact with SIRT1, resulting in epithelial-to-mesenchymal transition via control of E-cadherin. The mechanism of SIRT7 as a poor prognostic factor in HCC may be more related to other roles in tumor cells than its role as a suppressor of tumor suppressor genes.[29]

High ELK4 expression did not show a correlation with SIRT7 or H3K18ac in the present study. However, high ELK4 expression was an independent factor of good prognosis in HCC patients. The most studied mechanism of ELK4 in tumorigenesis is the role as a cofactor of SIRT7 in deacetylation of H3K18, which is located in tumor suppressor genes or ribosome-related genes. Additionally, ELK4 fundamentally forms complexes with SRF dimers on SREs found in the c-fos and other immediate early gene promoters,[15] and this process is stimulated by the activated mitogen-activated protein kinase (MAPK) signaling pathway.[15,30] Therefore, we can assume that high ELK4 status would induce the oncogenic pathway, but this has not been investigated. Furthermore, ELK4 is expected to inhibit gene transcription, due to its resemblance to ELK3/NET. ELK3/NET acts as a transcription repressor of target promoters through its NET inhibitory domain (NID) and C-terminal-binding protein inhibition domain in the absence of the MAPK signal.[31,32] Thus, loss of ELK3 expression has been reported in malignant mesothelioma, suggesting the role of ELK3 as a repressor of tumors.[33] ELK4 also has a similar NID region to ELK3/NET,[34,35] suggesting that ELK4 may also inhibit gene transcription during the inactivated MAPK condition.[36] The role of ELK4 in HCC requires more investigation, but this transcriptional repression could be associated with inhibition of tumor progression.

In conclusion, high expression of ELK4 and low expression of H3K18ac were independent and good prognostic factors in HCC patients. High SIRT7 expression in HCC was associated with poor overall survival rate, although it was not an independent prognostic factor. In HCC tissue samples, these proteins had significant prognostic values independently; however, we did not find an integrated tumorigenic effect. Since these proteins have not been widely investigated, more comprehensive studies for interactions and mechanisms of ELK4, SIRT7, and H3K18ac are needed in HCC.

## Conflicts of Interest

No potential conflict of interest relevant to this article was reported.

## REFERENCES


1. Jung KW, Won YJ, Kong HJ, Oh CM, Lee DH, Lee JS. Cancer statistics in Korea: incidence, mortality, survival, and prevalence in 2011. Cancer Res Treat 2014; 46: 109-23.
2. Kim HS, Shen Q, Nam SW. Histone deacetylases and their regulatory microRNAs in hepatocarcinogenesis. J Korean Med Sci 2015; 30: 1375-80.
3. Ma L, Chua MS, Andrisani O, So S. Epigenetics in hepatocellular carcinoma: an update and future therapy perspectives. World J Gastroenterol 2014; 20: 333-45.
4. Hung SY, Lin HH, Yeh KT, Chang JG. Histone-modifying genes as biomarkers in hepatocellular carcinoma. Int J Clin Exp Pathol 2014; 7: 2496-507.
5. Li L, Bhatia R. The controversial role of sirtuins in tumorigenesis: SIRT7 joins the debate. Cell Res 2013; 23: 10-2.
6. Mellini P, Valente S, Mai A. Sirtuin modulators: an updated patent review (2012 - 2014). Expert Opin Ther Pat 2015; 25: 5-15.
7. Kleszcz R, Paluszczak J, Baer-Dubowska W. Targeting aberrant cancer metabolism: the role of sirtuins. Pharmacol Rep 2015; 67: 1068-80.
8. Jang KY, Noh SJ, Lehwald N, *et al*. SIRT1 and c-Myc promote liver tumor cell survival and predict poor survival of human hepatocellular carcinomas. PLoS One 2012; 7: e45119.
9. Chen J, Chan AW, To KF, *et al*. SIRT2 overexpression in hepatocellular carcinoma mediates epithelial to mesenchymal transition by

protein kinase B/glycogen synthase kinase-3beta/beta-catenin signaling. Hepatology 2013; 57: 2287-98.
10. Zhang B, Qin L, Zhou CJ, Liu YL, Qian HX, He SB. SIRT3 expression in hepatocellular carcinoma and its impact on proliferation and invasion of hepatoma cells. Asian Pac J Trop Med 2013; 6: 649-52.
11. Zhang ZG, Qin CY. Sirt6 suppresses hepatocellular carcinoma cell growth via inhibiting the extracellular signalregulated kinase signaling pathway. Mol Med Rep 2014; 9: 882-8.
12. Kim JK, Noh JH, Jung KH, *et al*. Sirtuin7 oncogenic potential in human hepatocellular carcinoma and its regulation by the tumor suppressors MiR-125a-5p and MiR-125b. Hepatology 2013; 57: 1055-67.
13. Zheng Y, Chen H, Yin M, *et al*. MiR-376a and histone deacetylation 9 form a regulatory circuitry in hepatocellular carcinoma. Cell Physiol Biochem 2015; 35: 729-39.
14. Barber MF, Michishita-Kioi E, Xi Y, *et al*. SIRT7 links H3K18 deacetylation to maintenance of oncogenic transformation. Nature 2012; 487: 114-8.
15. Buchwalter G, Gross C, Wasylyk B. Ets ternary complex transcription factors. Gene 2004; 324: 1-14.
16. Edge SB, Byrd DR, Compton CC, Fritz AG, Greene FL, Trotti A. AJCC cancer staging manual. 7th ed. New York: Springer, 2010.
17. Edmondson HA, Steiner PE. Primary carcinoma of the liver: a study of 100 cases among 48,900 necropsies. Cancer 1954; 7: 462-503.
18. Eskandarian HA, Impens F, Nahori MA, *et al*. A role for SIRT2-dependent histone H3K18 deacetylation in bacterial infection. Science 2013; 341: 1238858.
19. Tasselli L, Xi Y, Zheng W, *et al*. SIRT6 deacetylates H3K18ac at pericentric chromatin to prevent mitotic errors and cellular senescence. Nat Struct Mol Biol 2016; 23: 434-40.
20. Vakhrusheva O, Smolka C, Gajawada P, *et al*. Sirt7 increases stress resistance of cardiomyocytes and prevents apoptosis and inflammatory cardiomyopathy in mice. Circ Res 2008; 102: 703-10.
21. Pokholok DK, Harbison CT, Levine S, *et al*. Genome-wide map of nucleosome acetylation and methylation in yeast. Cell 2005; 122: 517-27.
22. Sinha I, Wirén M, Ekwall K. Genome-wide patterns of histone modifications in fission yeast. Chromosome Res 2006; 14: 95-105.
23. Juliano CN, Izetti P, Pereira MP, *et al*. H4K12 and H3K18 acetylation associates with poor prognosis in pancreatic cancer. Appl Immunohistochem Mol Morphol 2016; 24: 337-44.
24. Tzao C, Tung HJ, Jin JS, *et al*. Prognostic significance of global histone modifications in resected squamous cell carcinoma of the esophagus. Mod Pathol 2009; 22: 252-60.
25. Liu BL, Cheng JX, Zhang X, *et al*. Global histone modification patterns as prognostic markers to classify glioma patients. Cancer Epidemiol Biomarkers Prev 2010; 19: 2888-96.
26. Seligson DB, Horvath S, Shi T, *et al*. Global histone modification patterns predict risk of prostate cancer recurrence. Nature 2005; 435: 1262-6.
27. Seligson DB, Horvath S, McBrian MA, *et al*. Global levels of histone modifications predict prognosis in different cancers. Am J Pathol 2009; 174: 1619-28.
28. Liu JP, Chen R. Stressed SIRT7: facing a crossroad of senescence and immortality. Clin Exp Pharmacol Physiol 2015; 42: 567-9.
29. Malik S, Villanova L, Tanaka S, *et al*. SIRT7 inactivation reverses metastatic phenotypes in epithelial and mesenchymal tumors. Sci Rep 2015; 5: 9841.
30. Sharrocks AD. The ETS-domain transcription factor family. Nat Rev Mol Cell Biol 2001; 2: 827-37.
31. Criqui-Filipe P, Ducret C, Maira SM, Wasylyk B. Net, a negative Ras-switchable TCF, contains a second inhibition domain, the CID, that mediates repression through interactions with CtBP and deacetylation. EMBO J 1999; 18: 3392-403.
32. Maira SM, Wurtz JM, Wasylyk B. Net (ERP/SAP2) one of the Ras-inducible TCFs, has a novel inhibitory domain with resemblance to the helix-loop-helix motif. EMBO J 1996; 15: 5849-65.
33. van Riggelen J, Buchwalter G, Soto U, *et al*. Loss of net as repressor leads to constitutive increased c-fos transcription in cervical cancer cells. J Biol Chem 2005; 280: 3286-94.
34. Stinson J, Inoue T, Yates P, Clancy A, Norton JD, Sharrocks AD. Regulation of TCF ETS-domain transcription factors by helix-loop-helix motifs. Nucleic Acids Res 2003; 31: 4717-28.
35. Yates PR, Atherton GT, Deed RW, Norton JD, Sharrocks AD. Id helix-loop-helix proteins inhibit nucleoprotein complex formation by the TCF ETS-domain transcription factors. EMBO J 1999; 18: 968-76.
36. Kaikkonen S, Makkonen H, Rytinki M, Palvimo JJ. SUMOylation can regulate the activity of ETS-like transcription factor 4. Biochim Biophys Acta 2010; 1799: 555-60.

 http://dx.doi.org/10.4132/jptm.2016.05.20

*Journal of Pathology and Translational Medicine 2016; 50: 345-354*
*http://dx.doi.org/10.4132/jptm.2016.06.14*

■ ORIGINAL ARTICLE ■

# Differential Immunohistochemical Profiles for Distinguishing Prostate Carcinoma and Urothelial Carcinoma

Woo Jin Oh* · Arthur Minwoo Chung*
Jee Soon Kim · Ji Heun Han
Sung Hoo Hong[1] · Ji Yeol Lee[1]
Yeong Jin Choi

Departments of Hospital Pathology and [1]Urology, Seoul St. Mary's Hospital, College of Medicine, The Catholic University of Korea, Seoul, Korea

**Received:** February 20, 2016
**Revised:** May 21, 2016
**Accepted:** June 14, 2016

**Corresponding Author**
Yeong Jin Choi, MD, PhD
Department of Hospital Pathology,
Seoul St. Mary's Hospital, College of Medicine,
The Catholic University of Korea, 222 Banpo-daero,
Seocho-gu, Seoul 06591, Korea
Tel: +82-2-2258-1616
Fax: +82-2-2258-1627
E-mail: mdyjchoi@catholic.ac.kr

*Woo Jin Oh and Arthur Minwoo Chung contributed equally to this work.

**Background:** The pathologic distinction between high-grade prostate adenocarcinoma (PAC) involving the urinary bladder and high-grade urothelial carcinoma (UC) infiltrating the prostate can be difficult. However, making this distinction is clinically important because of the different treatment modalities for these two entities. **Methods:** A total of 249 patient cases (PAC, 111 cases; UC, 138 cases) collected between June 1995 and July 2009 at Seoul St. Mary's Hospital were studied. An immunohistochemical evaluation of prostatic markers (prostate-specific antigen [PSA], prostate-specific membrane antigen [PSMA], prostate acid phosphatase [PAP], P501s, NKX3.1, and α-methylacyl coenzyme A racemase [AMACR]) and urothelial markers (CK34βE12, p63, thrombomodulin, S100P, and GATA binding protein 3 [GATA3]) was performed using tissue microarrays from each tumor. **Results:** The sensitivities of prostatic markers in PAC were 100% for PSA, 83.8% for PSMA, 91.9% for PAP, 93.7% for P501s, 88.3% for NKX 3.1, and 66.7% for AMACR. However, the urothelial markers CK34βE12, p63, thrombomodulin, S100P, and GATA3 were also positive in 1.8%, 0%, 0%, 3.6%, and 0% of PAC, respectively. The sensitivities of urothelial markers in UC were 75.4% for CK34βE12, 73.9% for p63, 45.7% for thrombomodulin, 22.5% for S100P, and 84.8% for GATA3. Conversely, the prostatic markers PSA, PSMA, PAP, P501s, NKX3.1, and AMACR were also positive in 9.4%, 0.7%, 18.8%, 0.7%, 0%, and 8.7% of UCs, respectively. **Conclusions:** Prostatic and urothelial markers, including PSA, NKX3.1, p63, thrombomodulin, and GATA3 are very useful for differentiating PAC from UC. The optimal combination of prostatic and urothelial markers could improve the ability to differentiate PAC from UC pathologically.

**Key Words:** Prostatic adenocarcinoma; Urinary bladder; Immunohistochemistry; Pathologic diagnosis; Urothelial carcinoma

Prostate involvement by urothelial carcinoma (UC) can occur from direct invasion of an infiltrating UC into the prostate stroma and from intraductal extension of the UC with or without subsequent stromal invasion of the prostate.[1] The involvement of the urinary bladder by prostate adenocarcinoma (PAC) as a metastasis or by direct extension occurs in 12% of all secondary bladder tumors[1] and is the second most common origin of this bladder cancer.[2] A common diagnostic problem in this circumstance is to differentiate between high-grade UC and high-grade PAC. Distinguishing between these two entities is crucial because the treatment for PAC is very different from that of infiltrating UC. Advanced UC is generally managed with chemotherapy, whereas advanced PAC is often managed with anti-androgen hormone therapy.

In the absence of a papillary UC or noninvasive flat component, distinguishing high-grade PAC involving the bladder from infiltrating UC on routine hematoxylin and eosin stain can be challenging.[3] Even in cases in which a known history of PAC is available, superimposed histologic changes, such as squamous metaplasia caused by prior radiation or hormonal therapy or poor differentiation, lead to difficulty in differentiating a primary UC from a recurrent PAC on a needle biopsy or transurethral resection of prostate.[2] Given the equivocal histologic features and significant differences in treatment modality and prognosis, immunohistochemistry is necessary whenever the differential diagnosis cannot be made with complete certainty based on histologic features only.

Prostate-specific antigen (PSA) and prostate acid phosphatase (PAP) have been known to assist in verifying the prostatic lineage in cases of metastatic carcinoma of unknown origin.[4] However, in poorly differentiated carcinomas, the sensitivities of PSA and PAP decrease.[3] Newer prostatic markers, such as prostein (P501s), prostate-specific membrane antigen (PSMA), proPSA, and NKX3.1, may provide added utility.[3] Urothelial markers, such

pISSN 2383-7837
eISSN 2383-7845

as CK34βE12, p63, thrombomoculin, S100P, and GATA binding protein 3 (GATA3), have been reported to be useful in identifying tumors of urothelial origin. However, thrombomodulin is only moderately sensitive compared with CK34βE12 and p63 in identifying UC.[2,3] Cytokeratin 7 and cytokeratin 20 are of limited utility in the differential diagnosis of these tumors because they may both be positive in a subset of PAC and UC.[5-7]

In the present study, we analyzed and evaluated the diagnostic utility of prostatic and urothelial immunohistochemical markers in PAC and UC with variable differentiation.

## MATERIALS AND METHODS

### Patients and materials

We performed a retrospective analysis of a prospectively maintained database of patients approved by the Institutional Review Board of Seoul St. Mary's Hospital, the Catholic University of Korea (KC13SISI0909). We enrolled a total of 111 patients with PAC and 138 patients with UC who were treated at Seoul St. Mary's Hospital between June 1995 and July 2009.

Cases of PAC were divided according to low (Gleason score < 7) and high grade (Gleason score ≥7). Of the 111 PACs from radical prostatectomy specimens, 64 cases (57.6%) were low grade and 47 (42.3%) were high grade. Cases of UC, whether noninvasive papillary or infiltrating, were divided into low and high grade according to the World Health Organization classification. Of the 138 UCs from cystectomy or tranurethral resection of bladder specimens, 28 cases (20.3%) were noninvasive papillary low grade, and 110 (79.7%) were noninvasive papillary or infiltrating cases with high-grade morphology. The male: female ratio was 7:1. None of the patients received neoadjuvant chemotherapy, hormone, or radiation therapy.

### Immunohistochemistry

We analyzed and evaluated the immunoprofile of urothelial and prostatic markers using tissue microarrays (TMAs). Needle punches (0.5-mm diameter) of paraffin-embedded tissue blocks were transferred and arrayed in the recipient block. Tissue punches yielding equivocal results were excluded from data analysis. Only interpretable positive or negative staining was accepted as a positive or negative result. Five-micrometer sections from the TMA blocks were prepared for immunohistochemical staining. All tissues were fixed in neutral buffered formalin, paraffin embedded, and processed in a standard tissue processor.

The immunohistochemical stains were performed on an automated immunostainer (LV-1 Autostainer, Lab Vision, Fremont, CA, USA) using the standard avidin-biotin peroxidase method after antigen retrieval according to the manufacturer's instructions. The immunohistochemical stains for this study included PSA, PSMA, PAP, P501s, NKX3.1, α-methylacyl coenzyme A racemase (AMACR), CK34βE12, p63, thrombomodulin, S100P, and GATA3. Primary antibodies used in this study were as follows: PSA (polyclonal, Dako, Carpinteria, CA, USA), PSMA (monoclonal, Novocastra Lab, Ltd., Newcastle upon Tyne, UK), PAP (monoclonal, Dako), P501s (monoclonal, Dako), NKX3.1 (monoclonal, Athena ES, Baltimore, MD, USA), AMACR (monoclonal, Cell Marque, Rocklin, CA, USA), CK34βE12 (monoclonal, Dako), p63 (monoclonal, Lab Vision), thrombomodulin (monoclonal, Dako), S100P (monoclonal, Dako), and GATA3 (monoclonal, prediluted, Cell Marque). Detailed information about the antibodies used in this study is included in Table 1. The staining patterns for PSA, PSMA, AMACR, and thrombomodulin were cytoplasmic. The P501s staining was in a perinuclear cytoplasmic location and had a speckled pattern. CK34βE12 showed membranous and/or cytoplasmic staining. Only nuclear stains with or without cytoplasmic staining were accepted as positive results for the p63, NKX3.1, S100P, and GATA3 stains. All immunohistochemical staining reactions were reviewed by experienced genitourinary pathologists. The patterns of all immunostaining markers in this study were diffuse and homogeneous. The immunohistochemical staining results were recorded as positive stains when ≥10% of cells showed positive reaction regardless of the intensity of the staining. SPSS ver. 16.0 (SPSS Inc., Chicago, IL, USA) was used for statistic analysis. We used chi-square tests to analyse the reactivity of all antibody panels. p-values ≤.05 were considered statistically significant.

**Table 1.** Antibodies used in immunohistochemical staining

| Antibody | Clone | Dilution | Vendor |
|---|---|---|---|
| PSA | Polyclonal | 1:1,000 | Dako |
| PSMA | Monoclonal | 1:100 | Novocastra |
| PAP | Monoclonal | Prediluted | Dako |
| P501s | Monoclonal | 1:200 | Dako |
| NKX3.1 | Monoclonal | 1:500 | Athena ES |
| AMACR | Monoclonal | 1:200 | Cell Marque |
| CK34βE12 | Monoclonal | 1:50 | Dako |
| p63 | Monoclonal | 1:800 | Lab Vision |
| TM | Monoclonal | 1:1,000 | Dako |
| S100P | Monoclonal | 1:800 | Dako |
| GATA3 | Monoclonal | Prediluted | Cell Marque |

PSA, prostate-specific antigen; PSMA, prostate-specific membrane antigen; PAP, prostate acid phosphatase; AMACR, α-methylacyl coenzyme A racemase; TM, thrombomodulin; GATA3, GATA binding protein 3.


http://dx.doi.org/10.4132/jptm.2016.06.14

## RESULTS

The results for PSA, PSMA, PAP, P501s, NKX3.1, AMACR, CK34βE12, p63, thrombomodulin, S100P, and GATA3 were summarized (Table 2).

### Prostatic markers in the PAC group

The sensitivities of prostatic markers in PAC were as follows: PSA (100%), PSMA (83.8%), PAP (91.9%), P501s (93.7%), NKX3.1 (88.3%), and AMACR (66.7%). The specificities of prostatic markers in PAC were as follows: PSA (90.6%), PSMA (99.3%), PAP (81.2%), P501s (99.3%), NKX3.1 (100%), and AMACR (91.3%). The positive predictive values (PPVs) of prostatic markers in PAC were as follows: PSA (89.5%), PSMA (98.9%), PAP (79.7%), P501s (99.1%), NKX3.1 (100%), and AMACR (86.1%). The negative predictive values (NPVs) of prostatic markers in PAC were as follows: PSA (100%), PSMA (88.4%), PAP (92.6%), P501s (95.1%), NKX3.1 (91.4%), and AMACR (77.3%) (Fig. 1).

### Urothelial markers in the PAC group

Only a small number of PAC was positive for urothelial markers. CK34βE12, p63, thrombomodulin, S100P, and GATA3 immunostains were positive in 1.8%, 0%, 0%, 3.6%, and 0% of PAC, respectively. The specificities of urothelial markers in PAC were as follows: CK34βE12 (24.6%), p63 (26.1%), thrombomodulin (54.3%), S100P (77.5%), and GATA3 (15.2%). The PPVs of urothelial markers in PAC were as follows: CK34βE12 (1.9%), p63 (0%), thrombomodulin (0%), S100P (11.4%), and GATA3 (0%). The NPVs of urothelial markers in PAC were as follows: CK34βE12 (23.8%), p63 (24.5%), thrombomodulin (40.3%), S100P (50.0%), and GATA3 (15.9%) (Fig. 1).

### Urothelial markers in the UC group

The sensitivities of urothelial markers in the UC group were as follows: CK34βE12 (75.4%), p63 (73.9%), thrombomodulin (45.7%), S100P (22.5%), and GATA3 (84.8%). The specificities of urothelial markers in UC were as follows: CK34βE12 (98.2%), p63 (100%), thrombomodulin (100%), S100P (96.4%), and GATA3 (100%). The PPVs of urothelial markers in UC were as follows: CK34βE12 (98.1%), p63 (100%), thrombomodulin (100%), S100P (88.6%), and GATA3 (100%). The NPVs of urothelial markers in UC were as follows: CK34βE12 (76.2%), p63 (75.5%), thrombomodulin (59.7%), S100P (50.0%), and GATA3 (84.1%) (Figs. 2, 3).

**Table 2.** Comparison of immunohistochemical results for PAC and UC including low- and high-grade tumors

| Variable | PSA | PSMA | PAP | P501s | NKX3.1 | AMACR | CK34βE12 | p63 | TM | S100P | GATA3 |
|---|---|---|---|---|---|---|---|---|---|---|---|
| PAC | | | | | | | | | | | |
| Sensitivity | 111/111 (100) | 93/111 (83.8) | 102/111 (91.9) | 104/111 (93.7) | 98/111 (88.3) | 74/111 (66.7) | 2/111 (1.8) | 0/111 (0) | 0/111 (0) | 4/111 (3.6) | 0/111 (0) |
| Specificity | 125/138 (90.6) | 137/138 (99.3) | 112/138 (81.2) | 137/138 (99.3) | 138/138 (100) | 126/138 (91.3) | 34/138 (24.6) | 36/138 (26.1) | 75/138 (54.3) | 107/138 (77.5) | 21/138 (15.2) |
| PPV | 111/124 (89.5) | 93/94 (98.9) | 102/128 (79.7) | 104/105 (99.1) | 98/98 (100) | 74/86 (86.1) | 2/106 (1.9) | 0/102 (0) | 0/63 (0) | 4/35 (11.4) | 0/117 (0) |
| NPV | 125/125 (100) | 137/155 (88.4) | 112/121 (92.6) | 137/144 (95.1) | 138/151 (91.4) | 126/163 (77.3) | 34/143 (23.8) | 36/147 (24.5) | 75/186 (40.3) | 107/214 (50) | 21/132 (15.9) |
| UC | | | | | | | | | | | |
| Sensitivity | 13/138 (9.4) | 1/138 (0.7) | 26/138 (18.8) | 1/138 (0.7) | 0/138 (0) | 12/138 (8.7) | 104/138 (75.4) | 102/138 (73.9) | 63/138 (45.7) | 31/138 (22.5) | 117/138 (84.8) |
| Specificity | 0/111 (0) | 18/111 (16.2) | 9/111 (8.1) | 7/111 (6.3) | 13/111 (11.7) | 37/111 (33.3) | 109/111 (98.2) | 111/111 (100) | 111/111 (100) | 107/111 (96.4) | 111/111 (100) |
| PPV | 13/124 (10.5) | 1/94 (1.1) | 26/128 (20.3) | 1/105 (0.9) | 0/87 (0) | 12/86 (13.9) | 104/106 (98.1) | 102/102 (100) | 63/63 (100) | 31/35 (88.6) | 117/117 (100) |
| NPV | 0/25 (0) | 18/155 (11.6) | 9/21 (42.9) | 7/144 (4.9) | 13/151 (8.6) | 37/163 (22.7) | 109/143 (76.2) | 111/147 (75.5) | 111/186 (59.7) | 107/214 (50) | 106/127 (84.1) |

Values are presented as number (%).
PAC, prostatic adenocarcinoma; UC, urothelial carcinoma; PSA, prostate-specific antigen; PSMA, prostate-specific membrane antigen; PAP, prostate acid phosphatase; AMACR, α-methylacyl coenzyme A racemase; TM, thrombomodulin; GATA3, GATA binding protein 3; PPV, positive predictive value; NPV, negative predictive value.

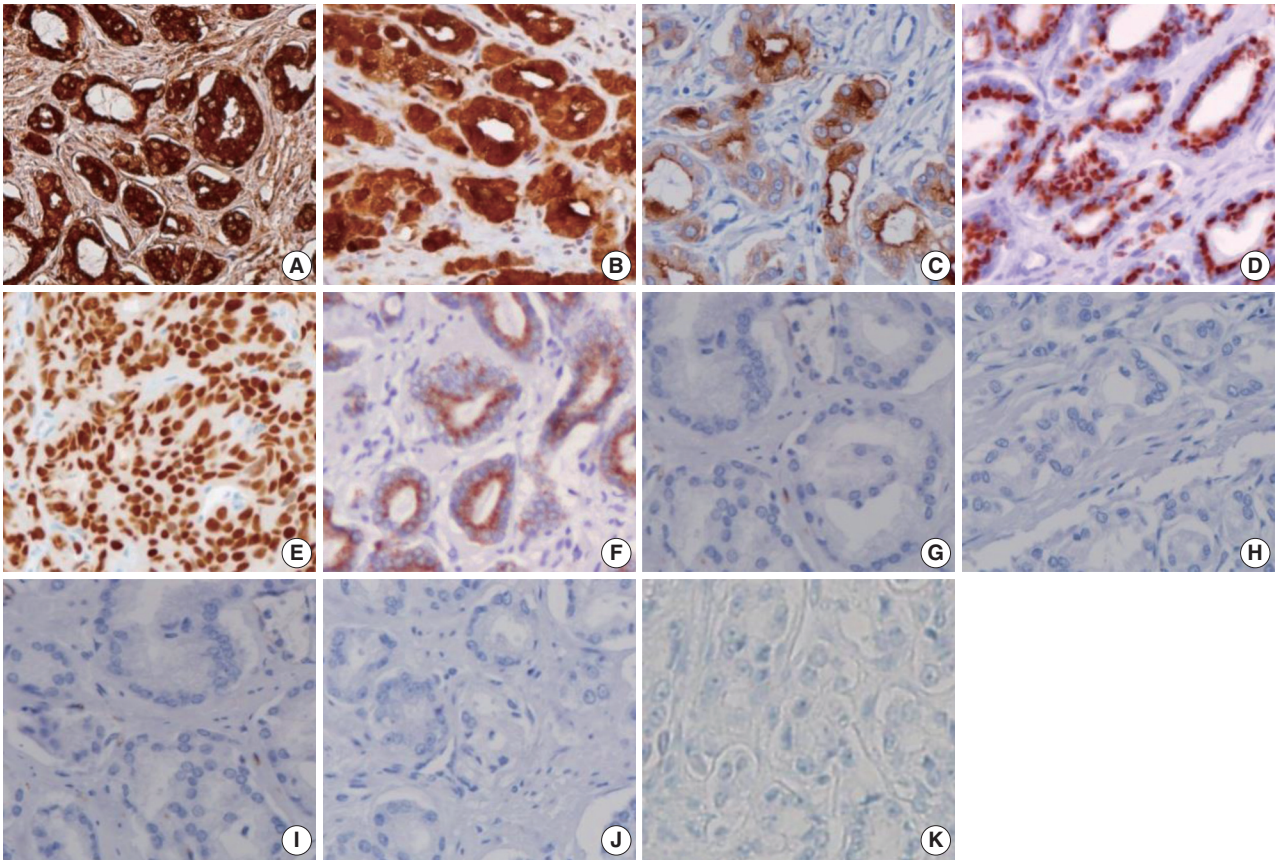


**Fig. 1.** Representative panel of immunohistochemical markers in most cases of prostate adenocarcinoma. Positive immunoreactivity for prostate-specific antigen (A), prostate-specific membrane antigen (B), prostate acid phosphatase (C), P501s (D), NKX3.1 (E), and α-methylacyl coenzyme A racemase (F). Negative immunoreactivity for CK34βE12 (G), p63 (H), thrombomodulin (I), S100P (J), and GATA binding protein 3 (K).

### Prostatic markers in the UC group

The prostatic markers PSA, PSMA, PAP, P501s, NKX3.1, and AMACR were also positive in 9.4%, 0.7%, 18.8%, 0.7%, 0%, and 8.7% of UC, respectively. The specificities of prostatic markers in UC were as follows: PSA (0%), PSMA (16.2%), PAP (8.1%), P501s (6.3%), and NKX3.1 (11.7%), and AMACR (33.3%). The PPVs of prostatic markers in the UC group were as follows: PSA (10.5%), PSMA (1.1%), PAP (20.3%), P501s (0.9%), NKX3.1 (0%), and AMACR (13.9%). The NPVs of prostatic markers in UC were as follows: PSA (0%), PSMA (11.6%), PAP (42.9%), P501s (4.9%), NKX3.1 (8.6%), and AMACR (22.7%) (Figs. 2, 3).

### Subanalysis of high-grade PAC and high-grade UC

We only included the patients with high-grade PAC (47 cases) and high-grade UC (110 cases) and analyzed the sensitivities and specificities of prostatic and urothelial markers. The results for high-grade PAC and high-grade UC were in the same range. No significant differences in the sensitivities and specificities were observed between the entire tumor groups and the high-grade groups (Table 3).

## DISCUSSION

Although the pathologic identification of PAC and UC using hematoxylin and eosin staining is not difficult in most cases, some cases may present a challenging diagnosis because the histologic appearance of poorly differentiated PAC can be very similar to that of high-grade UC.[3]

High-grade PAC may have enlarged nuclei and prominent nucleoli similar to UC, but little variability in the nuclear size or shape is generally observed in PAC compared with UC.[2,3] Additionally, even in high-grade PAC, there are few mitosis and pleomorphism compared with high-grade UC.[3] Although high-grade UC commonly exhibits more pronounced pleomorphism compared with PAC,[2,3] there have been cases of high-grade UC that were indistinguishable from high-grade PAC in terms of pleomorphism and cytologic atypia.[3] UC tends to grow in nests


http://dx.doi.org/10.4132/jptm.2016.06.14

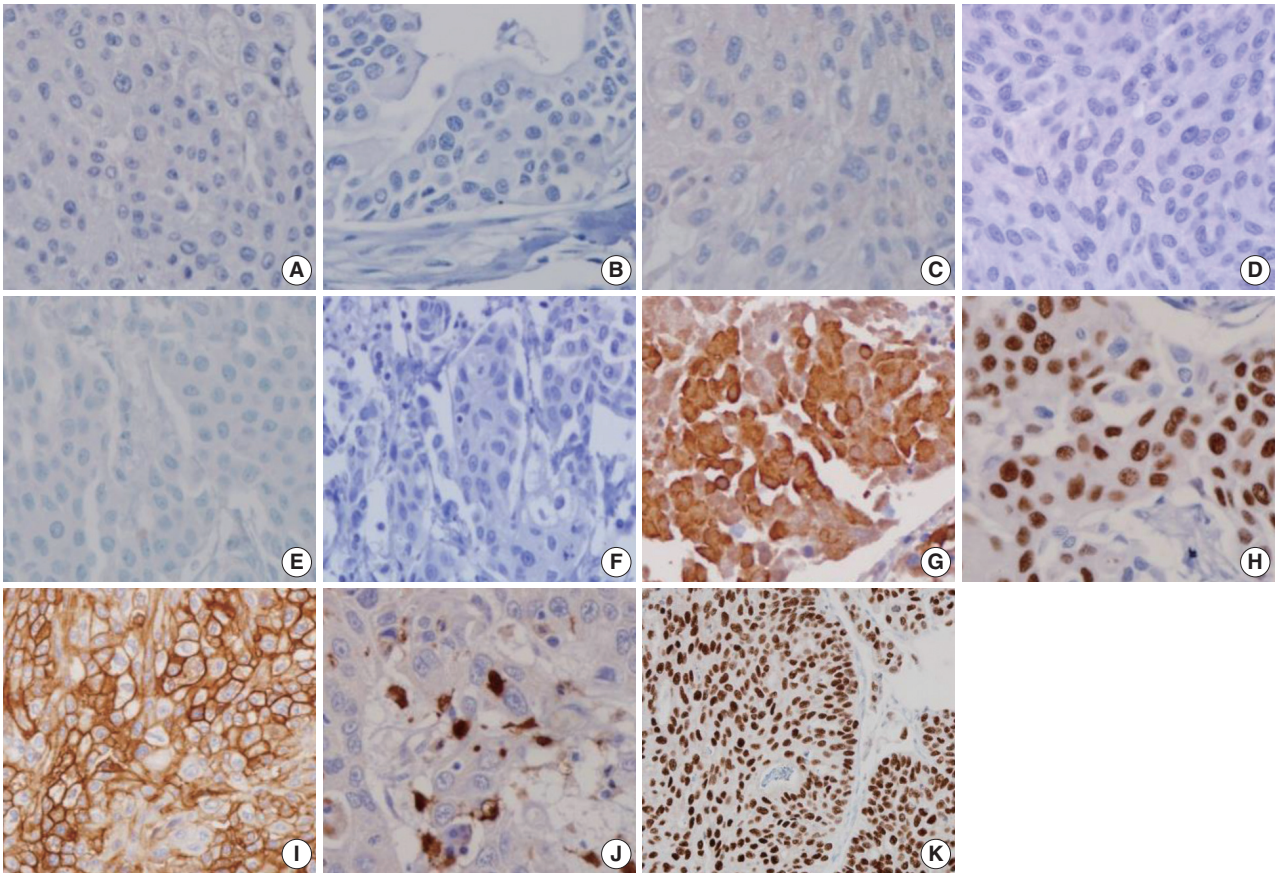


**Fig. 2.** Representative panel of immunohistochemical markers in most cases of urothelial adenocarcinoma. Negative immunoreactivity for prostate-specific antigen (A), prostate-specific membrane antigen (B), prostate acid phosphatase (C), P501s (D), NKX3.1 (E), and α-methylacyl coenzyme A racemase (F). Positive immunoreactivity for CK34βE12 (G), p63 (H), thrombomodulin (I), S100P (J), and GATA binding protein 3 (K).

and often shows conspicuous squamous differentiation and glassy eosinophilic cytoplasm. In contrast, the cytoplasm of PAC is generally pale and foamy.[3] Additionally, the findings of focal cribriform glandular differentiation or infiltrating cords of cells are more typical features of PAC than UC.[2,3] As the findings with routine hematoxylin and eosin staining may overlap, immunohistochemical staining may help solve the diagnostic dilemma.[3] Particularly, in poorly differentiated carcinomas involving both the prostate and bladder without any glandular differentiation, the pathology of the case should be evaluated immunohistochemically (Table 4).

PSA, a serine protease member of the human glandular kallikrein family, is almost exclusively synthesized in the prostate ductal and acinar epithelium, making it a highly specific marker for the prostatic lineage.[2] However, PSA has also been reported to be present in some non-prostatic tissue, such as the urethral, periurethral, and perianal glands.[4] Extraprostatic neoplasms that frequently express PSA include urethral and periurethral adenocarcinoma, cloacogenic carcinoma, salivary gland pleomorphic adenoma, salivary duct carcinoma, and rare breast carcinomas.[8] PSA has been shown to be a highly specific marker, but some authors suggest that there is an inverse correlation between the Gleason score and PSA staining intensity.[9] Previous studies have reported that high-grade PAC that was completely negative for PSA stain ranged from 3% to 27%.[3,5,6,9,10] However, in our study, no PAC specimens were devoid of PSA expression, including high-grade PAC, with 100% sensitivity. Therefore, PSA expression is very useful and valuable for clarifying the prostatic origin of tumors.

PSMA, a 750 amino acid type II membrane glycoprotein, is expressed by benign and malignant prostatic epithelial cells, with stronger staining observed in the latter.[11] Although PSMA is a very specific marker of prostatic lineage, it is also expressed in non-prostatic tissues, such as the duodenal mucosa, neuroendocrine cells of colonic crypts, endothelial cells of some neoplasms, and proximal renal tubules.[12,13] Some studies have re-

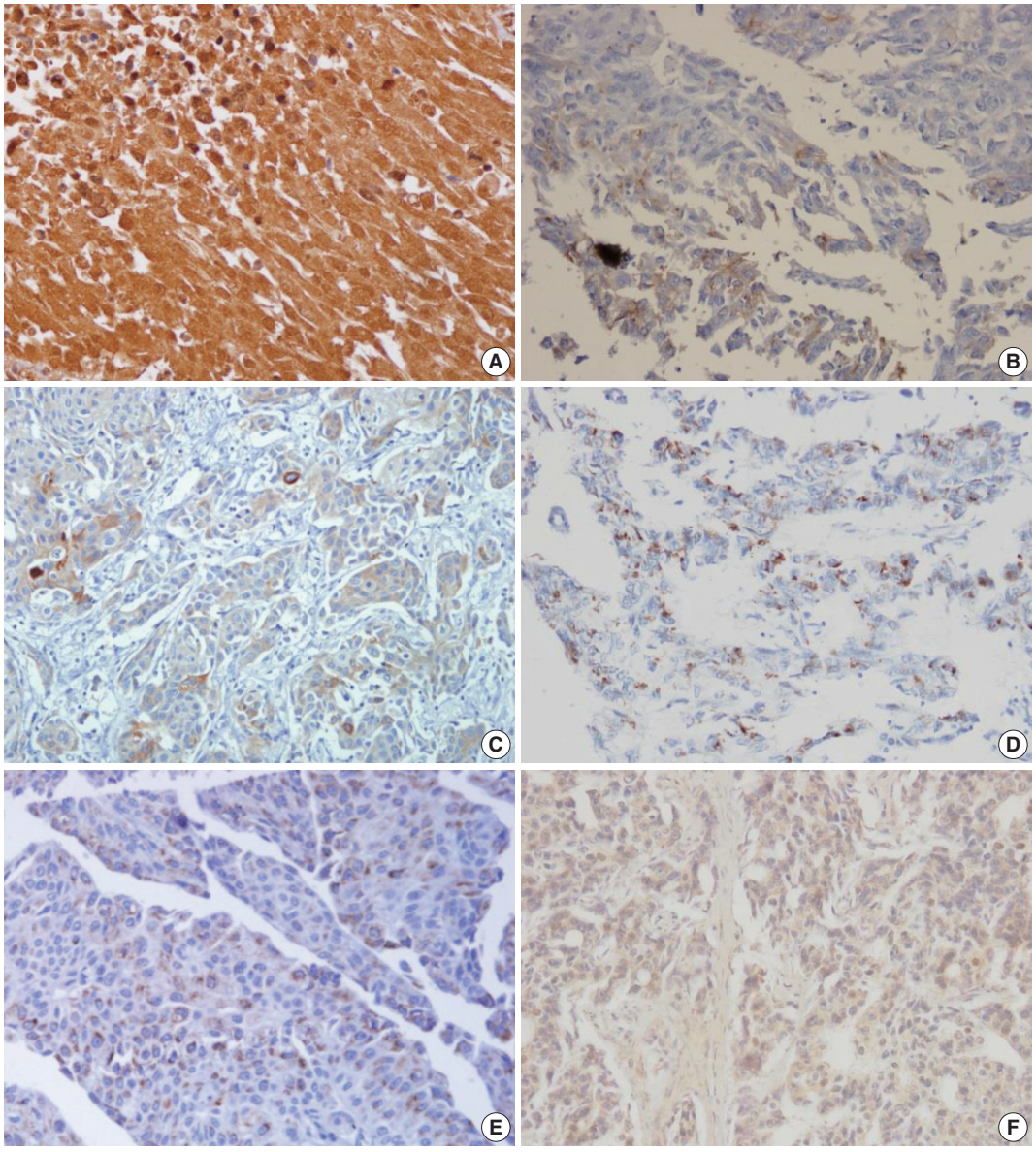


**Fig. 3.** (A) Prostate-specific antigen shows cytoplasmic staining of urothelial carcinoma. (B) Prostate-specific membrane antigen shows focal cytoplasmic staining of urothelial carcinoma. (C) Prostate acid phosphatase shows positivity in urothelial carcinoma. (D) P501S shows focal perinuclear cytoplasmic staining of urothelial carcinoma. (E) α-Methylacyl coenzyme A racemase shows weakly positive staining of urothelial carcinoma. (F) S100P shows weak nuclear staining of prostate adenocarcinoma.

ported an inverse correlation between PSMA staining and the Gleason score.[11,12] The sensitivities of PSMA for PAC ranged from 86.8% to 100% in various studies.[3,12-15] In our study, the sensitivity of PSMA in PAC (83.8%) was lower than PSA, but its specificity (99.3%) was higher than PSA. PSMA has been reported to stain 11% of urinary bladder adenocarcinomas, a fact worth noting.[16] We detected scattered patterns of positive PSMA staining in only one from 138 cases (0.7%) of UC.

PAP is an early prostatic marker used to confirm the diagnosis of PAC5,[15] and remains a specific marker for prostate tissue. Mhawech *et al*.[5] reported that 87% of high-grade PAC showed immunopositivity for PAP and observed an inverse correlation between the Gleason score and PAP staining. In this study, PAP was stained in 91.9% of PAC and showed a relative lack of specificity compared with PSMA (81.2% vs 99.3%), with a more variable staining pattern. Monoclonal antibodies to PAP have been reported to have lower sensitivities than their polyclonal counterparts but be more specific.[2] PAP staining has been known to be consistently negative in UC,[5,10,17] but a recent study reported immunopositivity in 11.1% of UC.[6] Unexpectedly, we


http://dx.doi.org/10.4132/jptm.2016.06.14

**Table 3.** Comparison of immunohistochemical results for high-grade PAC and high-grade UC

| Variable | PSA | PSMA | PAP | P501s | CK34βE12 | p63 | S100P | GATA3 |
|---|---|---|---|---|---|---|---|---|
| PAC | | | | | | | | |
| Sensitivity | 47/47 (100) | 39/47 (83) | 43/47 (91.5) | 44/47 (93.6) | 0/47 (0) | 1/47 (2.1) | 2/47 (4.3) | 0/47 (0) |
| Specificity | 95/110 (86.4) | 109/110 (99.1) | 85/110 (77.3) | 109/110 (99.1) | 23/110 (20.9) | 27/110 (24.6) | 84/110 (76.4) | 17/110 (15.5) |
| PPV | 47/62 (75.8) | 39/40 (97.5) | 43/68 (63.2) | 44/45 (98.8) | 0/87 (0) | 1/84 (1.2) | 2/28 (7.1) | 0/93 (0) |
| NPV | 95/95 (100) | 109/117 (93.2) | 85/90 (95.5) | 109/112 (97.3) | 23/70 (32.9) | 27/73 (37) | 84/129 (65.1) | 17/64 (26.6) |
| UC | | | | | | | | |
| Sensitivity | 15/110 (13.6) | 1/110 (0.9) | 25/110 (22.7) | 1/110 (0.9) | 87/110 (79.1) | 83/110 (75.5) | 26/110 (23.6) | 93/110 (84.5) |
| Specificity | 0/47 (0) | 8/47 (17.0) | 4/47 (8.5) | 3/47 (6.4) | 47/47 (100) | 46/47 (97.9) | 45/47 (95.7) | 47/47 (100) |
| PPV | 15/62 (24.2) | 1/40 (2.5) | 25/68 (36.8) | 1/45 (2.2) | 87/87 (100) | 83/84 (98.8) | 26/28 (92.9) | 93/93 (100) |
| NPV | 0/95 (0) | 8/117 (6.8) | 4/89 (4.5) | 3/112 (2.7) | 47/70 (67.1) | 46/73 (63) | 45/129 (34.9) | 46/63 (74.6) |

Values are presented as number (%).
PAC, prostatic adenocarcinoma; UC, urothelial carcinoma; PSA, prostate-specific antigen; PSMA, prostate-specific membrane antigen; PAP, prostate acid phosphatase; GATA3, GATA binding protein 3; PPV, positive predictive value; NPV, negative predictive value.

also detected PAP staining with a scattered pattern in 26 of 138 cases of UC (18.8%).

P501s, a 553-amino acid protein located in the Golgi complex, is a newer prostate-specific protein identified by a combination of high-throughput microarray screening with cDNA subtraction.[18] P501s is expressed by benign and malignant prostatic epithelium and has not been detected in the urothelium or non-prostatic tissue.[19] P501s was reported to be expressed in 94% of a total of observed 113 PAC cases, independent of the metastatic status and Gleason score.[19] Chuang *et al*.[3] reported that P501s was expressed in all 38 high-grade PAC cases. In the current study, P501s showed high sensitivity (93.7%) and specificity (99.3%) for PAC, and only one of 138 cases of UC (0.7%) was positive for that marker. To date, P501s expression has not been shown in tumors except PAC, making it of great utility in differentiating poorly differentiated PAC from high-grade UC.[3,16]

NKX3.1, a prostate specific androgen regulated homeobox gene,[20] is expressed in the prostatic epithelium, rare ureteral and urothelial cells, normal testis, lobular carcinoma of the breast, and bronchial mucous glands.[21,22] Gelmann *et al*.[22] reported that all 40 observed cases of UC were negative for NKX3.1. In the current study, none of the 138 cases of UC was positive for NKX3.1. The sensitivities of NKX3.1 for PAC reported in previous studies were 92.1%, 89.5%, 87.4%, and 69.2%.[3,21-23] This study also showed a comparable result, with 88.3% sensitivity of NKX3.1 for PAC.

The AMACR, localized predominantly in peroxisomal structures, plays a critical role in peroxisomal beta oxidation of branched chain fatty acid. Jiang *et al*.[24] demonstrated that both PAC and high-grade prostate intraepithelial neoplasia (HG-PIN) consistently revealed a significantly higher expression than normal epithelium. However, AMACR expression has repeatedly been demonstrated in HG-PIN and some benign mimickers of PAC. Moreover, Kunju *et al*.[6] reported that AMACR is expressed in 36% of UC cases. In our study, AMACR was expressed in 66.7% of 111 cases of PAC and 8.7% of 138 cases of UC. AMACR is less sensitive than other prostate markers for PAC and is of limited utility in resolving the difficult problems involving both the prostate and urinary bladder.

Although PSA, PSMA, PAP, P501s, and NKX3.1 are sensitive and specific markers for evaluating the prostatic origin of tumors, lack of staining was also detected for most markers, except PSA, in this study, at 16.2% for PSMA, 8.1% for PAP, 6.3% for P501s, and 11.7% for NKX3.1 of 111 PAC cases. Therefore, the lack of immunoreactivity of prostate markers in a poorly differentiated carcinoma does not exclude the possibility of a prostatic origin. In addition, false-positives were detected in UC in five of six established prostate markers in this study, ranging from 0.7% to 18.8%, suggesting that the immunohistochemical panel is necessary and useful to discriminate poorly differentiated high-grade carcinomas involving both the prostate and bladder.

Many immunohistochemical stains have been investigated for UC, but no single marker has been found to be unequivocally diagnostic of urothelial origin. Thus, investigators have recommended a panel of markers to demonstrate the urothelial origin of tumor, such as CK34βE12, p63, thrombomodulin, S100P, and GATA3.

The monoclonal antibody CK34βE12, which reactive specifically against high-molecular-weight cytokeratins (CKs), including CK1, CK5, CK14, and CK20,[2] is an extremely sensitive marker of urothelial lineage. It is reported to match the sensitivity of p63 and surpass that of uroplakin III and thrombomodulin.[3,25] Compared with previous studies showing sensitivities of 97.2%, 91.4%, and 65.2% for CK34βE12 in UC,[3,6,10] our study found 75.4% sensitivity in UC. It is worth noting that CK34βE12 can label squamous epithelia, including areas

**Table 4.** Reported sensitivities of immunohistochemical markers for PAC and UC

| Immunohistochemical marker | Current study (2016) | | Chuang *et al.* (2007)[3] | | Kunju *et al.* (2006)[6] | | Mhawech *et al.* (2002)[5] | | Genega *et al.* (2000)[10] | |
|---|---|---|---|---|---|---|---|---|---|---|
| | PAC | UC | PAC | UC | PAC | UC | PAC | UC | PAC | UC |
| PSA | 111/111 (100) | 16/138 (11.6) | 37/38 (97.4) | 0/35 (0) | 40/42 (95.2) | 0/36 (0) | 34/40 (85.0) | 0/45 (0) | 32/34 (94.1) | 0/46 (0) |
| PSMA | 93/111 (83.8) | 1/138 (0.7) | 35/38 (92.1) | 0/35 (0) | - | - | - | - | - | - |
| PAP | 102/111 (91.9) | 26/138 (18.8) | - | - | 40/42 (95.2) | 4/36 (11.1) | 38/40 (95.0) | 0/45 (0) | 32/34 (94.1) | 0/46 (0) |
| P501s | 104/111 (93.7) | 1/138 (0.7) | 38/38 (100) | 2/35 (5.7) | - | - | - | - | - | - |
| NKX3.1 | 98/111 (88.3) | 2/138 (1.4) | 36/38 (94.7) | 0/35 (0) | - | - | - | | - | - |
| AMACR | 74/111 (66.7) | 12/138 (8.7) | - | - | 37/42 (88.1) | 13/36 (36.1) | - | - | - | - |
| CK34βE12 | 2/111 (1.8) | 104/138 (75.4) | 3/38 (7.9) | 32/35 (91.4) | 1/42 (2.4) | 35/36 (97.2) | - | - | 2/34 (5.9) | 30/46 (65.2) |
| p63 | 0/111 (0) | 102/138 (73.9) | 0/38 (0) | 29/35 (82.9) | 0/42 (0) | 33/36 (91.7) | - | - | - | - |
| TM | 0/111 (0) | 63/138 (45.7) | 2/38 (5.3) | 24/35 (68.6) | - | - | 0/40 (0) | 22/45 (48.8) | - | - |
| S100P | 4/111 (3.6) | 31/138 (22.5) | 3/38 (7.9) | 25/35 (71.4) | - | - | - | - | - | - |
| GATA3 | 0/111 (0) | 117/138 (95.9) | - | - | - | - | - | - | - | - |
| CK7 | - | - | - | - | 4/42 (9.5) | 34/36 (94.4) | 11/40 (27.5) | 39/45 (86.6) | 4/34 (11.8) | 38/46 (82.6) |
| CK20 | - | - | - | - | 2/42 (4.8) | 19/36 (52.8) | 4/40 (10.0) | 30/45 (66.6) | 8/34 (23.5) | 10/46 (21.7) |
| Uroplakin III | - | - | - | - | - | - | 0/40 (0) | 27/45 (60) | - | - |

Values are presented as number (%).
PAC, prostatic adenocarcinoma; UC, urothelial carcinoma; PSA, prostate-specific antigen; PSMA, prostate-specific membrane antigen; PAP, prostate acid phosphatase; AMACR, α-methylacyl coenzyme A racemase; TM, thrombomodulin; GATA3, GATA binding protein 3; CK, cytokeratin.

of squamous differentiation in recurrent PAC after therapy. Thus, Parwani *et al.*[26] argued that immunopositivity for CK34βE12 restricted to areas of squamous differentiation does not exclude the possibility of PAC.

p63, a homologue of the p53 tumor suppressor gene, encodes at least six different proteins with a wide range of biologic functions, including a role in urothelial differentiation.[2] Immunostaining for p63 is typically present in more than 90% of the nuclei of the normal urothelia.[2] Many UCs retain a pattern of p63 expression, but p63 expression may be partially lost in high-grade UC.[3,27] Although p63 sensitivity for UC in our study (73.9%) was lower than that of previous studies (82.9%–91.7%),[3,6] its specificity was 100% for UC.

Thrombomodulin, also designated CD141, is an endothelial cell associated cofactor for the thrombin-mediated activator of protein C.[2] Previous studies have shown that thrombomodulin was immunostained in 48.8%–68.6% of UC,[3,5] but our study found a slightly lower expression at 45.7%.

S100P is highly expressed in the urothelial epithelium.[28] Higgins *et al.*[28] reported that the polyclonal antibody against S100P labeled 85% of UC and 3% of PAC, whereas the monoclonal antibody against S100P detected 77% of UC and 2% of PAC. Chuang *et al.*[3] also reported that the monoclonal S100P detected 51.4% of UC and 7.9% of PAC. In our study with a monoclonal antibody against S100P, 22.5% of UC and 3.6% of PAC were stained, which was less than in previous studies.[3,28]

Although CK34βE12 and p63 have been reported to intermittently label PAC in a non-basal cell distribution, thrombomodulin has not been reported to show cross reactivity.[5,6,10] We found that CK34βE12 and p63 immunostains were superior to thrombomodulin or S100P as differential markers of urothelial origin. Only a few scattered cells of PAC were labeled with CK34βE12 (1.8%) and S100P (3.6%), but no PAC was immunopositive for thrombomodulin or p63 in our study.

GATA3 is a member of a zinc finger transcription factor family that plays an important role in promoting and directing cell proliferation, differentiation, and development.[2] GATA3 is a very sensitive marker for UC, and it is also highly specific in excluding high-grade PAC.[29] Chang *et al.*[29] reported that none of the 38 high-grade PACs was positive for GATA3. In this study, the sensitivity of GATA3 was 0% in PAC and 84.8% in UC. Uroplakin III is considered the most specific marker for urothelial differentiation, but it has not received popularity due to the lack of uniform expression in UCs.[29] Our study has some limitations because we did not include studies of Uroplakin III.

In conclusion, prostatic markers, including PSA, PSMA, PAP,


http://dx.doi.org/10.4132/jptm.2016.06.14

and P501s, are very useful for distinguishing PAC from UC. Urothelial markers are less sensitive in identifying UC but rarely stain PAC. In the current study, we found that PSA is most sensitive prostatic marker for distinguishing PAC from UC cases with high sensitivity and negative predictive value. In addition, NKX3.1 is the most specific prostatic marker for distinguishing PAC from UC cases with high specificity and positive predictive value. p63 and thrombomodulin are the most specific urothelial markers for distinguishing UC from PAC cases with high specificities. GATA3 was positive in 117 of 137 cases of UCs and none of the 111 PACs was positive for GATA3. We found that the best combination of immunohistochemical markers for distinguishing PAC from UC is panels consisting of PSA, NKX3.1, p63, thrombomodulin, and GATA3. The optimal combination of immunohistochemical panels of prostatic and urothelial markers could improve the ability to establish the pathologic diagnosis of poorly differentiated high-grade carcinomas involving either the prostate or urinary bladder.

## Conflicts of Interest

No potential conflict of interest relevant to this article was reported.

## REFERENCES


1. Bates AW, Baithun SI. Secondary neoplasms of the bladder are histological mimics of nontransitional cell primary tumours: clinicopathological and histological features of 282 cases. Histopathology 2000; 36: 32-40.
2. Dabbs DJ. Diagnostic imunohistochemistry. 3rd ed. Philadelphia: Saunders-Elsevier, 2010; 621-5.
3. Chuang AY, DeMarzo AM, Veltri RW, Sharma RB, Bieberich CJ, Epstein JI. Immunohistochemical differentiation of high-grade prostate carcinoma from urothelial carcinoma. Am J Surg Pathol 2007; 31: 1246-55.
4. Varma M, Jasani B. Diagnostic utility of immunohistochemistry in morphologically difficult prostate cancer: review of current literature. Histopathology 2005; 47: 1-16.
5. Mhawech P, Uchida T, Pelte MF. Immunohistochemical profile of high-grade urothelial bladder carcinoma and prostate adenocarcinoma. Hum Pathol 2002; 33: 1136-40.
6. Kunju LP, Mehra R, Snyder M, Shah RB. Prostate-specific antigen, high-molecular-weight cytokeratin (clone 34betaE12), and/or p63: an optimal immunohistochemical panel to distinguish poorly differentiated prostate adenocarcinoma from urothelial carcinoma. Am J Clin Pathol 2006; 125: 675-81.
7. Chibber PJ, McIntyre MA, Hindmarsh JR, Hargreave TB, Newsam JE, Chisholm GD. Transitional cell carcinoma involving the prostate. Br J Urol 1981; 53: 605-9.
8. Kamoshida S, Tsutsumi Y. Extraprostatic localization of prostatic acid phosphatase and prostate-specific antigen: distribution in cloacogenic glandular epithelium and sex-dependent expression in human anal gland. Hum Pathol 1990; 21: 1108-11.
9. Goldstein NS. Immunophenotypic characterization of 225 prostate adenocarcinomas with intermediate or high Gleason scores. Am J Clin Pathol 2002; 117: 471-7.
10. Genega EM, Hutchinson B, Reuter VE, Gaudin PB. Immunophenotype of high-grade prostatic adenocarcinoma and urothelial carcinoma. Mod Pathol 2000; 13: 1186-91.
11. Marchal C, Redondo M, Padilla M, *et al*. Expression of prostate specific membrane antigen (PSMA) in prostatic adenocarcinoma and prostatic intraepithelial neoplasia. Histol Histopathol 2004; 19: 715-8.
12. Bostwick DG, Pacelli A, Blute M, Roche P, Murphy GP. Prostate specific membrane antigen expression in prostatic intraepithelial neoplasia and adenocarcinoma: a study of 184 cases. Cancer 1998; 82: 2256-61.
13. Silver DA, Pellicer I, Fair WR, Heston WD, Cordon-Cardo C. Prostate-specific membrane antigen expression in normal and malignant human tissues. Clin Cancer Res 1997; 3: 81-5.
14. Chang SS, Reuter VE, Heston WD, Gaudin PB. Comparison of anti-prostate-specific membrane antigen antibodies and other immunomarkers in metastatic prostate carcinoma. Urology 2001; 57: 1179-83.
15. Sweat SD, Pacelli A, Murphy GP, Bostwick DG. Prostate-specific membrane antigen expression is greatest in prostate adenocarcinoma and lymph node metastases. Urology 1998; 52: 637-40.
16. Lane Z, Hansel DE, Epstein JI. Immunohistochemical expression of prostatic antigens in adenocarcinoma and villous adenoma of the urinary bladder. Am J Surg Pathol 2008; 32: 1322-6.
17. Bassily NH, Vallorosi CJ, Akdas G, Montie JE, Rubin MA. Coordinate expression of cytokeratins 7 and 20 in prostate adenocarcinoma and bladder urothelial carcinoma. Am J Clin Pathol 2000; 113: 383-8.
18. Xu J, Kalos M, Stolk JA, *et al*. Identification and characterization of prostein, a novel prostate-specific protein. Cancer Res 2001; 61: 1563-8.
19. Kalos M, Askaa J, Hylander BL, *et al*. Prostein expression is highly restricted to normal and malignant prostate tissues. Prostate 2004; 60: 246-56.
20. He WW, Sciavolino PJ, Wing J, *et al*. A novel human prostate-spe-

cific, androgen-regulated homeobox gene (NKX3.1) that maps to 8p21, a region frequently deleted in prostate cancer. Genomics 1997; 43: 69-77.
21. Bowen C, Bubendorf L, Voeller HJ, *et al*. Loss of NKX3.1 expression in human prostate cancers correlates with tumor progression. Cancer Res 2000; 60: 6111-5.
22. Gelmann EP, Bowen C, Bubendorf L. Expression of NKX3.1 in normal and malignant tissues. Prostate 2003; 55: 111-7.
23. Aslan G, Irer B, Tuna B, Yorukoglu K, Saatcioglu F, Celebi I. Analysis of NKX3.1 expression in prostate cancer tissues and correlation with clinicopathologic features. Pathol Res Pract 2006; 202: 93-8.
24. Jiang Z, Li C, Fischer A, Dresser K, Woda BA. Using an AMACR (P504S)/34betaE12/p63 cocktail for the detection of small focal prostate carcinoma in needle biopsy specimens. Am J Clin Pathol 2005; 123: 231-6.
25. Parker DC, Folpe AL, Bell J, *et al*. Potential utility of uroplakin III, thrombomodulin, high molecular weight cytokeratin, and cytokeratin 20 in noninvasive, invasive, and metastatic urothelial (transitional cell) carcinomas. Am J Surg Pathol 2003; 27: 1-10.
26. Parwani AV, Kronz JD, Genega EM, Gaudin P, Chang S, Epstein JI. Prostate carcinoma with squamous differentiation: an analysis of 33 cases. Am J Surg Pathol 2004; 28: 651-7.
27. Comperat E, Camparo P, Haus R, *et al*. Immunohistochemical expression of p63, p53 and MIB-1 in urinary bladder carcinoma: a tissue microarray study of 158 cases. Virchows Arch 2006; 448: 319-24.
28. Higgins JP, Kaygusuz G, Wang L, *et al*. Placental S100 (S100P) and GATA3: markers for transitional epithelium and urothelial carcinoma discovered by complementary DNA microarray. Am J Surg Pathol 2007; 31: 673-80.
29. Chang A, Amin A, Gabrielson E, *et al*. Utility of GATA3 immunohistochemistry in differentiating urothelial carcinoma from prostate adenocarcinoma and squamous cell carcinomas of the uterine cervix, anus, and lung. Am J Surg Pathol 2012; 36: 1472-6.

 http://dx.doi.org/10.4132/jptm.2016.06.14

*Journal of Pathology and Translational Medicine 2016; 50: 355-360*
*http://dx.doi.org/10.4132/jptm.2016.05.19*

■ ORIGINAL ARTICLE ■

# Difference of the Nuclear Green Light Intensity between Papillary Carcinoma Cells Showing Clear Nuclei and Non-neoplastic Follicular Epithelia in Papillary Thyroid Carcinoma

Hyekyung Lee · Tae Hwa Baek[1]
Meeja Park · Seung Yun Lee
Hyun Jin Son · Dong Wook Kang
Joo Heon Kim · Soo Young Kim[2]

Department of Pathology Eulji University Hospital, Eulji University School of Medicine, Daejeon; [1]Medical Examiner's Office, National Forensic Service, Wonju; [2]Department of Occupational Medicine, Eulji University Hospital, Eulji University School of Medicine, Daejeon, Korea

**Received:** March 11, 2016
**Revised:** May 3, 2016
**Accepted:** May 19, 2016

**Corresponding Author**
Soo Young Kim, MD
Department of Pathology, Eulji University Hospital, 95 Dunsanseo-ro, Seo-gu, Daejeon 35233, Korea
Tel: +82-42-611-3782
Fax: +82-42-611-3776
E-mail: kimsooy@eulji.ac.kr

**Background:** There is subjective disagreement regarding nuclear clearing in papillary thyroid carcinoma. In this study, using digital instruments, we were able to quantify many ambiguous pathologic features and use numeric data to express our findings. **Methods:** We examined 30 papillary thyroid carcinomas. For each case, we selected representative cancer cells showing clear nuclei and surrounding non-neoplastic follicular epithelial cells and evaluated objective values of green light intensity (GLI) for quantitative analysis of nuclear clearing in papillary thyroid carcinoma. **Results:** From 16,274 GLI values from 600 cancer cell nuclei and 13,752 GLI values from 596 non-neoplastic follicular epithelial nuclei, we found a high correlation of 94.9% between GLI and clear nuclei. GLI between the cancer group showing clear nuclei and non-neoplastic follicular epithelia was statistically significant. The overall average level of GLI in the cancer group was over two times higher than the non-neoplastic group despite a wide range of GLI. On a polygonal line graph, there was a fluctuating unique difference between both the cancer and non-neoplastic groups in each patient, which was comparable to the microscopic findings. **Conclusions:** Nuclear GLI could be a useful factor for discriminating between carcinoma cells showing clear nuclei and non-neoplastic follicular epithelia in papillary thyroid carcinoma.

**Key Words:** Image processing, computer-assisted; Light intensity; Cell nucleus; Thyroid cancer, papillary

In the diagnosis of papillary thyroid carcinoma, nuclear characteristics are important. Among the nuclear triad composed of clear nuclei, nuclear grooves and pseudoinclusions, nuclear clearing is the most subjective and most ambiguous finding.[1] Currently, with the use of digital instruments, we are able to quantify many ambiguous pathologic features and express our findings with numeric data.[2-6] Based on a previous study that described the meaningful data of nuclear green light intensity (GLI) in neuroendocrine tumors,[7] we hypothesized that the nuclear clearing of papillary thyroid carcinoma could be also expressed using GLI because both tumors share similar nuclear features with relatively homogeneous nuclei without irregular chromatin clumping. We measured the GLI of cancer cells showing clear nuclei and surrounding non-neoplastic follicular epithelial nuclei in papillary thyroid carcinoma patients and evaluated the significance of GLI as a discriminator between the two groups.

## MATERIALS AND METHODS

A total of 30 thyroidectomy specimens with papillary carcinoma were retrospectively selected from the Department of Pathology and Laboratory Medicine archives of the Eulji University Hospital. We cut formalin-fixed, paraffin-embedded tissues into 3-μm sections, and stained all sections simultaneously with hematoxylin and eosin using an automatic slide staining machine under standard conditions. We reviewed the slides on an Olympus BX51 microscope (Olympus Corp., Tokyo, Japan) with ×40 magnification of the apochromatic objective lens and a 0.85 numeric aperture. We maintained the same light source conditions throughout the analysis. Clear nuclei were determined by two pathologists (H.L. and M.P.). We captured digital images (1,360×1,024 pixels) of typical areas showing cancer cells with clear nuclei and surrounding non-neoplastic nuclei by using an Olympus DP71 digital camera (Olympus Corp.) and saved the

pISSN 2383-7837
eISSN 2383-7845

**Table 1.** The number of GLI of cancer cells and non-neoplastic cells in 30 papillary thyroid carcinoma patients

| Patient No. | No. of cancer cells | No. of GLI of cancer | No. of non-neoplastic cells | No. of GLI of non-neoplastic cells |
|---|---|---|---|---|
| 1 | 20 | 533 | 16 | 354 |
| 2 | 20 | 542 | 20 | 470 |
| 3 | 20 | 558 | 20 | 435 |
| 4 | 20 | 485 | 20 | 443 |
| 5 | 20 | 463 | 20 | 417 |
| 6 | 20 | 372 | 20 | 377 |
| 7 | 20 | 483 | 20 | 467 |
| 8 | 20 | 433 | 20 | 373 |
| 9 | 20 | 466 | 20 | 401 |
| 10 | 20 | 497 | 20 | 342 |
| 11 | 20 | 476 | 20 | 367 |
| 12 | 20 | 423 | 20 | 415 |
| 13 | 20 | 442 | 20 | 345 |
| 14 | 20 | 452 | 20 | 380 |
| 15 | 20 | 449 | 20 | 427 |
| 16 | 20 | 546 | 20 | 434 |
| 17 | 20 | 496 | 20 | 424 |
| 18 | 20 | 635 | 20 | 428 |
| 19 | 20 | 519 | 20 | 459 |
| 20 | 20 | 537 | 20 | 455 |
| 21 | 20 | 547 | 20 | 417 |
| 22 | 20 | 521 | 20 | 414 |
| 23 | 20 | 508 | 20 | 437 |
| 24 | 20 | 575 | 20 | 425 |
| 25 | 20 | 750 | 20 | 605 |
| 26 | 20 | 623 | 20 | 662 |
| 27 | 20 | 798 | 20 | 604 |
| 28 | 20 | 760 | 20 | 692 |
| 29 | 20 | 630 | 20 | 625 |
| 30 | 20 | 755 | 20 | 658 |
| Total | 600 | 16,274 | 596 | 13,752 |

GLI, green light intensity.

images in Tagged Image File Format format. We reviewed each digital image and removed any image that did not fulfill the minimum requirements (bad nuclear mask, out-of-focus image, pyknotic nucleus). For each case, we selected 20 representative cancer cells with clear nuclei and 20 surrounding non-neoplastic follicular epithelial nuclei except for case 1. For each cell, we drew line profiles using computerized image analyzer (Image Pro program Plus ver. 6.5, Media Cybertics Co., Silver Spring, MD, USA) and obtained graph files and Excel data on GLIs of consecutive pixels along the line profiles. For comparison between the two groups, statistical analysis was performed with a nonparametric Mann-Whitney U test and $p < .05$ was considered significant.

## RESULTS

A total of 600 cancer cell nuclei and 596 non-neoplastic fol-

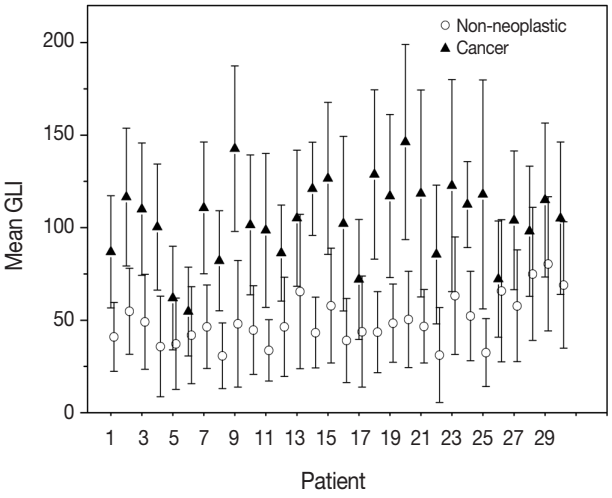


**Fig. 1.** Plot box graph of green light intensity (GLI) of cancer cells and non-neoplastic cells in 30 papillary thyroid carcinoma patients. Error bar, 5th and 95th percentiles; line, central 50th percentile; triangle for cancer, circle for non-neoplastic group, mean GLI.


http://dx.doi.org/10.4132/jptm.2016.05.19

licular epithelial nuclei were selected from 30 papillary thyroid carcinoma patients. The 16,274 GLI values from 600 cancer cell nuclei and 13,752 GLI values from 596 non-neoplastic follicular epithelial nuclei were studied (Table 1, Fig. 1). We sought to determine whether GLI could be used to identify clear nuclei of the cancer group by comparison with the non-neoplastic group. There was a high correlation of 94.9% between GLI and clear nuclei on the receiver operating characteristic (ROC) curve (Fig. 2). There was a significant increase in GLI in the cancer group (GLI median, standard deviation); with values of 51, 20 for the non-neoplastic group compared to 105, 29 for the cancer group, which was statistically significant (Fig. 3). On a polygonal line graph of an equal number of GLI from the cancer group and non-neoplastic group in each patient, there was a fluctuating difference between each patient, but there was a higher difference in the cancer group (Fig. 4). The microscopic findings of cases 9, 14, and 25 who showed more GLI difference between the two groups revealed more clear nuclei in cancer cells (Fig. 5A), whereas cases 5, 6, and 26 showed less GLI difference between the two groups with less clear nuclei in cancer cells (Fig. 5B). Each patient showed unique identifiable patterns in both the cancer and non-neoplastic groups.

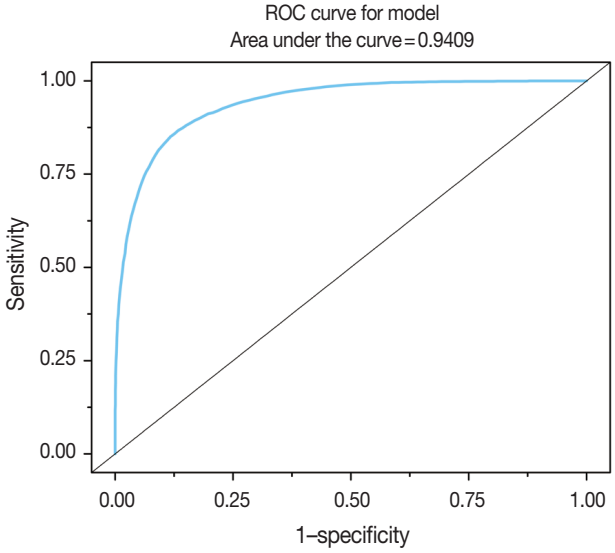


**Fig. 2.** High correlation of green light intensity with nuclear clearing in receiver operating characteristic curve (ROC).

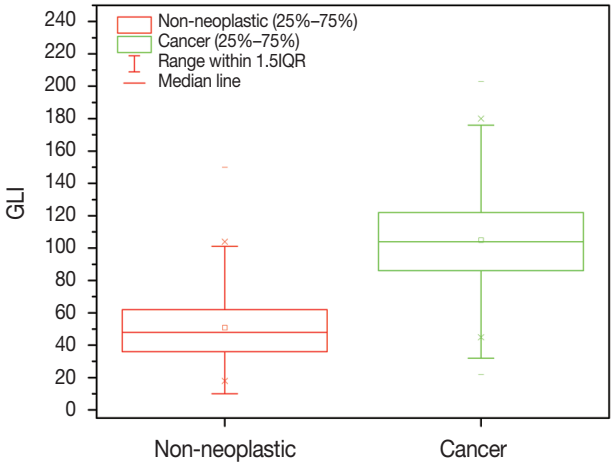


**Fig. 3.** Comparison of green light intensity (GLI) between papillary thyroid carcinoma showing clear nuclei and surrounding non-neoplastic follicular epithelial cells.

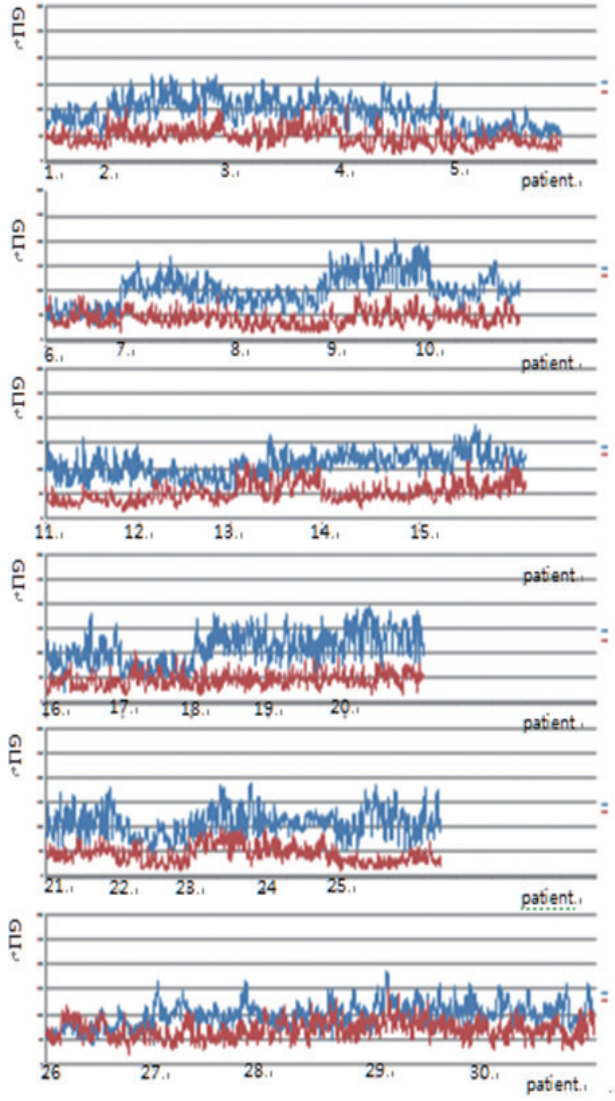


**Fig. 4.** Fluctuating difference of green light intensity (GLI) in both cancer and non-neoplastic groups between each patient on polygonal line graph (red, non-neoplastic cells; blue, cancer).

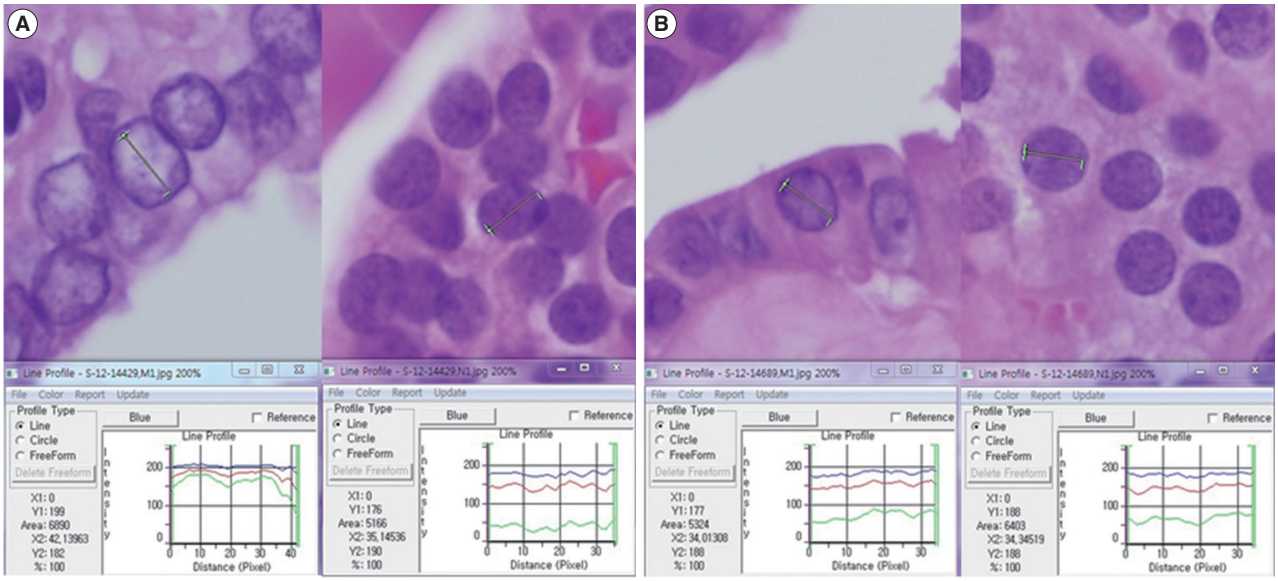


**Fig. 5.** (A) Comparison of green light intensity (GLI) of cancer cells and non-neoplastic cells in case 25, which shows a large difference (left, cancer; right, non-neoplastic cells). (B) Comparison of GLI of cancer cells and non-neoplastic cells in case 26, where there is no significant difference (left, cancer; right, non-neoplastic cells). Note the similarity in red, green, and blue light intensities of non-neoplastic follicular epithelial cells in panel A and B.

## DISCUSSION

Nuclear examination of cells is important in pathology. Several characteristic nuclear features of clinical significance have been described. Hyperchromatism is an expression of increased DNA content due to cellular proliferation and mitosis is an expression of rapid cellular division. Coffee bean-like nuclear grooves, ground glass nuclei, and nuclear pseudoinclusions are meaningful in the diagnosis for specific diseases such as papillary thyroid carcinoma. Among those nuclear features, pseudoinclusions or grooves are relatively objective findings with either presence or absence documented. However, some features such as clear nuclei, vesicular nuclei, and homogenized nuclei are relatively subjective findings and their diagnosis is subject to interobserver variability. Many pathologists have been trying to minimize interobserver variability for some time. Currently, by using a more developed digital imaging system, we are able to translate subjective and ambiguous pathologic findings into objective data. With these data, we can reduce interobserver variability and introduce a new era of data based research. Papillary thyroid carcinoma is a well-known tumor in the sense that appropriate nuclear features are essential for making the diagnosis. Among these diagnostic nuclear features, clear nuclei are relatively subjective and shows significant interobserver variability. Several questions regarding clear nuclei remain, including the following. What degree of clearance is enough for the diagnosis of clear nuclei of papillary carcinoma? Is the level of clearing the same in usual papillary thyroid carcinomas? Is there any recommended method to measure the clearing? Unfortunately, the recommended and standard method for measuring nuclear clearing is not yet known. When we considered these issues, we realized the necessity of measurable data regarding the degree and level of nuclear clearing. In addition to quantitative studies regarding nuclear morphometry characteristics such as variation in nuclear size, irregularity in nuclear contours, and chromatin texture[3-7] red, green, and blue color charts have also been used to calibrate digital graphic devices.[8,9] A recent study described red, green, and blue light intensities for nuclear chromatin pattern of neuroendocrine cells and stressed the importance of GLI.[7] We attempted to answer the above questions by quantitatively measuring objective GLI values. In the materials and methods section, we questioned whether single line profile can be used instead of different orientations (0°, 45°, 90°, and 135°). In a short preliminary study (unpublished data) we could not find big differences between those groups and in practice, it was not easy to draw a line profile of different angles because we had to avoid nuclear grooves and pseudoinclusions. In the results analysis, by comparing the GLI between the cancer group with clear nuclei and the non-neoplastic internal control group, we were able to reduce the possible errors that affect digital image analysis, namely specimen thickness, staining, and interference due to the brightness around the line profiles. Fig. 2 shows a high con-


http://dx.doi.org/10.4132/jptm.2016.05.19

cordance of 94.9% between the carcinoma groups and GLI in the ROC curve study. Fig. 3 shows the difference in GLI between the cancer group showing clear nuclei and the non-neoplastic group, which was statistically significant. Based on these results, we suggest that the presence of clear nuclei is highly correlated with GLI and that GLI could be a meaningful discriminator between cancer and non-neoplastic groups. Fig. 4 shows the fluctuating difference of GLI in both cancer and non-neoplastic groups in each case, with an even higher difference in the cancer group. The higher fluctuation in the cancer group seems to be related to the higher standard deviation described in Table 1. In cases 5, 6, and 26, the GLI difference between the cancer and non-neoplastic groups was not significant; however in cases 9, 14, and 25, the difference between the two groups was significant. These differences in GLI were easily identified by microscopic examination for clear nuclei (Fig. 5). Based on such differences in GLI compared with the microscopic findings in each case, we were able to answer the second question as follows: the level of clearing is not the same in all thyroid papillary carcinomas. When we considered that nuclear clearing can be related to nuclear microfilament localization or hypochromatism in tumor progression[10,11] with the wide range of light intensity, the nuclear clearing could be an expression of gradual tumor progression rather than a sudden onset phenomenon. The pathogenesis of a clear nucleus is not completely understood. The effects of thyroid hormone on Na/K-ATPase activity have been studied and the functions of the Na/K-ATPase of the nuclear envelope in ion transport and chromatin modulation have been described.[12-15] Therefore, the characteristic nuclear triad of papillary thyroid carcinoma, which consists of nuclear grooves, pseudoinclusions, and clearing, can be secondary findings due to an abnormal Na/K-ATPase affected by abnormal thyroid hormone in papillary thyroid carcinoma. Because of the wide range of GLI, we could not generate a diagnostically helpful cut-off value or function for the discrimination between the cancer group showing clear nuclei and non-neoplastic group. However, with over 30,000 GLI data points, we believe that an average level of GLI at least two times higher in the cancer group (104.9) than the non-neoplastic group (50.8) is meaningful. For example, in thyroid tissue section showing big difference over two times of GLI of each cell, although we can't definitely discriminate between cancer cells showing clear nuclei and normal cells only by GLI values, we could consider the possibility of papillary carcinoma in the tissue section. Moreover we can apply these results in cytology, where automatic screening is relatively popular. However, there are still many problems to be solved, such as common nuclear clearing in autoimmune thyroiditis and proper quality control and adjustment for different samples. Recently, Louis *et al*.[16,17] defined computational pathology as an approach to extract clinically actionable knowledge from variable data, including digital images, and suggested that computational pathology should serve as a hub for data-related research in modern health care systems. By using newly developed information and technology tools, we can review and reanalyze our traditional pathologic findings and with those efforts, we can expand our understanding of diseases and obtain more objective and reproducible methods of diagnosis. In conclusion, quantitative analysis of the nuclear GLI for the discrimination between cancer cells showing clear nuclei and non-neoplastic follicular epithelial cells in papillary thyroid carcinoma revealed meaningful results comparable to traditional microscopic findings. Nuclear GLI could be a useful factor for the discrimination between these two groups.

## Conflicts of Interest

No potential conflict of interest relevant to this article was reported.

## REFERENCES


1. LiVolsi VA. Papillary thyroid carcinoma: an update. Mod Pathol 2011; 24 Suppl 2: S1-9.
2. Neltner JH, Abner EL, Schmitt FA, *et al*. Digital pathology and image analysis for robust high-throughput quantitative assessment of Alzheimer disease neuropathologic changes. J Neuropathol Exp Neurol 2012; 71: 1075-85.
3. El Hallani S, Guillaud M, Korbelik J, Marginean EC. Evaluation of quantitative digital pathology in the assessment of Barrett eophagus-associated dysplasia. Am J Clin Pathol 2015; 144: 151-64.
4. Guillaud M, Zhang L, Poh C, Rosin MP, MacAulay C. Potential use of quantitative tissue phenotype to predict malignant risk for oral premalignant lesions. Cancer Res 2008; 68: 3099-107.
5. Huang W, Hennrick K, Drew S. A colorful future of quantitative pathology: validation of Vectra technology using chromogenic multiplexed immunohistochemistry and prostate tissue microarrays. Hum Pathol 2013; 44: 29-38.
6. Kayser K, Görtler J, Goldmann T, Vollmer E, Hufnagl P, Kayser G. Image standards in tissue-based diagnosis (diagnostic surgical pathology). Diagn Pathol 2008; 3: 17.
7. Park M, Baek T, Baek J, *et al*. Nuclear image analysis study of neuroendocrine tumors. Korean J Pathol 2012; 46: 38-41.

8. Yagi Y. Color standardization and optimization in whole slide imaging. Diagn Pathol 2011; 6 Suppl 1: S15.
9. Bautista PA, Hashimoto N, Yagi Y. Color standardization in whole slide imaging using a color calibration slide. J Pathol Inform 2014; 5: 4.
10. Johannessen JV, Gould VE, Jao W. The fine structure of human thyroid cancer. Hum Pathol 1978; 9: 385-400.
11. Fischer AH, Taysavang P, Weber CJ, Wilson KL. Nuclear envelope organization in papillary thyroid carcinoma. Histol Histopathol 2001; 16: 1-14.
12. Lin MH, Akera T. Increased (Na+,K+)-ATPase concentrations in various tissues of rats caused by thyroid hormone treatment. J Biol Chem 1978; 253: 723-6.
13. Kamitani T, Ikeda U, Muto S, *et al*. Regulation of Na,K-ATPase gene expression by thyroid hormone in rat cardiocytes. Circ Res 1992; 71: 1457-64.
14. Liu Y, Levine B. Autosis and autophagic cell death: the dark side of autophagy. Cell Death Differ 2015; 22: 367-76.
15. Garner MH. Na,K-ATPase in the nuclear envelope regulates Na+: K+ gradients in hepatocyte nuclei. J Membr Biol 2002; 187: 97-115.
16. Louis DN, Gerber GK, Baron JM, *et al*. Computational pathology: an emerging definition. Arch Pathol Lab Med 2014; 138: 1133-8.
17. Louis DN, Feldman M, Carter AB, *et al*. Computational pathology: a path ahead. Arch Pathol Lab Med 2016; 140: 41-50.

 http://dx.doi.org/10.4132/jptm.2016.05.19

*Journal of Pathology and Translational Medicine 2016; 50: 361-368*
*http://dx.doi.org/10.4132/jptm.2016.06.19*

■ ORIGINAL ARTICLE ■

# CD99 Is Strongly Expressed in Basal Cells of the Normal Adult Epidermis and Some Subpopulations of Appendages: Comparison with Developing Fetal Skin

Gawon Choi[1,2]* · Jin Roh[3]*
Chan-Sik Park[3]

[1]Graduate School of Medicine, University of Ulsan College of Medicine, Seoul; [2]Mizmedi Hospital, Seoul; [3]Department of Pathology, Asan Medical Center, University of Ulsan College of Medicine, Seoul, Korea

**Received:** March 23, 2016
**Revised:** June 6, 2016
**Accepted:** June 19, 2016

**Corresponding Author**
Chan-Sik Park, MD, PhD
Department of Pathology, Asan Medical Center, University of Ulsan College of Medicine, 88 Olympic-ro 43-gil, Songpa-gu, Seoul 05505, Korea
Tel: +82-2-3010-5838
Fax: +82-2-472-7898
E-mail: csikpark@amc.seoul.kr

*Gawon Choi and Jin Roh contributed equally to this work.

**Background:** CD99 is a cell surface transmembrane glycoprotein expressed in various tissues. CD99 is differentially expressed between subpopulations of each tissue and is highly expressed in certain hematopoietic and precursor cells. However, there has been no comprehensive study of CD99 expression in normal skin. We evaluated CD99 expression in normal human skin and developing fetal skin. **Methods:** Seventy-five adult skin samples containing normal skin and eight fetal skin samples of different gestational ages were collected. CD99 immunohistochemical staining was performed to evaluate expression pattern in adult and fetal skin samples. CD99 and CD34 expression were compared by double immunofluorescence. **Results:** In normal adult skin, CD99 was strongly expressed in the membrane of epidermal basal keratinocytes, hair follicle bulges and outer root sheaths, and inner secretory cells of eccrine sweat glands. In fetal skin, CD99 was not expressed on the periderm at 16 weeks of gestation but was expressed in basal cells of fetal skin at around 19 weeks of gestation. CD99 expression became comparable to that of the adult skin after 20 weeks of gestation. CD99 and CD34 were co-expressed in hair follicle outer root sheaths, as seen by double immunofluorescence study. **Conclusions:** This is the first study examining CD99 expression pattern in normal adult and fetal skin. CD99 tends to be expressed in the basal/precursor cells of epidermis and in hair follicles. These results provide a basis for future investigation on functions of CD99 in the skin and provide a novel potential target for the treatment of dermatologic lesions.

**Key Words:** CD99 protein; Skin; Immunohistochemistry

CD99 is a 32-kD type I transmembrane glycoprotein encoded by the *CD99* gene and its expression has been reported in many cell types, such as hematopoietic cells, endothelial cells, central nervous system ependymal cells, thymocytes, granular cells of the ovary, Sertoli cells, and pancreatic islet cells.[1-3] CD99 expression is seen in all leukocyte lineages but is differentially expressed with maturation and is particularly strong in immature thymic T-lineage cells.[2] Other studies also demonstrated high CD99 expression in tonsillar lymphoid progenitor cells[4] and in the subventricular zone of fetal brain (C.-S. Park, unpublished data), suggesting that CD99 may play important roles in these precursor cells. The functions of CD99 in cells in which CD99 was highly expressed have been studied and they were as follows: cell death of thymocytes and T lymphocytes,[5,6] migration through monocyte endothelial junctions by adhesion and diapedesis,[7] cell-cell adhesion in lymphocytes,[5,8] maintenance of cellular morphology in Hodgkin and Reed/Sternberg cells,[9] and recruitment of T cells to inflamed mouse skin.[10] Pathologically, CD99 is strongly expressed in various tumors including Ewing sarcoma/peripheral neuroectodermal tumors, T-lymphoblastic lymphoma, and others.[11] CD99 is a crucial marker for the diagnosis of these tumors.

Skin is the largest human organ and is structurally composed of epidermis, dermis, and appendages including hair follicles, sebaceous glands, and sweat glands (eccrine and apocrine). Microscopically, cells which composing the skin showed various stages of differentiation. The epidermis contains multiple layers of stratified keratinocytes, and basally located cells are morphologically undifferentiated. Hair follicles are cylindrical invaginations of surface epithelium, and are composed of the innermost hair shaft, the inner root sheath (IRS), and the outer root sheath (ORS). The bulge, the insertion site of the arrector pilli muscle, is the prominent epithelial protuberance of the ORS and it contains basaloid cells.[12] Sebaceous glands have central acini, mass-

pISSN 2383-7837
eISSN 2383-7845

es of rounded cells that are packed with lipid-filled vacuoles and peripheral undifferentiated basal cells. Eccrine sweat glands consist of a secretory portion lined with stratified cuboidal cells and an excretory portion lined with two layers of smaller cuboidal cells. Apocrine glands are large glands and secretory cells usually show cuboidal morphology with eosinophilic cytoplasm.[13]

CD99 expression levels differ in specific subpopulations according to cellular maturation. We identified strong CD99 expression in the basally located precursor cells of normal epidermis. We inferred that CD99 shows differential expression between the epidermis and appendageal subpopulations with maturation. No systemic evaluation of CD99 expression in normal skin or the appendages has yet been published. The aim of the present study was to evaluate CD99 expression patterns in normal adult epidermis and appendages by immunohistochemistry (IHC) and to ascertain CD99 expression in normal fetal skin during different gestational ages. We also investigated whether morphologically immature subpopulations that express CD99 correlate with skin precursor cells based on previously established marker.

## MATERIALS AND METHODS

### Skin samples

In this study, we retrospectively selected 75 cases of formalin-fixed, paraffin-embedded hair-bearing adult skin samples between 2002 and 2009 at Asan Medical Center. Samples were taken from the margins of routine surgical procedures such as excisional biopsy or excision for benign/malignant skin lesions that were diagnosed as following: various inflammatory lesions with parakeratosis (n = 16), keratinocytic tumors (n = 11), benign tumors with apocrine and eccrine differentiation (n = 14), malignant tumors with follicular differentiation (n = 1), benign tumors with follicular differentiation (n = 17), and tumors with sebaceous differentiation (n = 12). The rest were retrieved from mature cystic teratoma (n = 2) and normal scalp tissues biopsied for therapeutic reasons (n = 2). To analyze CD99 expression patterns in fetal skin, eight fetal skin samples were collected from the archives of Asan Medical Center. Gestational ages of the collected cases were 16, 17, 19 (2 cases), 20, 25, 26, and 28 weeks. All tissues were immediately fixed in 10% buffered formalin, and then processed in paraffin wax using standard procedures. Sections were serially cut into 4-μm sections and stained with hematoxylin and eosin for examination. The study protocol was approved by the Institutional Review Board (project number 2009-440) of Asan Medical Center.

### Immunohistochemical staining

All hematoxylin and eosin–stained slides were reviewed to ensure quality. When multiple blocks were available in a single case, one block containing representative tissue was selected. IHC staining for CD99 was performed using a BenchMark XT autoimmunostianer (Ventana Medical Systems, Tucson, AZ, USA) according to the manufacturer's instructions and using the reagents supplied with the kit. In brief, 4-μm sections were mounted on silanized charged slides, dried for 10 minutes at room temperature and then further dried for 20 minutes at 65°C. After deparaffinization, heat-induced epitope retrieval using standard Cell Conditioning Solution 1 was performed for 24 minutes. Subsequently, primary anti-CD99 (1:100, clone DN16, DiNonA, Seoul, Korea) was applied by an automated immunostaining system with the UltraView DAB Detection Kit (Ventana Medical Systems). Immunostained sections were counterstained with hematoxylin. Analysis of whole tissue section slides stained for CD99 by IHC was performed under a light microscope as previously described.[14-16] Lymphocytes and endothelial cells were used as internal positive controls. The results of CD99 immunostaining were classified into the following groups: consistently complete and strong membrane staining was assigned a value ++, weak to moderate membrane staining was assigned a value of +, variable membrane staining was assigned a value of +/–, and no staining was assigned a value of –. Occasional cytoplasmic staining was minimal and weak.

### Immunofluorescence assay

For immunofluorescence (IF) staining, 4-μm sections were incubated with mouse anti-CD99 (1:200, clone DN16, DiNonA) and rabbit anti-CD34 (1:10, #ab64480, rabbit polyclonal, Abcam, Cambridge, UK) for 60 minutes at room temperature. Sections were then incubated with tetramethylrhodamine-conjugated host anti-mouse IgG antibody and fluorescein isothiocyanate-conjugated host anti-rabbit IgG antibody for 60 minutes at room temperature. Nuclei were stained with DAPI. Sections incubated with the appropriate isotype control primary antibodies and fluorescently labeled secondary antibodies were utilized as necessary. Results were analyzed using confocal microscopy (Leica TCS_NP/SP, Leica Microsystems, Mannheim, Germany).

## RESULTS

### Basal cells showed strong CD99 expression in normal adult epidermis

To examine the expression pattern of CD99 in epidermal ke-


http://dx.doi.org/10.4132/jptm.2016.06.19

ratinocytes, immunostaining for CD99 was performed on non-pathologic adult skin samples (Fig. 1A). In the epidermis, cell membranes in the basal cell layer were strongly stained (Fig. 1B), whereas the keratinocytes in the prickle cell layer just above the basal cell layer showed markedly reduced staining and cells in the granular and hornified layers did not express CD99. We also identified intense CD99 expression in Langerhans' cells in the epidermal layer (Fig. 1B).

### Basaloid cells of bulge and ORS showed strong CD99 expression in normal adult hair follicle

Infundibula of hair follicles possessed a CD99 expression pattern similar to that of the epidermis. CD99 staining was strong in the basaloid cells (Fig. 1C) at the bulges, and basal cells of the follicular ORS were also strongly stained (Fig. 1D). Other subpopulations of hair follicles showed varying immunoreactivity. When observing CD99 staining in the central shaft of hair follicles, the cuticle was negative for CD99, the lower IRS was weakly positive, and the ORS was strongly positive (Fig. 1D).

### CD99 was differentially expressed in subpopulations of normal adult sweat glands and sebaceous glands

Secretory apocrine glands showed variable CD99 expression. Relatively thin to flat cell-lined apocrine glands were negative for CD99, but relatively tall cell-lined apocrine glands were positive for CD99. The apical luminal surfaces of both flat and tall

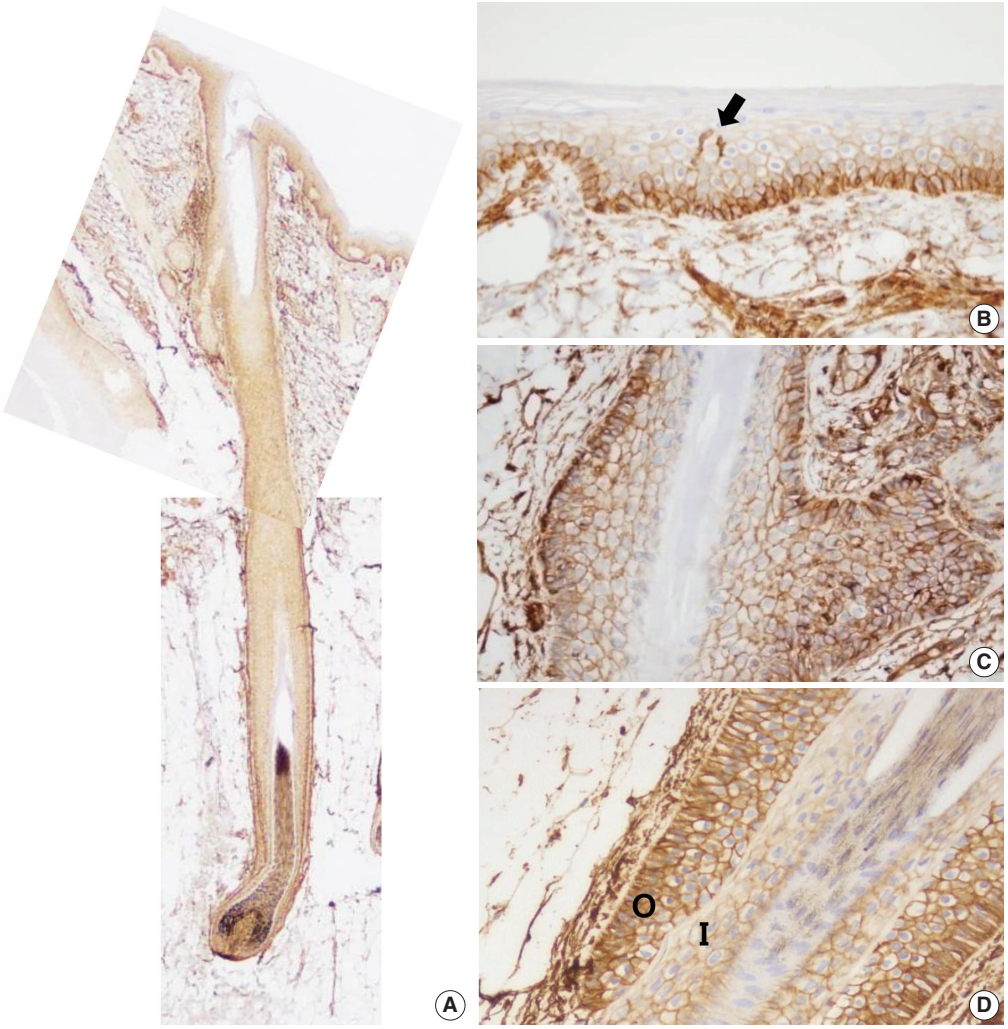


**Fig. 1.** CD99 expression in normal adult epidermis and hair follicles. (A) Overall CD99 expression pattern in normal adult skin. (B) Basal cells of the epidermis show strong immunopositivity for CD99. Epidermal Langerhans cells are also strongly immunopositive for CD99 (arrow). (C) Basaloid cells in the bulge, the insertion of the arrector pili muscle, show high CD99 expression. (D) In a terminal anagen hair follicle, the outer root sheath cells are strongly positive for CD99 stain. The inner root sheath cells are weakly positive for CD99 stain. O, outer root sheath; I, inner root sheath.

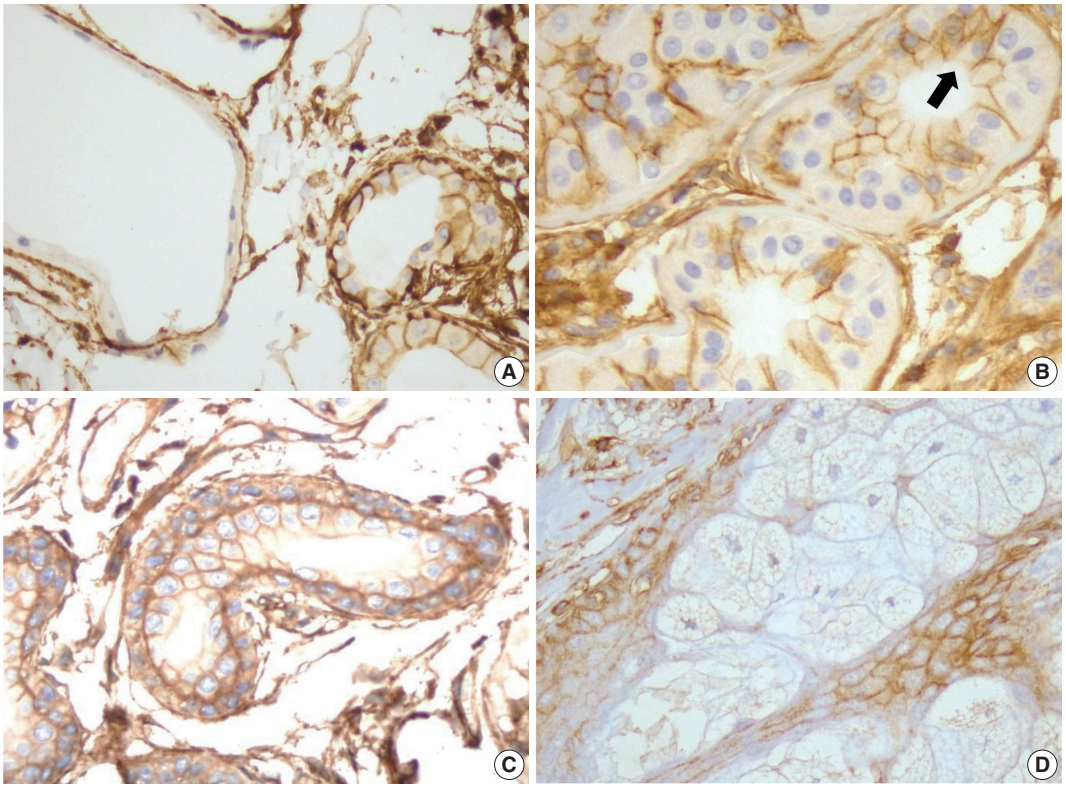


**Fig. 2.** CD99 expression in the normal adult sweat glands and sebaceous glands. (A) In apocrine glands, flattened lining cells are immunonegative for CD99 (left). Meanwhile, tall cells in apocrine glands express CD99 (right). (B) Inner small cells of eccrine glands express CD99 in opposition to outer large cells (arrow). Apicoluminal surface of the eccrine glands are immunonegative for CD99. (C) Two layers of excretory ductal cells are immunopositive for CD99. (D) In sebaceous glands, outer basal cells express CD99. However, mature sebocytes do not express CD99.

cell-lined glands were CD99-negative (Fig. 2A). Secretory coils of eccrine sweat glands are composed of outer clear cells and inner cuboidal cells; the outer clear cells were immunonegative and scattered inner cuboidal cells were immunopositive for CD99 (Fig. 2B). The excretory duct is composed of two-layered cuboidal cells, and both layers were immunopositive for CD99 (Fig. 2C). The apical luminal surfaces of inner eccrine cells and inner excretory ducts also lacked CD99 expression (Fig. 2B, C). In the sebaceous glands, basal cells surrounding the sebaceous alveolus were CD99 immunopositive, but mature sebocytes containing central lipid droplets were immunonegative for CD99 (Fig. 2D). Cells that were positive for CD99 immunostaining in normal adult epidermis and skin appendages are summarized in Table 1.

**Table 1.** Summary of CD99 expression in normal adult epidermis and skin appendages

| | | Immunoreactivity |
|---|---|---|
| Epidermis | Basal cells | ++ |
| | Prickle cells | + |
| | Granular cells | – |
| | Horny cells (cornified cells) | – |
| Hair follicle | Bulge | ++ |
| | Cortex | – |
| | Cuticle | – |
| | Inner root sheath–lower | + |
| | Outer root sheath | ++ |
| | Glassy membrane | – |
| Sweat glands | | |
| Eccrine secretory coil | Inner dark cells | ++[a] |
| | Outer clear cells | – |
| Apocrine secretory acinus | Secretory cells | +/–[a] |
| Excretory duct | Inner layer cells | +[a] |
| | Outer layer cells | ++ |
| Sebaceous glands | Mature sebocytes | – |
| | Basal cells | ++ |

++, consistently strong and complete membranous staining; +, consistently weak to moderate staining; +/–, variable staining; –, negative.
[a]Apico-luminal surfaces are negative for CD99.

## CD99-positive epidermal basal cells appeared in fetal skin early in the second trimester

Eight developing fetal human skin samples were obtained from aborted fetuses of 16–28 gestational weeks. In early stages, fetal skin is called periderm and is composed of 2–3 epider-


http://dx.doi.org/10.4132/jptm.2016.06.19

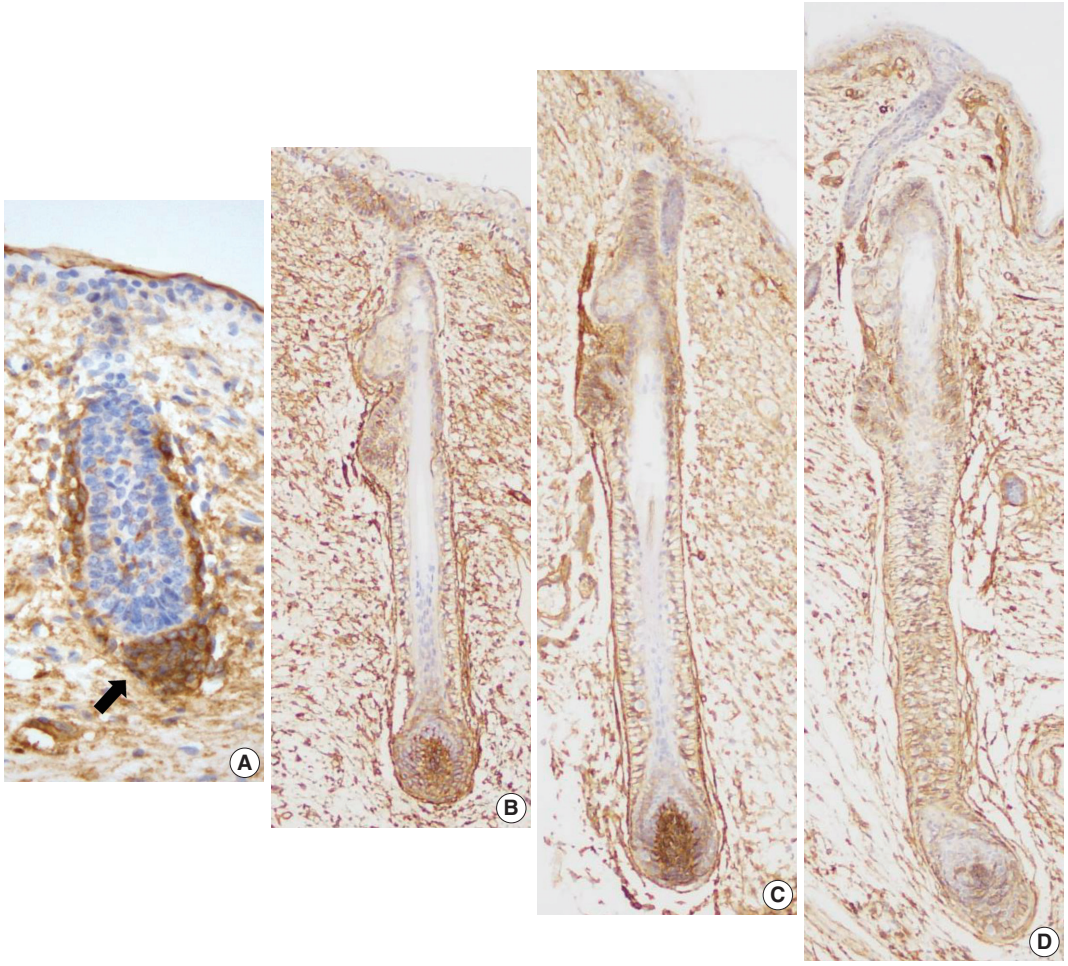


**Fig. 3.** CD99 expression pattern during normal development of the hair follicles. (A) At 16 weeks of gestation, only mesenchymal cells around the hair germ express CD99 (arrow). (B) CD99 positive epidermal basal cells appear at 19 weeks of gestation. Basaloid cells in the bulge and basal cells of the outer root sheath and lower inner root sheath also express CD99. (C, D) CD99 expression pattern is identical to that of adult skins at 20 and 25 weeks of gestation.

mal cell layers.[17] At 16 weeks of gestation, the periderm, including the epidermal basal layer and hair follicle germ, was negative for CD99, whereas mesenchymal cells around the hair germ were strongly positive for CD99 (Fig. 3A). At 19 weeks of gestation, the fetal epidermis and skin appendages start to resemble normal adult skin; basal cell layer, intermediate cell layer, hair follicles, sweat glands, and sebaceous glands appear at this stage. CD99 was expressed in the epidermal basal cell layer, hair bulge, ORS, and dermal papilla (Fig. 3B). At 20 and 25 weeks of gestation, fetal skin is histologically similar to adult skin, showing CD99 immunoreactivity patterns identical to those of adult skins (Fig. 3C, D).

### CD99 and CD34 were co-expressed in lower ORS cells, but they did not co-localize

In our study, CD99 staining was particularly strongly positive in immature epidermal basal cells and cells at the bulge. We therefore compared CD99-positive subpopulations of normal epidermis and skin appendages to CD34-positive subpopulations that have been reported as cutaneous precursor cells using double-IF. We focused on expression patterns of these markers in the basal cells of epidermis and hair follicles. In the adult epidermis and skin appendages, CD99 and CD34 expression partially overlapped at the lower ORS (Fig. 4A, D). Epidermal basal cells and basaloid cells of the bulge were CD34-negative (Fig. 4A–C). In the 20-week-old fetal skin, CD99 and CD34 were not co-expressed in the basal cells of epidermis (Fig. 5B), bulge (Fig. 5C), or ORS; however, mesencymal cells of dermal papilla showed co-expression (Fig. 5A).

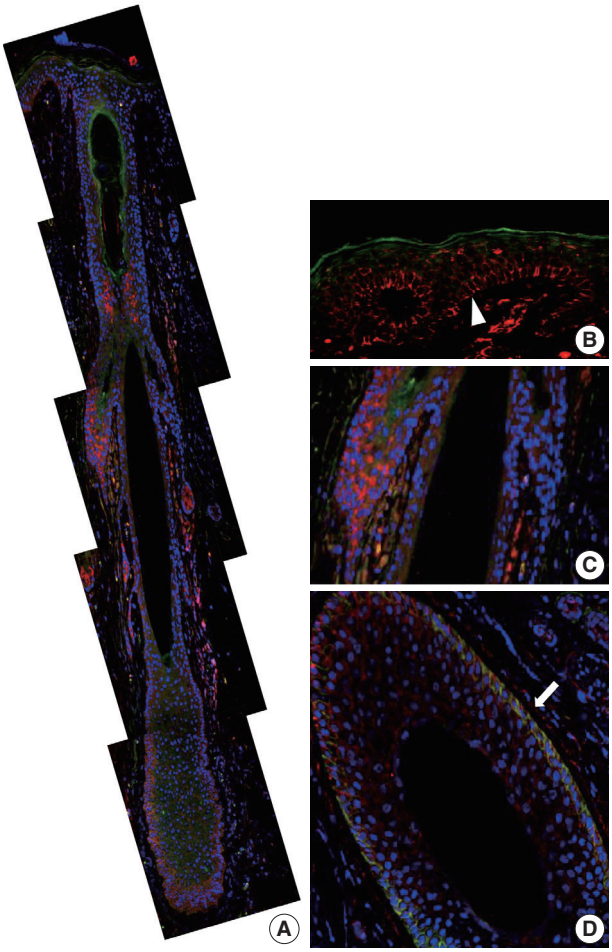


**Fig. 4.** CD99 and CD34 expression pattern by double-immunofluorescence staining in normal adult epidermis and hair follicles. (A) Overall expression pattern of CD99 (red) and CD34 (green). Epidermal basal cells (arrowhead) (B) and basaloid cells (C) in the bulge only express CD99 but not CD34. (D) Some cells in the lower outer root sheath show co-expression of CD99 and CD34 (arrow) (horizontal section).

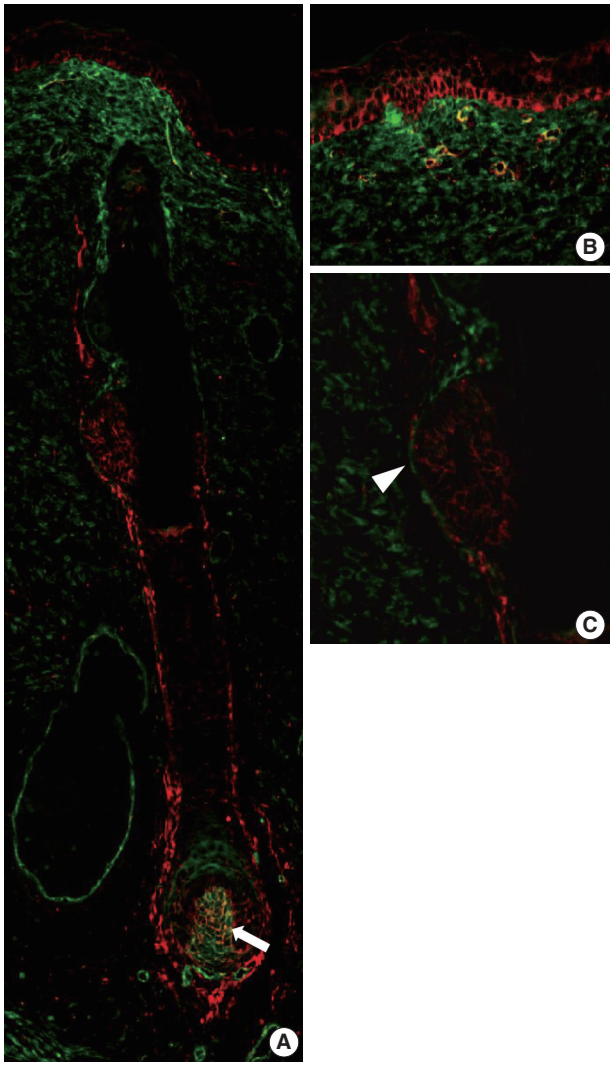


**Fig. 5.** CD99 and CD34 expression pattern by double-immunofluorescence staining in the fetal epidermis and hair follicles at 20 weeks of gestation. (A) Overall expression pattern of CD99 (red) and CD34 (green). Dermal papilla expresses both CD99 (red) and CD34 (green) (arrow). (B, C) Epidermal basal cells and basaloid cells in the bulge (arrowhead) express only CD99.

## DISCUSSION

The aim of the current study was to examine CD99 expression in normal human skin and skin appendages; no such study has been performed to date. Differential expression of CD99 was observed in the epidermis and appendages. We demonstrated that CD99 was strongly expressed in the immature epidermal basal cells, but the fully differentiated granular layer did not show CD99 positivity in normal adult skin. This result is consistent with the findings of a previous study,[18] in which CD99 expression was evaluated in a large series of cutaneous melanoma samples and was described briefly as a crisp membranous staining on normal epidermal basal cells. Our study showed that in skin appendages, CD99 showed differential immunoreactivity in each subpopulation. Bulge cells, basal cells of the ORS, and eccrine inner cuboidal cells were consistently and strongly positive. However, CD99 expression was variably positive in apocrine secretory glands. Relatively tall cells with luminal decapitation tended to be CD99-positive, but thin to flat cells without decapitation tended to be negative. These findings suggest that CD99 expression can differ according to cellular functional status.

Analysis of CD99 expression was also performed during different developmental stages of fetal skin. In fetal skin, peridermal cells persist until about week 21 and gradually disappear as stratum corneum. In the early stages of epidermal development,


http://dx.doi.org/10.4132/jptm.2016.06.19

mitotic activity occurs in all the epidermal layers; however, when differentiation begins, mitotic activity becomes restricted to the cells of the basal layer.[17] Angiotensin converting enzyme (ACE), keratin 19, β1-integrin, and p63 were used as stem cell markers in examining the various developmental stages of fetal skin by double IF.[19] The expression of ACE, β1-integrin, keratin 19, and p63 was seen in all epidermal layers of the developing fetal skin at 11–20 weeks of gestation. From 21 weeks of gestation onward, their expression was mainly confined to the basal layer of epidermal cells. In our study, CD99 was not seen in the periderm at 16 weeks of gestation but was consistently expressed at 19 weeks of gestation. Based on this result, we suggest that CD99 expression precedes the expression of ACE, β1-integrin, keratin 19, and p63 in the fetal basal layer.

Based on the particularly strong CD99 expression in immature thymic T-lineage cells,[2] tonsillar lymphoid progenitor cells,[4] and subventricular zone of fetal brain (C.-S. Park, unpublished data), we attempted to correlate CD99 expression with immature subpopulations of epidermis and appendages. CD99 was strongly expressed in immature basal keratinocytes. In hair follicles, the bulge is a prominent epithelial protuberance of the ORS. There is evidence for populations of stem cells located at the basal layer of the epidermis and the hair follicle bulge. CD99 is also strongly expressed in the bulge.

According to previous reports that analyzed expression patterns of various precursor markers, CD34 is more specific for the peripheral layer of the ORS, cytokeratin (CK) 15 for bulge and epidermal basal cells, nestin for inner portions of the ORS, CK19 for basal keratinocytes in the upper and lower third of the ORS, p63 for the basal/suprabasal layer, hair matrix, and ORS, and CD200 for the bulge.[20-24] We found CD99 was more broadly expressed in the epidermis and appendages. We showed that CD34, which was thought to have similar expressions patterns to CD99, shows different expression by double IF. In the present study, CD34 and CD99 were only co-expressed in the lower ORS. Therefore, we assumed that precursor cell subpopulations in the skin are more varied than previously thought.

In conclusion, this study examined CD99 expression in normal adult and fetal skin. CD99 is strongly expressed in the immature epidermal basal cells in the bulge and basal cells of the hair follicle ORS. These findings suggest that CD99 may carry out a specific function in the structures where it is expressed. Interestingly, CD99-expressing cell subpopulations partially overlapped with sites harboring epidermal precursor cells. Therefore, we present that CD99 is a unique and previously unreported marker of epidermis and its appendages. Future studies should focus on functions of CD99 in the epidermis and its appendages and investigate its feasibility as a novel target for the treatment of dermatologic lesions.

## Conflicts of Interest

No potential conflict of interest relevant to this article was reported.

## Acknowledgments

This work was supported by the National Research Foundation of Korea, Grant No. 2008-0062286 (http://www.nrf.re.kr/) and the Asan Institute for Life Sciences, Grant No. 2012-527 (http://en.ails. amc.seoul.kr/).

## REFERENCES

1. Aussel C, Bernard G, Breittmayer JP, Pelassy C, Zoccola D, Bernard A. Monoclonal antibodies directed against the E2 protein (MIC2 gene product) induce exposure of phosphatidylserine at the thymocyte cell surface. Biochemistry 1993; 32: 10096-101.
2. Dworzak MN, Fritsch G, Buchinger P, *et al*. Flow cytometric assessment of human MIC2 expression in bone marrow, thymus, and peripheral blood. Blood 1994; 83: 415-25.
3. Gordon MD, Corless C, Renshaw AA, Beckstead J. CD99, keratin, and vimentin staining of sex cord-stromal tumors, normal ovary, and testis. Mod Pathol 1998; 11: 769-73.
4. Strauchen JA, Miller LK. Lymphoid progenitor cells in human tonsils. Int J Surg Pathol 2003; 11: 21-4.
5. Bernard G, Zoccola D, Deckert M, Breittmayer JP, Aussel C, Bernard A. The E2 molecule (CD99) specifically triggers homotypic aggregation of CD4+ CD8+ thymocytes. J Immunol 1995; 154: 26-32.
6. Pettersen RD, Bernard G, Olafsen MK, Pourtein M, Lie SO. CD99 signals caspase-independent T cell death. J Immunol 2001; 166: 4931-42.
7. Schenkel AR, Mamdouh Z, Chen X, Liebman RM, Muller WA. CD99 plays a major role in the migration of monocytes through endothelial junctions. Nat Immunol 2002; 3: 143-50.
8. Hahn JH, Kim MK, Choi EY, *et al*. CD99 (MIC2) regulates the LFA-1/ICAM-1-mediated adhesion of lymphocytes, and its gene encodes both positive and negative regulators of cellular adhesion. J Immunol 1997; 159: 2250-8.
9. Kim SH, Choi EY, Shin YK, *et al*. Generation of cells with Hodgkin's and Reed-Sternberg phenotype through downregulation of CD99 (Mic2). Blood 1998; 92: 4287-95.
10. Bixel G, Kloep S, Butz S, Petri B, Engelhardt B, Vestweber D. Mouse

CD99 participates in T-cell recruitment into inflamed skin. Blood 2004; 104: 3205-13.
11. Ambros IM, Ambros PF, Strehl S, Kovar H, Gadner H, Salzer-Kuntschik M. MIC2 is a specific marker for Ewing's sarcoma and peripheral primitive neuroectodermal tumors: evidence for a common histogenesis of Ewing's sarcoma and peripheral primitive neuroectodermal tumors from MIC2 expression and specific chromosome aberration. Cancer 1991; 67: 1886-93.
12. Narisawa Y, Kohda H. Two- and three-dimensional demonstrations of morphological alterations of early anagen hair follicle with special reference to the bulge area. Arch Dermatol Res 1996; 288: 98-102.
13. Young B, Lowe JS, Stevens A, Heath JW. Wheater's functional histology: a text and colour atlas. 5th ed. Philadelphia: Elsevier, 2006; 167-85.
14. Park CK, Shin YK, Kim TJ, Park SH, Ahn GH. High CD99 expression in memory T and B cells in reactive lymph nodes. J Korean Med Sci 1999; 14: 600-6.
15. Cho EY, Choi Y, Chae SW, Sohn JH, Ahn GH. Immunohistochemical study of the expression of adhesion molecules in ovarian serous neoplasms. Pathol Int 2006; 56: 62-70.
16. Shin SJ, Lee H, Jung G, *et al*. Expression of CD99 in multiple myeloma: a clinicopathologic and immunohistochemical study of 170 cases. Korean J Pathol 2014; 48: 209-16.
17. Holbrook KA. Structure and function of the developing human skin. In: Goldsmith LA, ed. Biochemistry and physiology of the skin. New York: Oxford University Press, 1983; 64-101.
18. Wilkerson AE, Glasgow MA, Hiatt KM. Immunoreactivity of CD99 in invasive malignant melanoma. J Cutan Pathol 2006; 33: 663-6.
19. Liu HW, Cheng B, Li JF, *et al*. Characterization of angiotensin-converting enzyme expression during epidermis morphogenesis in humans: a potential marker for epidermal stem cells. Br J Dermatol 2009; 160: 250-8.
20. Jiang S, Zhao L, Purandare B, Hantash BM. Differential expression of stem cell markers in human follicular bulge and interfollicular epidermal compartments. Histochem Cell Biol 2010; 133: 455-65.
21. Inoue K, Aoi N, Sato T, *et al*. Differential expression of stem-cell-associated markers in human hair follicle epithelial cells. Lab Invest 2009; 89: 844-56.
22. Hoang MP, Keady M, Mahalingam M. Stem cell markers (cytokeratin 15, CD34 and nestin) in primary scarring and nonscarring alopecia. Br J Dermatol 2009; 160: 609-15.
23. Gho CG, Braun JE, Tilli CM, Neumann HA, Ramaekers FC. Human follicular stem cells: their presence in plucked hair and follicular cell culture. Br J Dermatol 2004; 150: 860-8.
24. Pellegrini G, Dellambra E, Golisano O, *et al*. p63 identifies keratinocyte stem cells. Proc Natl Acad Sci U S A 2001; 98: 3156-61.

 http://dx.doi.org/10.4132/jptm.2016.06.19

*Journal of Pathology and Translational Medicine 2016; 50: 369-376*
*http://dx.doi.org/10.4132/jptm.2016.06.06*

■ ORIGINAL ARTICLE ■

# Long Non-coding RNA HOTAIR Expression in Diffuse Large B-Cell Lymphoma: In Relation to Polycomb Repressive Complex Pathway Proteins and H3K27 Trimethylation

Eun Ji Oh[1,2]* · Soo Hee Kim[1,3,4]*
Woo Ick Yang[1] · Young Hyeh Ko[3]
Sun Och Yoon[1]

[1]Department of Pathology, Yonsei University College of Medicine, Seoul; [2]Department of Pathology, Seoul St. Mary's Hospital, College of Medicine, The Catholic University of Korea, Seoul; [3]Department of Pathology, Samsung Medical Center, Sungkyunkwan University School of Medicine, Seoul; [4]Anatomic Pathology Reference Lab, Seegene Medical Foundation, Seoul, Korea

**Received:** May 30, 2016
**Accepted:** June 6, 2016

**Corresponding Author**
Sun Och Yoon, MD, PhD
Department of Pathology, Yonsei University College of Medicine, 50-1 Yonsei-ro, Seodaemun-gu, Seoul 03722, Korea
Tel: +82-2-2228-1763
Fax: +82-2-362-0860
E-mail: soyoon@yuhs.ac; revita@naver.com

*Eun Ji Oh and Soo Hee Kim contributed equally to this work.

**Background:** A long non-coding RNA *hox* transcript antisense intergenic RNA (*HOTAIR*) is involved in epigenetic regulation through chromatin remodeling by recruiting polycomb repressive complex 2 (PRC2) proteins (EZH2, SUZ12, and EED) that induce histone H3 trimethylation at lysine 27 (H3K27me3). Deregulation of c-MYC and interaction between c-MYC and EZH2 are well known in lymphomagenesis; however, little is known about the expression status of *HOTAIR* in diffuse large B-cell lymphomas (DLBCLs). **Methods:** The expression status of PRC2 (EZH2, SUZ12, and EED), H3K27me3, c-MYC, and BCL2 was analyzed using immunohistochemistry (n = 231), and *HOTAIR* was investigated by a quantification real-time polymerase chain reaction method (n = 164) in DLBCLs. **Results:** The present study confirmed the positive correlation among PRC2 proteins, H3K27me3, and c-MYC in DLBCLs. Expression level of *HOTAIR* was also positively correlated to EZH2 ($p < .05$, respectively). Between c-MYC and *HOTAIR*, and between c-MYC/BCL2 co-expression and *HOTAIR*, however, negative correlation was observed in DLBCLs ($p < .05$, respectively). High level of H3K27me3 was determined as an independent prognostic marker in poor overall survival (hazard ratio, 2.0; $p = .023$) of DLBCL patients. High expression of *HOTAIR*, however, was associated with favorable overall survival ($p = .004$) in the univariate analysis, but the impact was not significant in the multivariate analysis. The favorable outcome of DLBCL with *HOTAIR* high expression levels may be related to the negative correlation with c-MYC expression or c-MYC/BCL2 co-expression. **Conclusions:** *HOTAIR* expression could be one of possible mechanisms for inducing H3K27me3 via EZH2-related PRC2 activation, and induced H3K27me3 may be strongly related to aggressive DLBCLs which show poor patient outcome.

**Key Words:** Lymphoma, large B-cell, diffuse; *HOTAIR*; *hox* transcript antisense intergenic RNA; Polycomb repressive complex2; Histone H3trimethylation at lysine 27

Long non-coding RNAs (lncRNAs) are molecules longer than 200 nucleotides that are not translated into proteins. The role of lncRNAs is mostly unknown. Recently, several types of cancer-related lncRNAs have been identified and studied in the field of translational research.[1-4] According to recent studies, some lncRNAs are involved in the epigenetic regulation of protein coding genes. *Hox* transcript antisense intergenic RNA (*HOTAIR*) is one of most actively studied lncRNAs. Overexpression of *HOTAIR* is known to occur in various solid tumors of esophagus, stomach, colon, liver, pancreas, lung, and breast and is related to poor prognosis in those tumors.[3,5] *HOTAIR* is located within the *homeobox C* (*HOXC*) gene cluster on chromosome12 and is co-expressed with the *HOXC* genes. *HOTAIR* is involved in chromatin remodeling through recruiting polycomb repressive complex 2 (PRC2; enhancer of zeste homolog 2 [EZH2], suppressor of zeste 12 homolog [SUZ12], and embryonic ectoderm development [EED]) and then inducing histone modification such as histone H3 trimethylation at lysine 27 (H3K27me3) at the promoter site of protein-coding genes.[1-4] Chromatin remodeling and gene regulation via histone modification of the polycomb repressive complex is known to function in the development of embryonic stem cells as well as the development of many types of cancers including hematologic malignancies.[6,7]

In hematologic malignancies, especially in diffuse large B cell lymphomas (DLBCLs) and follicular lymphomas that are the most predominant lymphoma subtype, the deregulation of

pISSN 2383-7837
eISSN 2383-7845

EZH2 methyltransferase is well known. In our previous study, the high level of global H3K27me3 in DLBCL was associated with poor patient prognosis.[8] From these findings, it was suggested that *HOTAIR* might be involved in the PRC2-associated induction of H3K27me3 in DLBCLs; however, an association with *HOTAIR* and DLBCL has not yet been described. In the present study, the expression status of *HOTAIR* was investigated in DLBCL, and the association with PRC2 and H3K27me3 was analyzed.

## MATERIALS AND METHODS

### Patients and clinical data

A total of 231 cases of DLBCL treated with R-CHOP (rituximab, cyclophosphamide, doxorubicin, vincristine, and prednisone) or R-CHOP–like (with or without radiotherapy or surgery) chemotherapy were selected for the study. Cases were retrieved from the archival files from the Department of Pathology, Severance Hospital, from 2005 to 2011. All cases were independently reviewed by two pathologists (S.O.Y. and S.H.K.) based on current World Health Organization criteria,[9] and discordant cases were consulted to other expert hematopathologists. In *HOTAIR* expression analysis, 164 cases were selected from the above 231 cases and investigated after quality assessment of extracted RNA. Clinical data were obtained from medical records. All study protocols were performed according to the ethical guidelines of the "World Medical Association Declaration of Helsinki–Ethical Principles for Medical Research Involving Human Subjects." This study was approved by the Institutional Review Board of Severance Hospital.

### Analysis for *HOTAIR* expression

Formalin fixed paraffin embedded (FFPE) tissue sections were prepared and stained with hematoxylin and eosin, and then the tumor areas were confirmed and marked under the microscope. The marked areas mainly contained packed tumor cells, and the stromal component was less than 10% of the marked area. The unstained slides of FFPE tissues were prepared after dissecting FFPE tissue blocks at 10-mm thickness using a microtome, and the marked area was scraped using a scalpel blade. Generally, three slices of tissue section per case were used for RNA extraction. Total RNA was isolated using an RNeasy FFPE Kit (Qiagen, Hilden, Germany) according to the supplier's instructions. Extracts of RNA were verified by measuring the ratios ofA260/A280 and A260/A230 with a ND-1000 NanoDrop spectrophotometer (NanoDrop, Wilmington, DE, USA). Reverse transcription was performed using a QuantiTect Reverse Transcription kit (Qiagen). The expression patterns of *HOTAIR* were assayed by relative quantification using expression of the housekeeping gene glyceraldehyde-3-phosphate dehydrogenase (*GAPDH*). Primers for *HOTAIR* and *GAPDH* were as follows: HOTAIR (forward, 5'-AGCCAGAGGAGGGAAGAGAG-3'; reverse, 5'-TCCCGTTCCCTAGATTTTCC-3') and GAPDH (forward, 5'-CAAATTCCATGGCACCGTCA-3'; reverse, 5'-ATCGCCCCACTTGATTTTGG-3'). Primers of *HOTAIR* were designed to detect all three transcript variants (transcript variant 1, 3, and 2). In brief, a 20 μL mixture containing 1.0 μL of cDNA, power SYBR Green PCR Master Mix (Applied Biosystems, Carlsbad, CA, USA), 1.0 μL of 10 pmol/μL forward primer, 1.0 μL of 10 pmol/μL reverse primer, and 7.0 μL of tertiary distilled water was prepared. Amplification was performed using a Step One Plus Real-Time PCR instrument (Applied Biosystems) under the following conditions: denaturation at 94°C for 10 minutes, followed by 35 cycles of 94°C for 15 seconds, 55°C for 30 seconds, and 72°C for 30 seconds (fluorescence signal acquisition was performed at this phase). Immediately after amplification, melting curve analysis was performed for amplicon verification. All samples were analyzed in triplicate to confirm reproducibility. Using the Step One Plus Real-Time PCR System software ver. 2.1 (Applied Biosystems), the threshold cycle (Ct, beginning of the polymerase chain reaction exponential phase) value of amplified *HOTAIR* was normalized versus that of amplified *GAPDH* ($2^{-dCt}$). After quality assessment of extracted RNA and expression analysis of the housekeeping gene *GAPDH*, 164 cases were finally selected for the analysis of *HOTAIR* expression. Normal palatine tonsil tissue was obtained from 10 cancer-free individuals and used as age-matched cancer-free controls. The cutoff value for high expression of *HOTAIR* ($HOTAIR^{high}$) was determined at the uppermost value among those of normal control tonsil tissues.

### Tissue microarray preparation, immunohistochemistry, and analysis

The hematoxylin and eosin slides were reviewed and two representative core tissues of the tumor area were selected in each case. Core tissues (3 mm in diameter) were taken from the individual donor blocks and arranged in new recipient tissue microarray paraffin blocks using a trephine apparatus. Immunohistochemical staining and *in situ* hybridization were performed on 4-μm tissue microarray tissue sections. Immunohistochemistry of EZH2 (1:100, Invitrogen, Carlsbad, CA, USA), SUZ12 (1:50, Abcam, Cambridge, UK), EED (1:1,000, Abcam), H3K27me3


http://dx.doi.org/10.4132/jptm.2016.06.06

(1:100, clone C36B11, Cell Signaling Technology, Beverly, MA, USA) was performed using the Ventana BenchMark XT Autostainer (Ventana Medical Systems, Tucson, AZ, USA). Immunohistochemistry for c-MYC (1:50, clone Y69, Abcam), BCL2 (1:50, Novocastra, Newcastle, UK), CD10 (1:100, Novocastra), BCL6 (RTU, Novocastra), and MUM1 (1:200, Cell Marque, Rocklin, CA, USA) was performed using the LEICA BOND-III Autostainer (Leica Biosystems, Newcastle Upon Tyne, UK). For *in situ* hybridization for Epstein-Barr virus (EBV), the INFORM EBER probe (Ventana Medical Systems) was used with the Ventana BenchMark XT Autostainer (Ventana Medical Systems) and ISH iVIEW Blue Detection kit (Ventana Medical Systems).

For EZH2, SUZ12, EED, and H3K27me3, staining intensity (0, no staining to weak; 1, moderate to strong) and proportion of positive tumor cell nuclei (0, < 10%; 1, ≥ 10% and < 75%; 2, ≥ 75%) were semiquantitatively graded as in the previous study.[8] Based on the intensity multiplied by proportion, the protein expression was scored as low (0), intermediate (1), or high level (2). For CD10, BCL6, and MUM1, the positive cutoff value was determined according to the Hans classification criteria[10] and was considered positive if ≥ 30% of the tumor cells showed nuclear immunoreactivity for BCL6 and MUM1, and if ≥ 30% of cells showed membranous reactivity for CD10. Determination of the germinal center B-like (GCB) or non-GCB phenotype was based on the Hans algorithm 10.

For c-MYC and BCL2, staining intensity (0, no staining to weak; 1, moderate to strong) and areas of positive tumor cell nuclei by 10% increments (1 of < 10% to 10 of 90%–100%) were semiquantitatively graded. The cutoff value for high expression was determined by log-rank tests (Mantel-Cox) for overall survival as in the previous report, and the threshold value was determined for c-MYC at a score ≥ 4 (≥ 40% of tumor cells with moderate to strong expression), and BCL2 at a score ≥ 7 (≥ 70% of tumor cells with moderate to strong expression).[11,12] For EBV *in situ* hybridization, the threshold value was determined when

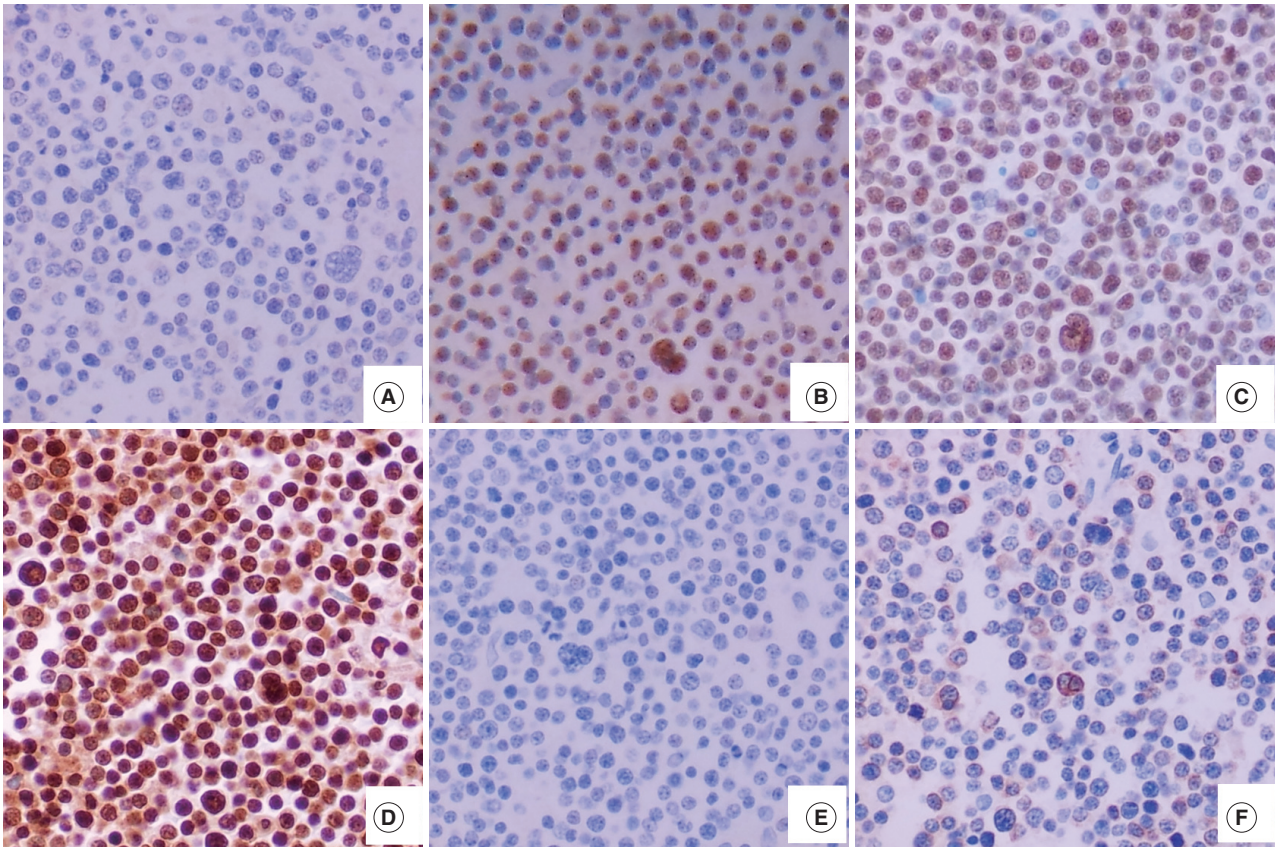


**Fig. 1.** A case of DLBCL with *HOTAIR*$^{high}$ (A–F) shows the various expression pattern of c-MYC (A), EZH2 (B), SUZ12 (C), EED (D), global H3K27me3 (E), and BCL2 (F). In a DLBCL case of *HOTAIR*$^{high}$ (A–F), many PRC2 protein (EZH2, SUZ12, and EED)–positive tumor cells show no expression of c-MYC and no mark of H3K27me3. BCL2 was negative in this case. DLBCL, diffuse large B-cell lymphoma; HOTAIR, hox transcript antisense intergenic RNA; EZH2, enhancer of zeste homolog 2; SUZ12, suppressor of zeste 12 homolog; EED, embryonic ectoderm development; PRC2, polycomb repressive complex 2.

≥10% of the tumor cells showed moderate to strong nuclear expression.

The features of expression of polycomb repressive complex proteins (EZH2, SUZ12, and EED), H3K27me3, c-MYC, and BLC2 in *HOTAIR*$^{high}$ or *HOTAIR*$^{low}$ cases are presented in Fig. 1.

### Statistical analysis

The t test and chi-square test were used to analyze the differences between the variables examined. Overall survival times were measured from the date of lymphoma diagnosis to the date of death or last follow-up visit. Patient survival rates were determined using the Kaplan-Meier method, and the differences in survival rates were compared using the log-rank test. Multivariate analysis was performed using the Cox proportional hazards model. A two-sided p-value < .05 was considered to be statistically significant. When a two-sided p-value was ≤ .05 and < .10, a trend toward statistical significance was considered. All statistical analyses were carried out using SPSS software ver. 20.0 for Windows (IBM Corp., Armonk, NY, USA).

## RESULTS

### The relations among PRC2 proteins, H3K27me3, c-MYC, BCL2, and *HOTAIR*

The DLBCL cases frequently showed high expression of PRC2 proteins and H3K27me3 (28.9%, 47.1%, 74.3%, and 35.7% for EZH2$^{high}$, SUZ12$^{high}$, EED$^{high}$, and H3K27me3$^{high}$, respectively). High expression of all PRC2 proteins (EZH2$^{high}$/

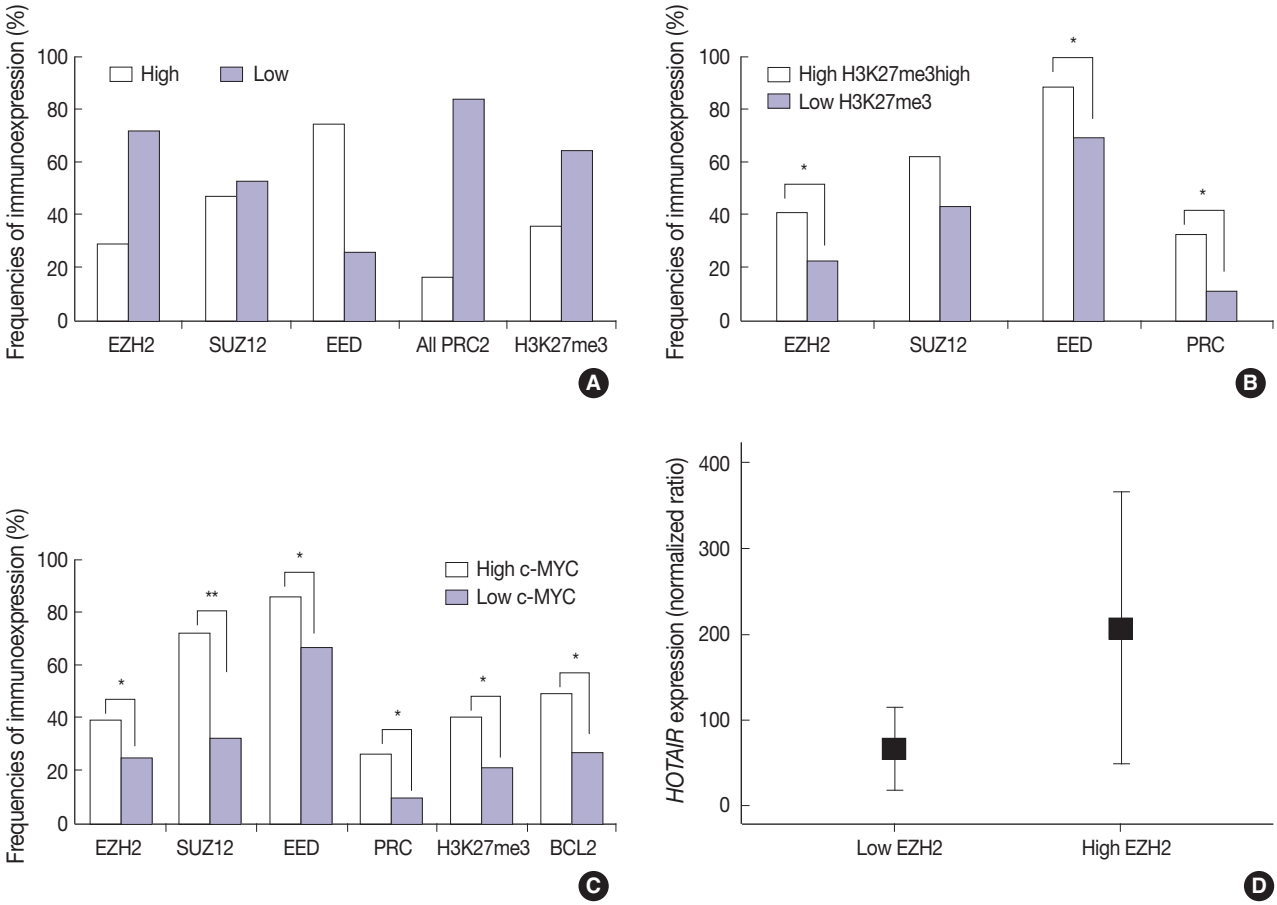


**Fig. 2.** (A) The DLBCL cases frequently show high expression of PRC2 proteins (EZH2, SUZ12, and EED), high expression of all PRC2 proteins (EZH2$^{high}$/SUZ12$^{high}$/EED$^{high}$), and high H3K27me3 level. (B) When compared to cases without high H3K27me3 expression (low H3K27me3), those with high H3K27me3 expression more frequently show high expression of EZH2, SUZ12, EED, and all PRC2 (EZH2$^{high}$/SUZ12$^{high}$/EED$^{high}$). (C) When compared to cases without high c-MYC expression (low c-MYC), those with high c-MYC expression more frequently show high expression of EZH2, SUZ12, EED, all PRC2 (EZH2$^{high}$/SUZ12$^{high}$/EED$^{high}$), H3K27me3, and BCL2. (D) The expression level of *HOTAIR* is significantly higher in cases with high EZH2 expression than those without high EZH2 expression (low EZH2). DLBCL, diffuse large B-cell lymphoma; HOTAIR, hox transcript antisense intergenic RNA; EZH2, enhancer of zeste homolog 2; SUZ12, suppressor of zeste 12 homolog; EED, embryonic ectoderm development; PRC2, polycomb repressive complex 2. *p < .05, **p < .001.


http://dx.doi.org/10.4132/jptm.2016.06.06

SUZ12$^{high}$/EED$^{high}$) was noted in 16.1% of cases (Fig. 2A). The expression of H3K27me3 was positively correlated to PRC2 markers. When compared to cases of H3K27me3$^{low}$, those of high H3K27me3 expression more frequently showed high expression of EZH2 (41.2% vs 22.2%, p = .003), SUZ12 (62.5% vs 43.0%, p = .053), EED (88.6% vs 69.7%, p = .026), and all PRC2 (EZH2$^{high}$/SUZ12$^{high}$/EED$^{high}$) (32.3% vs 11.3%, p = .005). These results are summarized in Fig. 2B.

The expression of c-MYC was positively correlated to PRC2 markers and H3K27me3. When compared to cases of c-MYC$^{low}$, those of high c-MYC expression more frequently showed high expression of EZH2 (39.1% vs 24.6%, p = .036), SUZ12 (72.2% vs 32.1%, p < .001), EED (85.7% vs 66.7%, p = .011), all PRC2 (EZH2$^{high}$/SUZ12$^{high}$/EED$^{high}$) (26.4% vs 9.5%, p = .009), and H3K27me3 (40.6% vs 21.2%; p = .004). BCL2 was positively correlated with c-MYC (49.3% vs 26.8%; p = .002). These results are summarized in Fig. 2C. BCL2 expression showed no significant correlation with the tested PRC2-related markers.

The expression level of HOTAIR was significantly higher in cases of EZH2$^{high}$ than those of EZH2$^{low}$ (mean ratio value, 207 vs 66; p = .027) (Fig. 2D). For other markers, no statistical significance was observed according to HOTAIR expression level.

### *HOTAIR* expression in in relation to clinicopathological variables of DLBCL

In the present study, 23.8% of cases (39/164) showed high *HOTAIR* expression levels (*HOTAIR*$^{high}$). In the correlation analysis between *HOTAIR*$^{high}$ and clinicopathological characteristics of DLBCL (Table 1), high expression of c-MYC protein was less frequent in *HOTAIR*$^{high}$ than in *HOTAIR*$^{low}$ (p = .037). The rate of co-expression of c-MYC and BCL2 was significantly lower in *HOTAIR*$^{high}$ than in *HOTAIR*$^{low}$ (p = .015). Other clinicopathological factors including EBV (p = .660) and Hans classification (p = .746) showed no significant correlation with *HOTAIR* expression (Table 1).

### Clinical significance of RNA and protein expression

In univariate analysis for overall survival of DLBCL patients (Table 2), the known prognostic factors including age > 60 (p < .001), Eastern Cooperative Oncology Group performance status ≥ 2 (p < .001), elevated lactate dehydrogenase (p < .001), extranodal sites ≥ 2 (p = .001), Ann-Arbor stage III–IV (p = .003), and International Prognostic Index (IPI) risk ≥ 3 (p < .001) showed significant association with reduced overall survival rate. Expression of c-MYC and co-expression of c-MYC/BCL2 were also related to inferior overall survival rate (p = .032 and p = .006, respectively). Among the PRC pathway markers (EZH2, SUZ12, EED, and H3K27me3), SUZ12$^{high}$ and H3K27me3$^{high}$ were related to inferior overall survival rate (p = .028 and p = .010, respectively) (Fig. 3A, B). *HOTAIR*$^{high}$, however, was significantly related to superior overall survival rate than *HOTAIR*$^{low}$ (p = .004) (Fig. 3C).

In multivariate analysis (Table 2), H3K27me3$^{high}$ revealed an independent effect on poor overall survival (hazard ratio, 2.0; p = .023). IPI risk ≥ 3 was still determined as an independent prognostic factor (hazard ratio, 3.5; p < .001), while *HOTAIR*$^{high}$ showed a tendency to be related to improved survival with marginal significance (hazard ratio, 0.5; p = .086).

## DISCUSSION

In our previous study, high level of global H3K27me3 was found to be a negative prognostic indicator in patients with DLBCL.[8] This subsequent study aimed to explore the role of *HOTAIR*, possibly functioning via induction of H3K27me3. We

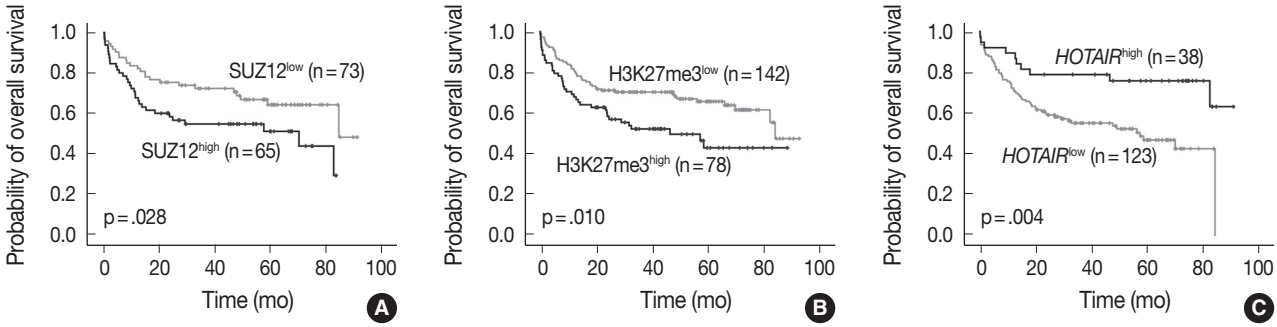


**Fig. 3.** Overall survival based on SUZ12 (A), H3K27me3 (B), and *HOTAIR* expression (C). High expression of SUZ12 (SUZ12$^{high}$) and H3K27me3 (H3K27me3$^{high}$) is related to inferior overall survival, while high expression of *HOTAIR* (*HOTAIR*$^{high}$) is correlated with longer overall survival than low levels of *HOTAIR* expression (*HOTAIR*$^{low}$). SUZ12, suppressor of zeste 12 homolog; HOTAIR, hox transcript antisense intergenic RNA.

**Table 1.** Clinicopathological characteristics, relation to outcome, and association with HOTAIR level in DLBCL patients

| Variable | No. (%) (n=164) | *HOTAIR* | | p-value |
|---|---|---|---|---|
| | | *HOTAIR*$^{low}$ | *HOTAIR*$^{high}$ | |
| Sex | | | | |
| Male | 98 (59.8) | 73 (58.4) | 25 (64.1) | .526 |
| Female | 66 (40.2) | 52 (41.6) | 14 (35.9) | |
| Age (yr) | | | | |
| ≤60 | 94 (57.3) | 69 (55.2) | 25 (64.1) | .326 |
| >60 | 70 (42.7) | 56 (44.8) | 14 (35.9) | |
| ECOG performance status[a] | | | | |
| <2 | 132 (80.5) | 96 (76.8) | 36 (92.3) | .033 |
| ≥2 | 32 (19.5) | 29 (23.2) | 3 (7.7) | |
| Ann-Arbor stage[a] | | | | |
| I–II | 89 (54.6) | 63 (50.8) | 26 (66.7) | .083 |
| III–IV | 74 (45.4) | 61 (49.2) | 13 (33.3) | |
| Extranodal sites[a] | | | | |
| <2 | 108 (66.3) | 81 (65.3) | 27 (69.2) | .653 |
| ≥2 | 55 (33.7) | 43 (34.7) | 12 (30.8) | |
| Lactate dehydrogenase[a] | | | | |
| Normal | 90 (55.2) | 65 (52.4) | 25 (64.1) | .201 |
| Elevated | 73 (44.8) | 59 (47.6) | 14 (35.9) | |
| IPI risk group[a] | | 79 (63.7) | 28 (71.8) | .354 |
| 0–2 | 107 (65.6) | 45 (36.3) | 11 (28.2) | |
| 3–5 | 56 (34.4) | | | |
| Hans classification[a] | | | | |
| GCB | 44 (28.0) | 32 (27.1) | 12 (30.8) | .660 |
| Non-GCB | 113 (72.0) | 86 (72.9) | 27 (69.2) | |
| EBV | | | | |
| Negative | 132 (88.0) | 98 (87.5) | 34 (89.5) | .746 |
| Positive | 18 (12.0) | 14 (12.5) | 4 (10.5) | |
| BCL2[a] | | | | |
| Negative expression | 84 (58.7) | 58 (54.7) | 26 (70.3) | .098 |
| Positive expression | 59 (41.3) | 48 (45.3) | 11 (29.7) | |
| c-MYC[a] | | | | |
| Negative expression | 92 (62.2) | 63 (57.3) | 29 (76.3) | .037 |
| Positive expression | 56 (32.8) | 47 (42.7) | 9 (23.7) | |
| c-MYC/BCL2[a] | | | | |
| No co-expression | 110 (77.5) | 76 (72.4) | 34 (91.9) | .015 |
| Co-expression | 32 (22.5) | 29 (27.6) | 3 (8.1) | |

Values are presented as number (%).
HOTAIR, hox transcript antisense intergenic RNA; DLBCL, diffuse large B-cell lymphoma; ECOG, Eastern Cooperative Oncology Group; IPI, International Prognostic Index; GCB, germinal center B-like; EBV, Epstein-Barr virus.
[a]Information not available in some cases.

found the positive correlation between PRC2 proteins, global H3K27me3 levels, and c-MYC in DLBCL as expected.

In the present study, the positive correlation among PRC2 proteins (EZH2, SUZ12, and EED), global H3K27me3 levels, and c-MYC was also confirmed in DLBCL as expected. In addition, *HOTAIR* expression was related to EZH2 expression. These findings could support that the lncRNA *HOTAIR* may be involved in inducing H3K27me3 through recruiting polycomb repressive complex, the methyltransferase EZH2 and core accessory proteins, SUZ12 and EED.

Based on many other studies, interaction between c-MYC and PRC2 (EZH2, SUZ12, and EED) is well known in the tumorigenesis of various cancer types including lymphomas. Protein c-MYC interacts with EZH2 as well as SUZ12/EED, and they induce the histone modification of H3K27me3 on the promoter of target genes, which then represses gene expression. Many other studies have shown that EZH2 and c-MYC activate each other.[13-15] From the present findings, it could be also suggested that c-MYC may be the possible mechanism for inducing H3K27me3 via PRC2-related pathways in DLBCLs.


http://dx.doi.org/10.4132/jptm.2016.06.06

**Table 2.** Cox proportional hazard analyses of overall survival

| Variable | Category | Univariate analysis p-value | Multivariate analysis p-value | HR | 95% CI |
|---|---|---|---|---|---|
| Age | >60 vs ≤60 | <.001 | - | - | - |
| ECOG PS | ≥2 vs <2 | <.001 | - | - | - |
| Ann-Arbor stage | III–IV vs I–II | .003 | - | - | - |
| Extranodal sites | ≥2 vs <2 | .001 | - | - | - |
| Lactate dehydrogenase | Elevated vs normal | <.001 | - | - | - |
| IPI risk group | 3–5 vs 0–2 | <.001 | <.001 | 3.5 | 1.9–6.3 |
| Hans classification | Non-GCB vs GCB | .16 | - | - | - |
| EBV | Positive vs negative | .611 | - | - | - |
| BCL2 | Positive vs negative | .076 | - | - | - |
| c-MYC | Positive vs negative | .032 | - | - | - |
| c-MYC/BCL2 | Co-expression vs no co-expression | .006 | .528 | 1.2 | 0.6–2.4 |
| EZH2 | High vs non-high | .883 | - | - | - |
| SUZ12 | High vs non-high | .028 | .183 | 1.5 | 0.8–2.7 |
| EED | High vs non-high | .25 | - | - | - |
| H3K27me3 | High vs non-high | .01 | .023 | 2 | 1.1–3.6 |
| *HOTAIR* | High vs non-high | .004 | .086 | 0.5 | 0.2–1.1 |

HR, hazard ratio; CI, confidence interval; ECOG PS, Eastern Cooperative Oncology Group performance status; IPI, International Prognostic Index; EBV, Epstein-Barr virus; EZH2, enhancer of zeste homolog 2; SUZ12, suppressor of zeste 12 homolog; EED, embryonic ectoderm development; HOTAIR, hox transcript antisense intergenic RNA.

In other studies of solid tumors originating from various organs, high expression of *HOTAIR* showed a close association with poor prognosis.[5] In the present study, however, high levels of *HOTAIR* expression showed an association with good prognosis in DLBCL, although the impact was not significant in the multivariate analysis. There are no comparable reports to support the present findings because this is the first study for the expression status of *HOTAIR* in hematologic malignancies.

Although interaction between c-MYC and *HOTAIR* has not been established in hematologic malignancies, a close relationship between them may be plausible when considering the close association of PRC2 and *HOTAIR*, and PRC2 and c-MYC. However, expression of c-MYC showed a negative correlation with *HOTAIR* in the present study. One of the possible reason is autoregulation of c-MYC reported in one study; c-MYC represses itself via forming autoregulatory loops with EZH[2,13] therefore, *HOTAIR* might be involved in that process via EZH2. Whether *HOTAIR* expression is directly linked to the suppression of c-MYC or H3K27me3 should be investigated in further functional studies. In the *HOTAIR*-related suppression of c-MYC, PRC2-associated histone modification (H3K27me3) might be induced in the promoter region of *c-MYC* gene. For confirmation of this possible modulation, further study should be followed.

The favorable outcome of DLBCLs with high *HOTAIR* expression might be associated with the negative correlation with c-MYC and/or BCL2. Recent evidence has shown that co-expression of c-MYC and BCL2 proteins is associated with poor prognosis in DLBCL patients regardless of gene signature.[11,12] This was also observed in the present study in the univariate survival analysis. When the factor of *HOTAIR* expression was added in the multivariate analysis; however, the prognostic effect of co-expression of c-MYC and BCL2 became weak, and only the factor of high H3K27me3 level was important as well as the IPI risk score. H3K27me3, the chromatin modification status induced via changes of *HOTAIR*, c-MYC, or other various known and unknown mechanisms, seems to be the most important factor in determining the fate of disease aggressiveness of DLBCL. Though little is known about the key role of *HOTAIR* in the malignant lymphoma, *HOTAIR* might be involved in regulation of various genes in the lymphomagenesis. Further study should follow to determine the explicit mechanism among the sophisticated modulatory networks of c-MYC, PRC2, H3K27me3, and *HOTAIR*.

Recent evidence has shown that inhibition of EZH2 methyltransferase activity provides a potential target therapy for EZH2-deregulated lymphomas. In addition, the pharmacological inhibition of EZH2 activity results in a decrease of global H3K27me3 levels and a reactivation of silenced *PRC2* gene targets, and it inhibits growth of DLBCL cells.[16,17] From these overall findings as well as the present findings, *HOTAIR* may also be used in a target therapy by modulating the c-MYC–EZH2/PRC2 loop in a subset of DLBCLs with a high level of H3K27me3.

In conclusion, we found frequent expression of PRC2 pro-

teins and H3K27me3 and positive correlation between these proteins and c-MYC in DLBCLs. High expression of H3K27me3 was determined as an independent predictor of poor prognosis, however, *HOTAIR* was associated with favorable overall survival, which can be partly explained by negative correlation with c-MYC. LncRNA *HOTAIR* expression could be one of the possible mechanisms to be involved in aggressive behavior of DLBCL via induction of H3K27me3 and EZH2-related PRC2 activation.

## Conflicts of Interest

No potential conflict of interest relevant to this article was reported.

## Acknowledgments

This work was supported by grant no. 2014-01 from the Korean Medical Women's Association.

## REFERENCES

1. Spizzo R, Almeida MI, Colombatti A, Calin GA. Long non-coding RNAs and cancer: a new frontier of translational research? Oncogene 2012; 31: 4577-87.
2. Wahlestedt C. Targeting long non-coding RNA to therapeutically upregulate gene expression. Nat Rev Drug Discov 2013; 12: 433-46.
3. Gupta RA, Shah N, Wang KC, *et al*. Long non-coding RNA *HOTAIR* reprograms chromatin state to promote cancer metastasis. Nature 2010; 464: 1071-6.
4. Qiu MT, Hu JW, Yin R, Xu L. Long noncoding RNA: an emerging paradigm of cancer research. Tumour Biol 2013; 34: 613-20.
5. Zhang S, Chen S, Yang G, *et al*. Long noncoding RNA *HOTAIR* as an independent prognostic marker in cancer: a meta-analysis. PLoS One 2014; 9: e105538.
6. Martin-Perez D, Piris MA, Sanchez-Beato M. Polycomb proteins in hematologic malignancies. Blood 2010; 116: 5465-75.
7. Bracken AP, Helin K. Polycomb group proteins: navigators of lineage pathways led astray in cancer. Nat Rev Cancer 2009; 9: 773-84.
8. Oh EJ, Yang WI, Cheong JW, Choi SE, Yoon SO. Diffuse large B-cell lymphoma with histone H3 trimethylation at lysine 27: another poor prognostic phenotype independent of c-Myc/Bcl2 coexpression. Hum Pathol 2014; 45: 2043-50.
9. Swerdlow SH, Campo E, Harris NL, *et al*. WHO classification of tumours of haematopoietic and lymphoid tissues. 4th ed. Lyon: IARC Press, 2008.
10. Hans CP, Weisenburger DD, Greiner TC, *et al*. Confirmation of the molecular classification of diffuse large B-cell lymphoma by immunohistochemistry using a tissue microarray. Blood 2004; 103: 275-82.
11. Johnson NA, Slack GW, Savage KJ, *et al*. Concurrent expression of MYC and BCL2 in diffuse large B-cell lymphoma treated with rituximab plus cyclophosphamide, doxorubicin, vincristine, and prednisone. J Clin Oncol 2012; 30: 3452-9.
12. Hu S, Xu-Monette ZY, Tzankov A, *et al*. MYC/BCL2 protein coexpression contributes to the inferior survival of activated B-cell subtype of diffuse large B-cell lymphoma and demonstrates high-risk gene expression signatures: a report from The International DLBCL Rituximab-CHOP Consortium Program. Blood 2013; 121: 4021-31.
13. Benetatos L, Vartholomatos G, Hatzimichael E. Polycomb group proteins and MYC: the cancer connection. Cell Mol Life Sci 2014; 71: 257-69.
14. Sander S, Bullinger L, Klapproth K, *et al*. MYC stimulates EZH2 expression by repression of its negative regulator miR-26a. Blood 2008; 112: 4202-12.
15. Neri F, Zippo A, Krepelova A, Cherubini A, Rocchigiani M, Oliviero S. Myc regulates the transcription of the *PRC2* gene to control the expression of developmental genes in embryonic stem cells. Mol Cell Biol 2012; 32: 840-51.
16. McCabe MT, Ott HM, Ganji G, *et al*. EZH2 inhibition as a therapeutic strategy for lymphoma with EZH2-activating mutations. Nature 2012; 492: 108-12.
17. Qi W, Chan H, Teng L, *et al*. Selective inhibition of Ezh2 by a small molecule inhibitor blocks tumor cells proliferation. Proc Natl Acad Sci U S A 2012; 109: 21360-5.

*Journal of Pathology and Translational Medicine 2016; 50: 377-384*
*http://dx.doi.org/10.4132/jptm.2016.07.25*

■ ORIGINAL ARTICLE ■

# Do Helper T Cell Subtypes in Lymphocytic Thyroiditis Play a Role in the Antitumor Effect?

Seok Woo Yang* · Seong-Ho Kang[1]* Kyung Rae Kim[2] · In Hong Choi[3] Hang Seok Chang[4] · Young Lyun Oh[5] Soon Won Hong[6]

Department of Medicine, Yonsei University Graduate School, Seoul; [1]Department of Laboratory Medicine, Chosun University College of Medicine, Gwangju; Departments of [2]Internal Medicine, [3]Microbiology, and [4]General Surgery, Yonsei University College of Medicine, Seoul; [5]Department of Pathology, Sungkyunkwan University College of Medicine, Seoul; [6]Department of Pathology, Rehabilitation Institute of Neuromuscular Disease, Yonsei University College of Medicine, Seoul, Korea

**Received:** April 25, 2016
**Revised:** July 8, 2016
**Accepted:** July 25, 2016

**Corresponding Author**
Soon Won Hong, MD
Department of Pathology, Yonsei University College of Medicine, 50-1 Yonsei-ro, Seodaemun-gu, Seoul 03722, Korea
Tel: +82-2-2019-3543
Fax: +82-2-3463-2103
E-mail: soonwonh@yuhs.ac

*Seok Woo Yang and Seong-Ho Kang contributed equally to this work.

**Background:** Papillary thyroid carcinoma (PTC) is frequently accompanied by lymphocytic thyroiditis (LT). Some reports claim that Hashimoto's thyroiditis (the clinical form of LT) enhances the likelihood of PTC; however, others suggest that LT has antitumor activity. This study was aimed to find out the relationship between the patterns of helper T cell (Th) cytokines in thyroid tissue of PTC with or without LT and the clinicopathological manifestation of PTC. **Methods:** Fresh surgical samples of PTC with (13 cases) or without (10 cases) LT were used. The prognostic parameters (tumor size, extra-thyroidal extension of PTC, and lymph node metastasis) were analyzed. The mRNA levels of two subtypes of Th cytokines, Th1 (tumor necrosis factor α [TNF-α], interferon γ [IFN-γ ], and interleukin [IL] 2) and Th2 (IL-4 and IL-10), were analyzed. Because most PTC cases were microcarcinomas and recent cases without clinical follow-up, negative or faint p27 immunoreactivity was used as a surrogate marker for lymph node metastasis. **Results:** PTC with LT cases showed significantly higher expression of TNF-α ($p = .043$), IFN-γ ($p < .010$), IL-4 ($p = .015$) than those without LT cases. Although the data were not statistically significant, all analyzed cytokines (except for IL-4) were highly expressed in the cases with higher expression of p27 surrogate marker. **Conclusions:** These results indicate that mixed Th1 (TNF-α, IFN-γ , and IL-2) and Th2 (IL-10) immunity might play a role in the antitumor effect in terms of lymph node metastasis.

**Key Words:** Thyroid cancer, papillary; Cytokines; Cyclin-dependent kinase inhibitor p27; T-lymphocytes, helper-inducer; Neoplasm metastasis; Lymphocytic thyroiditis

The annual incidence of thyroid cancer is variable across the globe; for males, 1.2–2.6 per 100,000 and for females, 2.0–3.8 per 100,000. The Unites States, Japan, Sweden, and France have higher than average incidence rates.[1,2] In South Korea, the incidence of thyroid cancer is 0.88 per 100,000 in males and 6.68 per 100,000 in females. Among thyroid cancers, papillary thyroid carcinoma (PTC) is the most common (83.8%).[3] Hence, the etiology, prognosis, and pathophysiology of PTC have been investigated extensively in research studies. Current studies focus on the molecular pathology (such as the roles of E-cadherin, c-Met, and epidermal growth factor receptor) and genetic alterations (such as *RET/PTC*, *TRK*, *BRAF*, and *p53*) of PTCs.[4] Most PTC cases are indolent and seldom behave aggressively, where aggressive behavior is characterized with frequent recurrences and metastases.[5] Shibru *et al*.[6] maintain that patients over the age of 45, with elevated expression levels of both cyclooxygenase 2 and vascular endothelial growth factor C, have a more aggressive PTC. Including this study, there have been many attempts to find prognostic factors for PTC. For instance, Kebebew *et al*.[7] has recently found that *BRAF* mutations are significantly associated with the aggressive behavior of thyroid cancer.

There have been many attempts to develop therapeutic vaccines for cancer.[8] Despite the many research studies on cancer immunotherapy, the role of immunity in the biological behavior

pISSN 2383-7837
eISSN 2383-7845

of PTC is still poorly understood. Among the limited data collected on the influence of immunity on PTC behavior are findings indicating an association between the immunity and the good prognosis in cases of PTC concomitant with Hashimoto's thyroiditis (HT) or lymphocytic thyroiditis (LT).[9,10]

It is traditionally assumed that tumor growth is suppressed by T-helper 1 cell (Th1) immunity and supported by T-helper 2 cell (Th2) immunity. However, even Th2 immunity can promote antitumor activity.[11] Th1 immunity activates cytotoxic CD8+ T lymphocytes (CTLs). Although CTLs can acquire antitumor immunity, some tumor cells escape CTL immune surveillance and survive. Hence, from a practical point of view, Th1 predominance in itself does not represent antitumor immunity. Th2 immunity provokes a humoral immune reaction, i.e., the antibody-synthesizing immunity. While components of the Th2 immunity, such as B cells and interleukin (IL) 10, make favorable conditions for tumor growth, tumor-infiltrating granulocyte-linked Th2 immunity promotes antitumor activity.[11]

Although there are relatively few reports about Th immunity and PTC, one by Mardente *et al*.[12] reported that a Th cytokine pattern from the peripheral blood of a patient with PTC with chronic LT has a predominantly Th2 immune reaction or mixed cell response. Intrathyroidal lymphocytes in HT are composed of both B cells and T cells, the majority of them are CD8+ T cells, which are cytotoxic to thyroid follicle cells.[13] PTCs are often associated with chronic LT and HT; for instance, Shull *et al*.[14] demonstrated that diffuse LT is associated with PTC without therapeutic histories. In addition, Mauras *et al*.[15] reported three cases of thyroid cancer with HT that did not have recurrent disease after a thyroidectomy. Therefore, it is difficult to determine which Th subtype immunity has superior antitumor activity over the other.

Several clinical trials have been conducted to induce cytotoxic immunity against thyroid cancers. Amino *et al*.[16] used saline homogenates of thyroid tumors, and Gerfo *et al*.[17] applied chemically altered thyroglobulins, but the clinical efficacy of these therapies have not been proven yet.

In the present work, we analyzed the pattern of Th immunity and investigated its relationship to the clinicopathological manifestation of PTC. With the current ease of early detection of PTCs, cases of advanced tumor stages are rare. Hence, we used a surrogate immunohistochemical marker, p27, to represent the possibility of lymph node metastasis, for it has been known that p27 expression is low in metastasizing PTC.[18]

## MATERIALS AND METHODS

### Case materials

After Institutional Review Board (IRB) approval (protocol No. 08-0194), 23 patients from the Department of Pathology, Gangnam Severance Hospital, were enrolled in this study. The patients ranged in age from 35 to 59 years old, with a mean age of 47. Fresh surgical samples of PTC with (13 cases) or without (10 cases) LT were collected from the records in the Department of Pathology with the patients' agreement and the formal permission of the IRB. The prognostic parameters (tumor size, extra-thyroidal extension of PTC, and lymph node metastasis) were analyzed. Among the subtypes of PTC samples in this group, 21 were of the most conventional type and two cases were follicular variants. The fresh thyroid tissues were divided into PTC and nontumor portions and sampled separately. The nontumor portions were used for measuring the mRNA quantities of the cytokines, and the PTC portions were subject to immunohistochemical staining of CIP1 (p21)/KIP1 (p27) for protein expression analysis, as described in more detail in later section.

### Measurement of cytokine expression levels in the thyroid tissue

The nontumor portions of the patient samples were used to measure the mRNA levels of the following cytokines: tumor necrosis factor α (TNF-α), interferon γ (IFN-γ), IL-2, IL-4, IL-10, and IL-1β. The 13 cases with concomitant PTC and LT were referred to as the objective group, and the 10 cases of PTC without LT were used as a reference or control group. Quantitative real-time polymerase chain reaction (PCR) was performed according to the manual of LightCycler 480 Real-Time PCR System (Roche Applied Science, Manheim, Germany).

The reference gene value (actin and 18S RNA) and IL-1β value were measured in every sample. Although it is known to be meaningless to compare the levels of cytokines from the same specimen, the expressed cytokine levels could be ranked and compared in this research via a quantitative real-time PCR method. Using the concept of relative quantification, the cytokine values were corrected for differences in quality and quantity by dividing the concentration of a target RNA by the concentration of a reference RNA in the same sample (relative ratio = concentration of target/concentration of reference). The most common way to compare expression levels of different samples is to designate one of the samples as calibrator, where all other samples are compared to this calibrator. For normalization of the final results, the target/reference ratio of each sample is divided by the


http://dx.doi.org/10.4132/jptm.2016.07.25

target/reference ratio of the calibrator sample: calibrator normalized ratio = (sample; concentration of target/concentration of reference)/(calibrator; concentration of target/concentration of reference).[19] In the present work, we applied the constitutively-expressed cytokine, IL-1β, as the calibrator. There were cytokine values expressed as "not detected." This means that the reference gene was calculated, but the target gene could not be detected despite many PCR amplification processes. In these cases, we adjusted these "not detected" values to zero (0).

### Immunohistochemistry

The immunohistochemistry (IHC) of the p27 protein expression in the PTC tumor tissue from all 23 cases was analyzed using paraffin-embedded tissue. Formalin-fixed paraffin-embedded sections (3 μm thick) were dewaxed in xylene and rehydrated through graded alcohols to water. Endogenous peroxidase activity was blocked in 3% hydrogen peroxide. Antigen retrieval was performed in citrate buffer (pH 6.0) within a microwave pressure cooker, and endogenous biotin detection was blocked with the Avidin-Biotin blocking kit (Vector Laboratories Inc., Burlingame, CA, USA).

Optimum primary antibody dilutions were predetermined, and appropriate positive control samples (tissues known to be positive for the immunohistochemical marker) and negative control samples (test tissue sections without the addition of primary antibody) were used for p27 (Novocastra, Newcastle upon Tyne, UK). The primary antibody incubation was diluted at 1:200 for 1 hour. After incubation, the slide was washed with phosphate buffered saline, and a secondary incubation was carried out with biotin anti-mouse/anti-rabbit IgG followed by streptavidin-HRP (Signet Pathology System, Dedham, MA, USA) for 30 minutes. The immunoreaction was revealed by incubation in 3-amino-9-ethylcarbazole. The slides were counterstained with hematoxylin and mounted in balsam.

When p27 immunoreaction was interpreted, only the nuclear staining on PTC cells was regarded as positive. Its measurement was evaluated by the following two-tiered grading system: low grade (negative staining or faint staining in less than 30% of the tumor cells) and high grade (positive staining in more than 30% of the tumor cells) (Fig. 1).[20] Nuclear p27 immunoreactivity was considered altered when the expression was less than 30% of previously published, clinically relevant levels. In 21 cases, the results of IHC were summarized in two groups: the cases with LT (n = 13) and the cases without LT (n = 8). Two cases were not performed, for the IHC sections for p27 were devoid of tumor tissue.

### Statistical analysis

The Pearson chi-square test was used to examine the relationships of cytokines (TNF-α, IFN-γ, IL-2, IL-4, IL-10, and IL-1β) and p27 expression with the clinicopathological characteristics. All reported p-values were 2-sided, and the significance was set at .05. All statistical tests were performed with SPSS ver. 17.0 (SPSS Inc., Chicago, IL, USA).

## RESULTS

### Clinical manifestations and histopathological findings

#### *PTC with LT (n = 13)*

The subtypes of the PTCs with LT were determined to be the

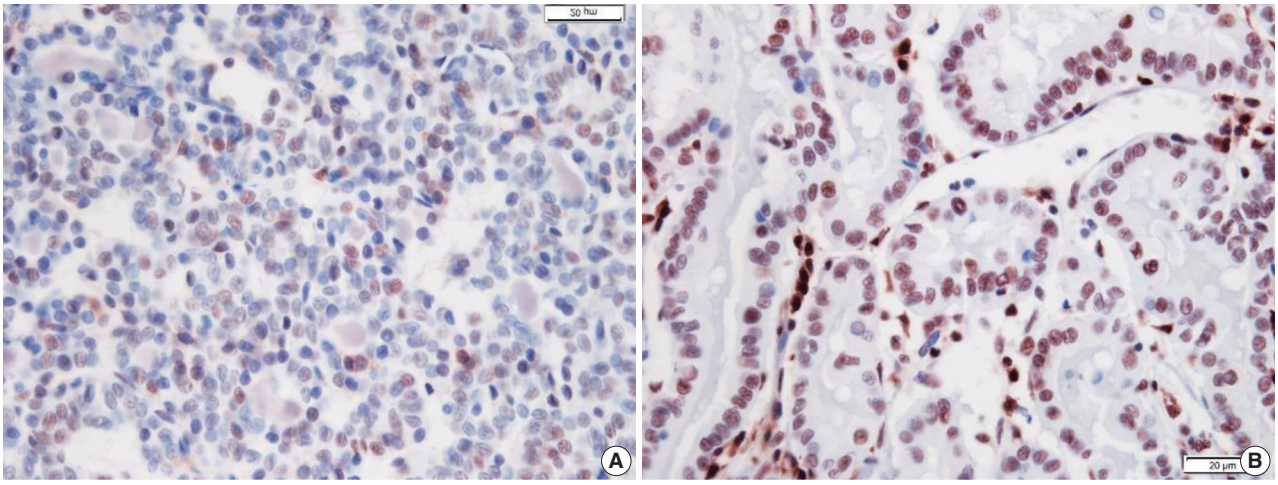


**Fig. 1.** p27 immunoreactivity (nuclear staining) on papillary thyroid carcinoma cells. Two-tiered grading system reveals a low grade (A, negative staining or faint staining less than 30% of tumor cells) and a high grade (B, positive staining more than 30% of tumor cells).

most conventional (11/13, 84.61%), and those of only two cases were follicular variants (2/13, 15.38%). The tumor sizes ranged from 0.2 to 1.1 cm, with an average of 0.55 cm. Of the 13 cases of this type, six cases showed extrathyroidal tumor extension (ET) (6/13, 46.15%), and two cases presented with lymph node metastasis (2/13, 15.38 %).

*PTC without LT (n = 10)*

The subtypes of the PTCs with LT were all conventional (10/10, 100%). Three cases with ET were present (3/10, 30%). Tumor sizes ranged from 0.1 to 1.5 cm, with an average of 0.61 cm. There were three cases with lymph node metastasis (3/10, 30%).

*Cytokine immune profiles*

In all 23 cases, the cytokine immune profiles were summarized into two groups: the cases with LT (n = 13) and the cases without LT (n = 10). The cytokines could have originated from inflammatory cells, thyroid tissue, and endothelial cells. In this research, the tissues were from the thyroid tissue near PTC.

*PTC with LT (n = 13)*

After manipulating the data using the concept of a calibrator with IL-1β, each sample of PTC with LT was compared (Table 1). Among the six cytokines analyzed, TNF-α, IL-4, and IFN-γ were relatively well expressed. Based on these factors, the cytokine expression in the PTC samples with LT represented a mixed Th1 (TNF-α and IFN-γ) and Th2 (IL-4 and IL-10) immunity.

*PTC without LT (n = 10)*

After manipulating data using the concept of a calibrator with IL-1β, each sample of PTC without LT was compared (Table 2). In contrast to the cases of PTC with LT, the cases without LT frequently exhibited nondetectable cytokine levels. Among the six cytokines analyzed, the expression levels of IFN-γ, IL-

**Table 1.** Cytokine and immune profiles of the cases with lymphocytic thyroiditis (n = 13)

| Case No. | TNF-α/IL-1β | IL-4/IL-1β | IFN-γ/IL-1β | IL-10/IL-1β | IL-2/IL-1β |
|---|---|---|---|---|---|
| 1 | 81.28 | 47.94 | 11.15 | 0.14 | 0 |
| 2 | 4,130.98 | 3173.80 | 1163.73 | 0 | 0 |
| 3 | 3,328.36 | 2686.57 | 946.27 | 0 | 0 |
| 4 | 198.41 | 145.50 | 64.68 | 0.20 | 0 |
| 5 | 276.08 | 258.27 | 93.89 | 0.73 | 0.09 |
| 6 | 5,275.74 | 4,871.32 | 1,875.00 | 0 | 0 |
| 7 | 2,454.55 | 2,227.27 | 954.55 | 7.88 | 3.10 |
| 8 | 108.88 | 91.54 | 40.36 | 1.39 | 0.25 |
| 9 | 242.84 | 242.84 | 46.20 | 0.18 | 0 |
| 10 | 141.74 | 135.65 | 43.39 | 0.20 | 0.10 |
| 11 | 4.21 | 0.03 | 0.05 | 0.04 | 0 |
| 14 | 5.81 | 1.54 | 0.39 | 0.11 | 0.09 |
| 16 | 2.32 | 0 | 0.12 | 0.05 | 0 |
| Median | 198.41 | 145.5 | 46.2 | 0.16 | 0 |

TNF-α, tumor necrosis factor α; IL, interleukin; IFN-γ, interferon γ.

**Table 2.** Cytokine and immune profiles of the cases without lymphocytic thyroiditis (n = 10)

| Case No. | TNF-α/IL-1β | IL-4/IL-1β | IFN-γ/IL-1β | IL-10/IL-1β | IL-2/IL-1β |
|---|---|---|---|---|---|
| 12 | 5.67 | 0.18 | 0 | 0.13 | 0 |
| 13 | 3.41 | 0 | 0.09 | 0 | 0 |
| 15 | 28.04 | 16.16 | 0 | 0 | 0 |
| 17 | 11.93 | 1.05 | 0 | 0.36 | 0 |
| 18 | 43.76 | 0 | 0 | 0 | 0 |
| 19 | 62.07 | 22.07 | 0 | 1.71 | 0.25 |
| 20 | 5.06 | 0.08 | 0 | 0.10 | 0 |
| 22 | 512.61 | 277.47 | 5.21 | 0 | 0 |
| 23 | 8.19 | 2.56 | 1.66 | 0.02 | 0.03 |
| 25 | 32.47 | 0 | 0 | 2.18 | 0 |
| Median | 19.98 | 0.61 | 0 | 0.06 | 0 |

TNF-α, tumor necrosis factor α; IL, interleukin; IFN-γ, interferon γ.


http://dx.doi.org/10.4132/jptm.2016.07.25

**Table 3.** Relationship between clinical parameters and the cases with lymphocytic thyroiditis

| Variable | LT (n=13) | Non-LT (n=10) | p-value |
|---|---|---|---|
| Tumor size (cm) | 0.50 (0.20–1.10) | 0.50 (0.10–1.50) | .707 |
| Extrathyroidal extension | 6 (46.15) | 3 (30) | .669 |
| Lymph nodal metastasis | 2 (15.38) | 3 (30) | .617 |
| LG p27 (n=14) | 8/13 (61.53) | 6/10 (60) | .655 |
| TNF-α | 198.41 (2.32–5,275.74) | 19.98 (3.41–512.61) | .043 |
| IL-4 | 145.50 (0–4,871.32) | 0.61 (0–277.47) | .015 |
| IFN-γ | 46.20 (0.05–1,875.00) | 0 (0–5.21) | <.001 |
| IL-10 | 0.14 (0–3.10) | 0.06 (0–0.25) | .508 |
| IL-2 | 0 (0–3.10) | 0 (0–0.25) | .322 |

Values are presented as median (range) or number (%).
The cytokine unit value is the ratio of each cytokine to IL-1β.
LT, cases with lymphocytic thyroiditis; Non-LT, cases without lymphocytic thyroiditis; LG p27, low-grade expression of p27 immunohistochemistry; TNF-α, tumor necrosis factor α; IL, interleukin; IFN-γ, interferon γ.

10, and IL-2 levels were too low to be measured. Based on these data, the cytokines expressed in PTC without LT represented a mixed Th1 (TNF-α) and Th2 (IL-4 and IL-1β) immunity.

### Prognostic parameters according to the presence of LT

The prognostic parameters (tumor size, ET, and lymph node metastasis) were not statistically related to LT, but the cases without LT had a tendency for lymph node metastasis (Table 3).

The cases with LT had enhanced expression of the cytokines (TNF-α, IFN-γ, IL-4, IL-10, and IL-2) compared to the samples of PTC without LT. Among the five cytokines, the expression levels of TNF-α, IFN-γ, and IL-4 were significantly higher in the cases with LT than in those without LT ($p < .05$).

In terms of p27 as a surrogate marker for lymph node metastasis, the degree of p27 expression was not correlated with lymph node metastasis in this study; high-grade expression of p27 had a tendency to occur in PTC cases with LT. In contrast, lymph node metastasis occurred slightly more frequently in PTC cases without LT. Conclusively, the degree of p27 expression did not show any correlation with lymph node metastasis in this study ($p = .15$) (Table 4).

### Cytokine immune profiles and clinical implications of the PTC cases with LT

Due to this unexpected finding, which revealed in the insufficiency of the PTC cases without LT to serve as a reference group, this study adopted a new goal to use the PTC cases with LT to analyze the relationship between cytokine immune profiles and prognostic parameters. In addition, the PTC cases in this study were mostly microcarcinomas, which might represent the incipient phase of the tumors. The incipient phase of tumors must always have a limitation in representing proper tumor staging, such as tumor size, nodal metastasis, and tumor extension. Hence, in this study, p27 was used as a surrogate marker of lymph node metastasis in the cases of microcarcinoma (as an incipient carcinoma).

**Table 4.** Relationship between p27 immunopositivity and lymph nodal metastasis

| Variable | Lymph nodal metastasis (n=5) | Without lymph nodal metastasis (n=18) |
|---|---|---|
| LG p27 (n=14) | 3/5 (60) | 11/18 (61.11) |
| HG p27 (n=7) | 1/5 (20) | 6/18 (33.33) |

Values are presented as number (%).
LG p27, low-grade expression of p27 immunohistochemistry; HG p27, high-grade expression of p27 immunohistochemistry.

Therefore, the statistical analysis of this profiles solely made use of the PTC cases with LT. Except for the IL-4 cytokine, the expression levels of the cytokines TNF-α, IFN-γ, and IL-10 were lower in the cases with low-grade expression of p27 than those with high-grade expression of p27, but there was no statistical significance (Table 5). The cases with ET had a tendency to demonstrate higher levels of cytokine expression than those with intrathyroidal tumor confinement (Table 6). Again, there was no statistical significance.

In summary, although the data were not statistically significant, the trends follow a pattern where higher cytokine levels were present in the cases with high grade expression of p27 (except for IL-4) and ET.

## DISCUSSION

This study revealed the presence of mixed Th1 (IFN-γ, TNF-α, and IL-2) and Th2 (IL-4 and IL-10) immunity in lymphocytes in cases of PTC with LT.

Although there is no statistical significance with a limited case number, this study could infer some meaningful results.

**Table 5.** Relationship between p27 immunopositivity and the cytokine immune profiles in the cases with lymphocytic thyroiditis (n=13)

| Cytokine | LG p27 (n=8) | HG p27 (n=5) | p-value |
|---|---|---|---|
| TNF-α | 76.32 (2.32–4,130.98) | 81.28 (5.81–5,275.74) | .390 |
| IL-4 | 53.85 (0–3,173.80) | 47.94 (1.54–4,871.32) | .313 |
| IFN-γ | 2.66 (0–1,163.73) | 11.15 (0–1,875) | .430 |
| IL-10 | 0.07 (0–7.88) | 0.11 (0–1.71) | 1.000 |
| IL-2 | 0 (0–3.10) | 0 (0–0.25) | .755 |

Values are presented as median (range). The cytokine unit value is the ratio of each cytokine to IL-1β.
LG p27, low-grade expression of p27 immunohistochemistry; HG p27, high grade expression of p27 immunohistochemistry; TNF-α, tumor necrosis factor α; IL, interleukin; IFN-γ, interferon γ.

**Table 6.** Relationship between cytokine levels and tumor extension in the cases with lymphocytic thyroiditis (n=13)

| Cytokine | ET (n=6) | IT (n=7) | p-value |
|---|---|---|---|
| TNF-α | 43.54 (2.32–4,130) | 28.04 (5.06–512.61) | 1.000 |
| IL-4 | 24.74 (0–3,173) | 16.16 (0.08–277.47) | 1.000 |
| IFN-γ | 5.77 (0.05–1,163.73) | 0 (0–5.21) | .153 |
| IL-10 | 0.08 (0–7.88) | 0 (0–0.10) | .237 |
| IL-2 | 0 (0–0.10) | 0 (0) | .376 |

Values are presented as median (range). The cytokine unit value is the ratio of each cytokine to IL-1β.
ET, extrathyroidal tumor extension; IT, intrathyroidal tumor confinement; TNF-α, tumor necrosis factor α; IL, interleukin; IFN-β, interferon β.

In the cases with LT, the higher expression of cytokine levels had a tendency to be associated with high p27 immuno-reactivity (Table 5). Furthermore, except for IL-4, all cytokines were decreased in the cases with LT and p27 underexpression, which represents the increased possibility of lymph node metastasis. Because IL-4 is associated with aggressive PTC, the fact that all cytokine except IL-4 were highly expressed in the cases with LT and increased p27 expression supports the hypothesis that high expression of cytokines except IL-4 may contribute to anticancer effect on the PTC in terms of lymph node metastasis.[21]

In contrast, the cases with ET revealed the higher expression of cytokines than those without ET. Based on these results, we propose that the higher expression of cytokines TNF-α, IFN-γ, IL-2, and IL-1 might inhibit nodal metastasis but not inhibit (or possibly enhance) the extrathyroidal extension. In view of helper T cell immunity, mixed Th1 and Th2 immunity seems to play a role in anticancer activity by inhibiting lymph node metastasis.

There have been several studies on the immune profiles of thyroiditis. Among them, Phenekos *et al*.[22] reported that HT and Graves' disease have two different helper T cell immunities. In their report, with the preferential expression of IL-2, IFN-γ, IL-12, and IL-18, a Th1 pattern of immune response which is characteristic of cellular immunity, is dominant in HT. In contrast, Ajjan *et al*.[23] reported a mixed Th1 and Th2 immune response in HT cases. They reported that reverse transcription polymerase chain reaction results showed both Th1 and Th2 immunity. The findings in our study corroborate these results.

Our findings demonstrated that IL-4 expression, together with other cytokines, has a tendency to be higher in the cases with ET. This may mean that IL-4 contributes to tumor extension. In contrast, in the cases with underexpression of p27, which may represent lymph node metastasis, IL-4 was higher than other cytokines. This may imply that IL-4 contributes to the lymphatic spread of the tumor, a concept that is supported by Vella *et al*.[21] who demonstrated that IL-4 levels were augmented in aggressive PTCs. They suggested that PTC cells receive protection from apoptosis by IL-4 production in the activated T lymphocytes of thyroid glands. To determine which of these conflicting results in terms of both nodal metastasis and capsular tumor extension are correct, further study may be necessary to disclose the role of IL-4 in PTC biological behavior.

A previous work by Yip *et al*.[24] demonstrated with *in vitro* tests that IL-1β was an anticancer factor, which suppressed the proliferation and reduced the invasive potential of human PTC cells. In this study, IL-1β was found to be constitutively expressed in all cases and was used as a calibrator to compare cytokine levels among the cases. Unfortunately, due to its use as a calibrator in this study, IL-1β expression levels in each case could not be compared.

It is generally accepted that there is a beneficial relationship between chronic LT and the biological behavior of PTC, which results in improved prognoses. Paulson *et al*.[25] suggested that chronic LT might have a protective role in tumor spread. Supporting this evidence, Mitsiades *et al*.[26] reported that Th1 cytokines, such as IFN-γ and TNF-α, increase the sensitivity of both normal and neoplastic thyrocytes to FasL and TRAIL, which lead to apoptosis. Furthermore, Ahn *et al*.[27] established that HT was associated with PTC, as was chronic inflammation with cancer in other locations. They also mentioned that the coexistence of HT in PTC cases introduced favorable clinical outcomes compared with those of PTC without HT.[27] Corroborating this idea, Yoon *et al*.[28] determined that patients with PTC and chronic LT had smaller tumor sizes, a lower incidence of capsular invasion, and a significantly lower incidence of lymph node metastases compared to patients without chronic LT. Several studies have also indicated that antithyroid antibodies are able to recognize these malignant cells and destroy them in the same way that they destroy normal follicular cells, contributing to the low rate of clinical progression of these lesions.[29,30]

The p27 protein was first identified as an inhibitor of cyclin E/


http://dx.doi.org/10.4132/jptm.2016.07.25

CDK2 complexes during transforming growth factor β–induced G1 arrest.[31] Phosphorylation is the mechanism primarily used for regulating p27 activity. The p27 protein possesses multiple tyrosine, serine, or threonine phosphorylation sites. The inhibitory roles of p27 towards cyclin/CDK complexes are weakened by phosphorylation directed by certain signal transduction pathways.[32] The current model delineates that p27 suppresses tumorigenesis by inhibiting cyclin/CDK activity in the nucleus, but it exerts other functions in the cytoplasm that are potentially oncogenic.[33]

There have been several clinical studies describing the relationship between the expression of p27 and lymph node metastasis. Karlidag *et al*.[18] reported that p27 expression in nonmetastasizing PTC was lower than that in normal thyroid tissue and higher than that in metastasizing PTC.

Our IHC analysis showed that p27 expression did not demonstrate any relationship to lymph node metastasis in PTC with LT, but this may be attributed to the early stage of the tumors, i.e., our study mainly included patients with microcarcinomas. There may be a chance that even PTC cases with low expression of p27 were too incipient to reveal lymph node metastasis. With this limitation in the evaluation of the relationship between cytokine levels and nodal metastasis, the common p27 marker was used as a surrogate marker to represent the possibility of nodal metastasis in early phase PTCs. As aforementioned, after focusing on the cases with LT, the cases with low-grade expression of p27 tended to be associated with lower levels of cytokines than those with high-grade expression of p27. This may implicate that the cases with lower levels of mixed Th1 and Th2 cytokines have a higher probability of having lymph node metastasis.

Considering the low cytokine expression in the cases with underexpression of p27 (except for IL-4), our results indicate that mixed Th1 and Th2 immune cytokines have a tendency toward anticancer effects in terms of lymph node metastasis. To predict tumor prognosis from cytokine levels, further studies determining the absolute values and IHC of cytokines will be necessary.

## Conflicts of Interest

No potential conflict of interest relevant to this article was reported.

## Acknowledgments

This work is funded by a grant of 2015 Korean Thyroid Association. We thank Su Jin Jeong. Without her endeavors and precise experimentation, the data for this research would not be as accurate.

## REFERENCES

1. Kuijpens JL, Coebergh JW, van der Heijden LH, Kruis H, Ribot JG, de Rooij HA. Thyroid cancer in Southeastern Netherlands, 1970-1989: trends in incidence, treatment and survival. Ned Tijdschr Geneeskd 1994; 138: 464-8.
2. Laurberg P, Nøhr SB, Pedersen KM, *et al*. Thyroid disorders in mild iodine deficiency. Thyroid 2000; 10: 951-63.
3. Ministry for Health, Welfare and Family Affairs; Korea Central Cancer Registry. Cancer incidence in Korea 1999-2002. Goyang: Korea Central Cancer Registry, 2008.
4. Sobrinho-Simoes M, Preto A, Rocha AS, *et al*. Molecular pathology of well-differentiated thyroid carcinomas. Virchows Arch 2005; 447: 787-93.
5. Siironen P, Louhimo J, Nordling S, *et al*. Prognostic factors in papillary thyroid cancer: an evaluation of 601 consecutive patients. Tumour Biol 2005; 26: 57-64.
6. Shibru D, Chung KW, Kebebew E. Recent developments in the clinical application of thyroid cancer biomarkers. Curr Opin Oncol 2008; 20: 13-8.
7. Kebebew E, Weng J, Bauer J, *et al*. The prevalence and prognostic value of *BRAF* mutation in thyroid cancer. Ann Surg 2007; 246: 466-70.
8. Finke LH, Wentworth K, Blumenstein B, Rudolph NS, Levitsky H, Hoos A. Lessons from randomized phase III studies with active cancer immunotherapies--outcomes from the 2006 meeting of the Cancer Vaccine Consortium (CVC). Vaccine 2007; 25 Suppl 2: B97-109.
9. McConahey WM, Hay ID, Woolner LB, van Heerden JA, Taylor WF. Papillary thyroid cancer treated at the Mayo Clinic, 1946 through 1970: initial manifestations, pathologic findings, therapy, and outcome. Mayo Clin Proc 1986; 61: 978-96.
10. Singh B, Shaha AR, Trivedi H, Carew JF, Poluri A, Shah JP. Coexistent Hashimoto's thyroiditis with papillary thyroid carcinoma: impact on presentation, management, and outcome. Surgery 1999; 126: 1070-6.
11. Ellyard JI, Simson L, Parish CR. Th2-mediated anti-tumour immunity: friend or foe? Tissue Antigens 2007; 70: 1-11.
12. Mardente S, Lenti L, Lococo E, *et al*. Phenotypic and functional characterization of lymphocytes in autoimmune thyroiditis and in papillary carcinoma. Anticancer Res 2005; 25: 2483-8.
13. Baker JR Jr, Fosso CK. Immunological aspects of cancers arising from thyroid follicular cells. Endocr Rev 1993; 14: 729-46.
14. Shull JH, Sharon N, Victor TA, Scanlon EF. Thyroid carcinoma: im-

munology, irradiation, and lymphocytic infiltration. Arch Surg 1979; 114: 729-31.
15. Mauras N, Zimmerman D, Goellner JR. Hashimoto thyroiditis associated with thyroid cancer in adolescent patients. J Pediatr 1985; 106: 895-8.
16. Amino N, Pysher T, Cohen EP, Degroot LJ. Immunologic aspects of human thyroid cancer: humoral and cell-mediated immunity, and a trial of immunotherapy. Cancer 1975; 36: 963-73.
17. Gerfo PL, Feind C, Weber C, Ting W. Immunotherapy of thyroid cancer by induction of autoimmune thyroiditis. Surgery 1983; 94: 959-65.
18. Karlidag T, Cobanoglu B, Keles E, *et al*. Expression of Bax, p53, and p27/kip in patients with papillary thyroid carcinoma with or without cervical nodal metastasis. Am J Otolaryngol 2007; 28: 31-6.
19. Pfaffl MW. A new mathematical model for relative quantification in real-time RT-PCR. Nucleic Acids Res 2001; 29: e45.
20. Resnick MB, Schacter P, Finkelstein Y, Kellner Y, Cohen O. Immunohistochemical analysis of p27/kip1 expression in thyroid carcinoma. Mod Pathol 1998; 11: 735-9.
21. Vella V, Mineo R, Frasca F, *et al*. Interleukin-4 stimulates papillary thyroid cancer cell survival: implications in patients with thyroid cancer and concomitant Graves' disease. J Clin Endocrinol Metab 2004; 89: 2880-9.
22. Phenekos C, Vryonidou A, Gritzapis AD, Baxevanis CN, Goula M, Papamichail M. Th1 and Th2 serum cytokine profiles characterize patients with Hashimoto's thyroiditis (Th1) and Graves' disease (Th2). Neuroimmunomodulation 2004; 11: 209-13.
23. Ajjan RA, Watson PF, McIntosh RS, Weetman AP. Intrathyroidal cytokine gene expression in Hashimoto's thyroiditis. Clin Exp Immunol 1996; 105: 523-8.
24. Yip I, Pang XP, Berg L, Hershman JM. Antitumor actions of interferon-gamma and interleukin-1 beta on human papillary thyroid carcinoma cell lines. J Clin Endocrinol Metab 1995; 80: 1664-9.
25. Paulson LM, Shindo ML, Schuff KG. Role of chronic lymphocytic thyroiditis in central node metastasis of papillary thyroid carcinoma. Otolaryngol Head Neck Surg 2012; 147: 444-9.
26. Mitsiades CS, Poulaki V, Mitsiades N. The role of apoptosis-inducing receptors of the tumor necrosis factor family in thyroid cancer. J Endocrinol 2003; 178: 205-16.
27. Ahn D, Heo SJ, Park JH, *et al*. Clinical relationship between Hashimoto's thyroiditis and papillary thyroid cancer. Acta Oncol 2011; 50: 1228-34.
28. Yoon YH, Kim HJ, Lee JW, Kim JM, Koo BS. The clinicopathologic differences in papillary thyroid carcinoma with or without co-existing chronic lymphocytic thyroiditis. Eur Arch Otorhinolaryngol 2012; 269: 1013-7.
29. Boi F, Lai ML, Marziani B, Minerba L, Faa G, Mariotti S. High prevalence of suspicious cytology in thyroid nodules associated with positive thyroid autoantibodies. Eur J Endocrinol 2005; 153: 637-42.
30. Lucas SD, Karlsson-Parra A, Nilsson B, *et al*. Tumor-specific deposition of immunoglobulin G and complement in papillary thyroid carcinoma. Hum Pathol 1996; 27: 1329-35.
31. Larrea MD, Liang J, Da Silva T, *et al*. Phosphorylation of p27Kip1 regulates assembly and activation of cyclin D1-Cdk4. Mol Cell Biol 2008; 28: 6462-72.
32. Lee J, Kim SS. The function of p27 KIP1 during tumor development. Exp Mol Med 2009; 41: 765-71.
33. Khoo ML, Beasley NJ, Ezzat S, Freeman JL, Asa SL. Overexpression of cyclin D1 and underexpression of p27 predict lymph node metastases in papillary thyroid carcinoma. J Clin Endocrinol Metab 2002; 87: 1814-8.

 http://dx.doi.org/10.4132/jptm.2016.07.25

*Journal of Pathology and Translational Medicine 2016; 50: 385-389*
*http://dx.doi.org/10.4132/jptm.2016.03.26*

■ CASE STUDY ■

# Mammary-Type Myofibroblastoma: A Report of Two Cases

Soyeon An · Joon Seon Song
Soonchan Park[1] · Jung Won Lee[2]
Kyung-Ja Cho

Department of Pathology, Asan Medical Center, University of Ulsan College of Medicine, Seoul; [1]Department of Radiology, Kyung Hee University Hospital at Gangdong, Kyung Hee University School of Medicine, Seoul; [2]Department of Surgery, Asan Medical Center, University of Ulsan College of Medicine, Seoul, Korea

**Received:** December 8, 2015
**Revised:** March 11, 2016
**Accepted:** March 26, 2016

**Corresponding Author**
Joon Seon Song, MD, PhD
Department of Pathology, Asan Medical Center, University of Ulsan College of Medicine, 88 Olympic-ro 43-gil, Songpa-gu, Seoul 05505, Korea
Tel: +82-2-3010-4548
Fax: +82-2-472-7898
E-mail: Songjs@amc.seoul.kr

Mammary-type myofibroblastoma (MFB) is a rare, benign spindle cell neoplasm occurring along the milkline, with extension from the mid-axilla to the medial groin. It is histologically and immunohistochemically identical to MFB of the breast and is part of a spectrum of lesions that includes spindle cell lipoma and cellular angiofibroma. Recently, we experienced two cases of mammary-type MFB involving male patients aged 30 and 58 years, respectively. The tumors were located in the right scrotal sac and in the right axilla. Wide excisions were performed. Microscopically, the masses were composed of haphazardly arranged, variably sized fascicles of bland spindle cells and were admixed with mature fat tissue. The spindle cells in both cases showed immunopositivity for desmin and CD34 and negativity for smooth muscle actin. Loss of retinoblastoma (RB)/13q14 loci is a characteristic genetic alteration of mammary-type MFB, and we identified loss of RB protein expression by immunohistochemical staining. We emphasize the importance of awareness of this rare neoplasm when a spindle cell neoplasm is accompanied by desmin immunopositivity. The second patient was alive without recurrence for 20 months, and the first patient had not been followed.

**Key Words:** Mammary-type myofibroblastoma; Milkline; 13q14

Mammary-type myofibroblastoma (MFB) is a rare, benign spindle cell neoplasm with myofibroblastic differentiation that is histologically identical to MFB of the breast and was first described by Wargotz *et al*. in 1987.[1] The tumor occurs mainly in older men and postmenopausal women. The age at presentation ranges from 35 to 85 years.[2,3] Common locations are along the embryonic milkline with extension from the mid-axilla to the medial groin.[2] The most common presentation is a painless, slowly growing mass.[2,4] The tumor is composed of bland spindle cells with myofibroblastic differentiation, prominent mast cells, fatty component, and hyalinized stroma. Recently, we experienced two cases of mammary-type MFB in the right scrotal sac of a 30-year-old man and in the right axilla of a 58-year-old man. In this report, we describe these two rare cases of mammary-type MFB.

## CASE REPORT

### Case 1

A 30-year-old previously healthy man presented with a solitary palpable mass in his right scrotal sac, which appeared 3 months earlier. He had no history of trauma or medical disease. The mass was painless, firm, and movable on physical examination. Abdominal/pelvic computed tomography (CT) showed a 5.0 cm mass in the right scrotal sac, separated from the adjacent testis and spermatic cord (Fig. 1A). Due the possibility of a mesenchymal tumor, excision was performed.

Grossly, the lesion was well-circumscribed and ovoid, measuring 5.0×3.5×2.0 cm. The cut surface of the mass was yellowish tan, rubbery, and trabeculated, without necrosis or hemorrhage (Fig. 2A). Microscopically, the mass was composed of bland spindle cells with haphazardly arranged collagen fibers and numerous mast cells. Some areas showed edematous stroma with hypocellularity. Numerous mast cells were scattered in the stroma (Fig. 2B). There was no cellular atypia or mitotic activity. Individual adipocytes and adipose tissue were admixed with the spindle cells, which showed immunopositivity for desmin (1:200, Dako, Glostrup, Denmark) and CD34 (1:500, Immunotech, Marseille, France) (Fig. 2C, D) and negativity for smooth muscle actin

pISSN 2383-7837
eISSN 2383-7845

(1:200, Dako), S-100 protein (1:100, Zymed, San Francisco, CA, USA), and human melanoma black 45 (1:50, Dako).

## Case 2

A 58-year-old man presented with a slowly growing right axillary mass that had appeared 15 months earlier. A chest CT revealed a 5.5-cm lobulated mass with infiltration of the surrounding soft tissue in the right axilla (Fig. 1B). Because of the possibility of metastatic carcinoma of unknown origin, a needle biopsy was performed. The diagnosis was low-grade spindle cell neoplasm with myofibroblastic differentiation. A wide excision was then performed. No evidence of recurrence was noted after 20 months of follow-up.

The mass was well-circumscribed, measuring 6.2×5.2×4.5


**Fig. 1.** Radiologic findings for the two study cases. (A) In case 1, a pelvis computed tomography (CT) shows 5.0 cm mass in the right scrotal sac separated from the adjacent testis and spermatic cord (arrow). (B) In case 2, a chest CT shows a 5.5 cm lobulated mass in the right axilla (arrowhead).

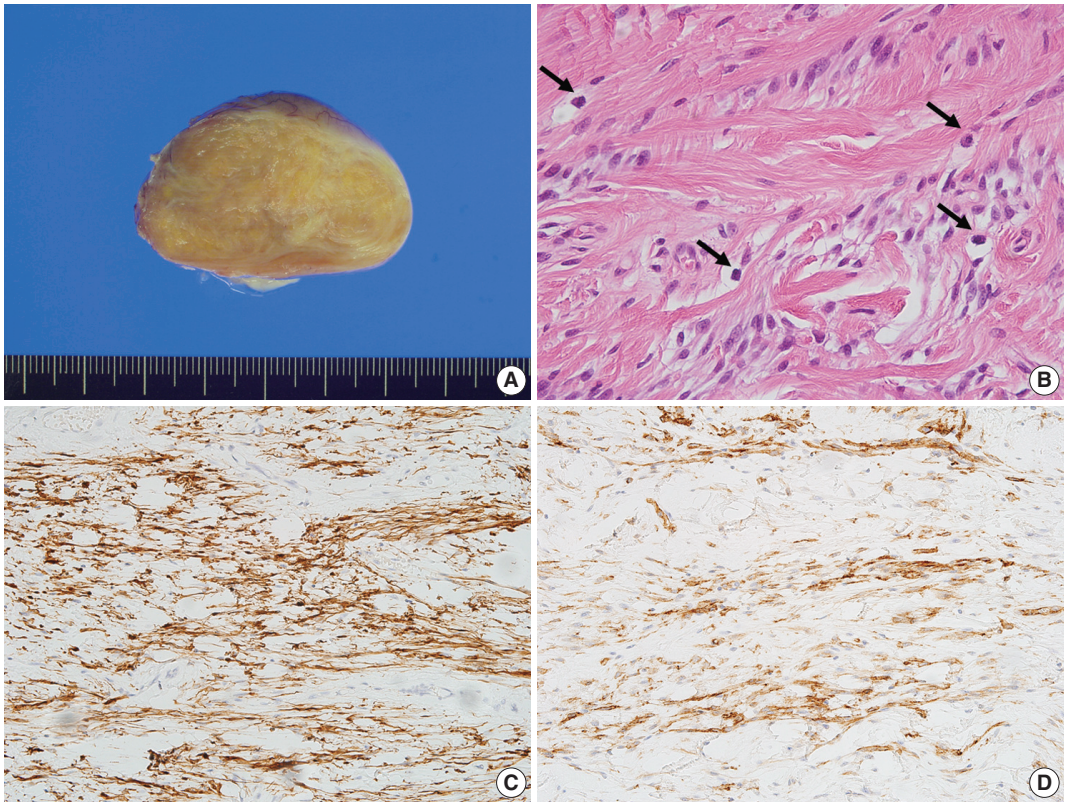


**Fig. 2.** Gross and microscopic findings of case 1. (A) The cut surface is yellowish tan, rubbery, and trabeculated, without necrosis or hemorrhage. (B) The mass is composed of haphazardly arranged and variably sized fascicles of bland spindle cells. Tumor cells have tapered nuclei and fine chromatin. Numerous mast cells are scattered (arrows). No mitosis is observed. The tumor cells show immunopositivity for desmin (C) and CD34 (D).


http://dx.doi.org/10.4132/jptm.2016.03.26

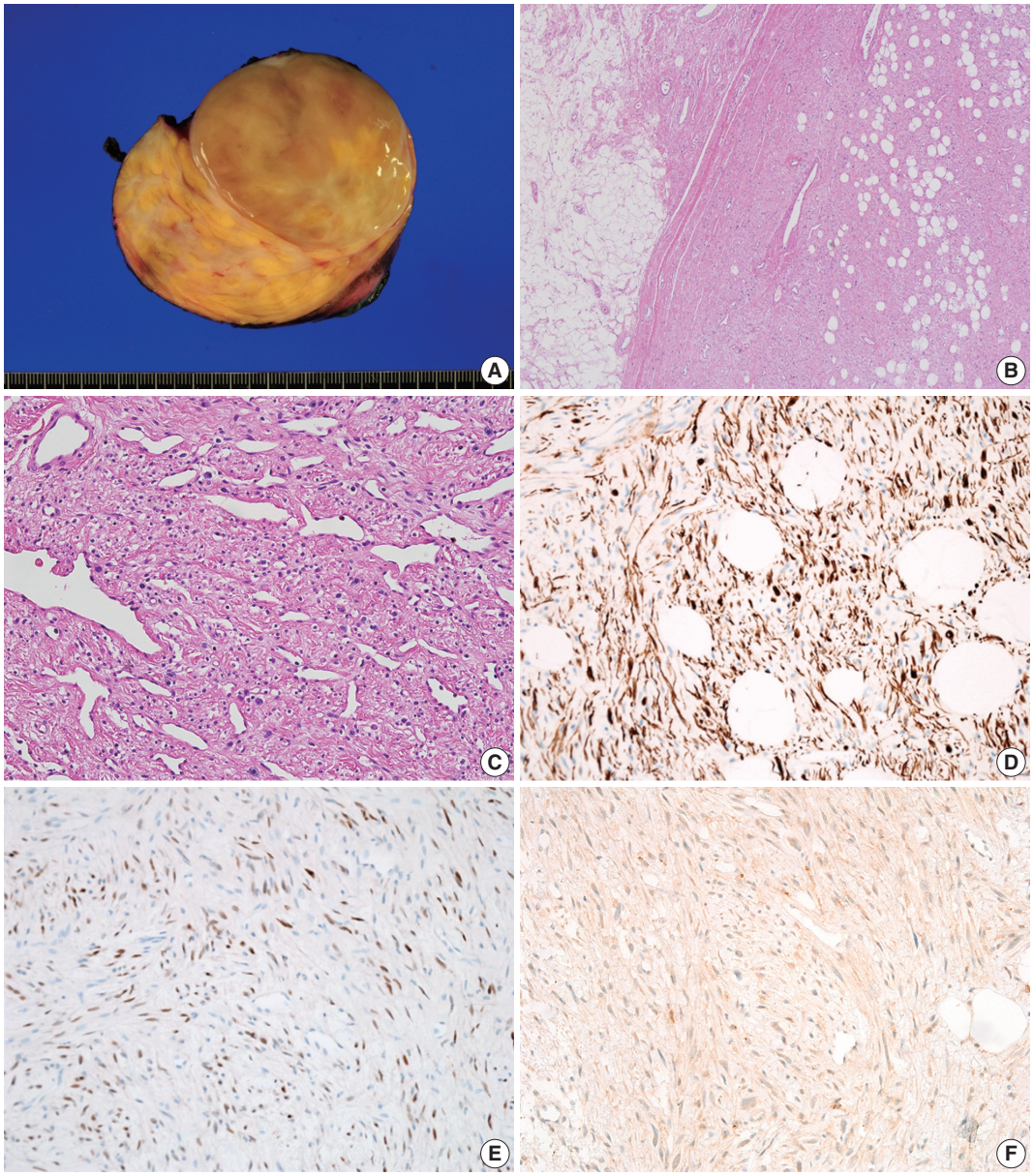


**Fig. 3.** Gross and microscopic findings of case 2. (A) The cut surface is yellowish tan, smooth, and glistening, and a focal myxoid change is observed. (B) The mass is well demarcated with mature adipocytes. (C) Staghorn-like blood vessels are present, with focal hyalinization. Tumor cells shows immunopositivity for desmin (D) and estrogen receptor (E). (F) Retinoblastoma immunostaining shows negativity.

cm. The cut surface was yellowish tan, smooth, and glistening with focal myxoid change. The peripheral portion showed a more prominent fatty component (Fig. 3A). Microscopically, the mass was composed of haphazardly arranged, variably sized fascicles of bland spindle cells and numerous mast cells. The spindle cells had tapered nuclei and fine chromatin. No cellular atypia or mitotic activity was identified. Hyalinized collagen fibers were abundant in the stroma. Adipose tissue was observed in both the intra-/extra-lesional portions. Staghorn-like blood vessels were present, with focal hyalinization (Fig. 3B, C). The spindle cells showed immunopositivity for desmin, CD34, and estrogen receptor (1:100, Novo, Newcastle upon Tyne, UK) and negativity for smooth muscle actin, S-100 protein, and retinoblastoma (1:20, Dako) (Fig. 3D–F).

The Institutional Review Board (IRB) of Asan Medical Center (IRB No. 2015-1303) approved this case report.

## DISCUSSION

Mammary-type MFB can occur along the embryonic milkline

and accessory breast. Nevertheless, in many previously reported cases, the tumor did not contain any breast tissue. McMenamin and Fletcher[2] described the possibility of ectopic breast in locations remote from the embryonic milkline. In addition, Millo *et al*.[5] suggested mesenchymal CD34-positive stem cells as an explanation for the hepatic location of mammary-type MFB.

MFB cells demonstrate immunopositivity for desmin and CD34.[2,6] In addition, at least focal expression of androgen, estrogen, and progesterone receptors has been reported.[4] Expression of smooth muscle actin is present in one-third of MFB cases.[7] In the two cases presented here, the tumor cells showed immunopositivity for desmin and CD34 and immunonegativity for smooth muscle actin. The differential diagnoses of mammary-type MFB include other low-grade spindle cell neoplasms such as spindle cell lipoma, cellular angiofibroma, and solitary fibrous tumors (SFTs). Desmin, CD34, and estrogen receptors are helpful markers for differential diagnosis.[4,6] Recently, Howitt and Fletcher[6] reported a large series of 143 cases of mammary-type MFB. They described complicated situations with mammary-type MFB, such as morphologic variation and CD34 and/or desmin negativity.[6] Spindle cell lipoma and cellular angiofibroma show overlapping histologic and immunophenotypic features with mammary-type MFB and share similar genetic findings, with loss of 13q14.[1,2,8,9]

Spindle cell lipoma has similar histologic features to MFB such as bland spindle cells, abundant mast cells in the stroma, and admixed adipose tissue. The morphological differences between these two tumor types are subtle. The spindle cells of mammary-type MFB show a fascicular arrangement, whereas those of spindle cell lipoma show a more haphazard arrangement. CD34 expression is present in both tumors, whereas desmin immunopositivity is rarely present in spindle cell lipoma (<2%).[2] Maggiani *et al*.[9] explained these different histologic features and immunoprofiles as due to stromal precursor cells with a variable capacity to differentiate into fibroblastic/lipocytic or myofibroblastic cells. Cellular angiofibroma usually involves the groin/pelvic area.[2,10] Histologically, cellular angiofibroma is composed of short spindle cells arranged without any pattern and numerous small- to medium-sized thick-walled hyalinized vessels. Some tumors contain a variable amount of adipose tissue.[2,10,11] Tumor cells can express CD34, but smooth muscle actin and desmin are usually negative.[10,11]

Mammary-type MFB, spindle cell lipoma, and cellular angiofibroma share not only histologic features, but also similar genetic alterations. The *RB1* gene, as well as the *FOXO1* (forkhead box protein O1, previously known as FKHR, forkhead in rhabdomyosarcoma) gene, is located in the 13q14 tumor suppressor locus, and deletion of this region, which was originally identified in spindle cell lipoma, has been reported in several cases of mammary-type MFB and cellular angiofibroma.[9] Maggiani *et al*.[9] described the loss of *RB*/13q14 and *FKHR*/13q14 loci in mammary-type MFB using fluorescence in situ hybridization (FISH) and suggested a genetic link with spindle cell lipoma, which has a characteristic loss of 13q and 16q. Hox *et al*.[8] reported a loss of *RB*/13q14 loci in mammary-type MFB of the head and neck region. Magro *et al*.[12] described a deletion of *FOXO1*, which is located on 13q14.11, both in mammary and vaginal MFB. In that study, five of seven cases of mammary-type MFB and three of five cases of vaginal MFB showed deletion of this locus. Hameed *et al*.[1] reported monosomy of chromosome 16 and loss of chromosome 13 in cellular angiofibroma. Flucke *et al*.[10] described the heterozygous loss of *RB1* in seven cases of cellular angiofibroma according to FISH. Magro[13] suggested the term benign stromal/mesenchymal tumor with 13q14 deletion, as these three entities share the same genetic alteration, and a minority of cases of spindle cell lipoma and cellular angiofibroma showed histologic similarity to mammary-type MFB.

SFT is another possible differential diagnosis. The tumor is composed of spindle cells surrounding thick-walled, branching staghorn-like blood vessels. An admixed adipocytic component can be present.[2,11] In SFT, the spindle cells show a haphazard arrangement with intertwining thin collagen fibers, whereas those in mammary-type MFB show short fascicles with broad interrupting collagen bands. Oval myoid cells with abundant eosinophilic cytoplasm, which are distinguishing features of mammary-type MFB, are not observed in SFT. SFT commonly expresses CD34 (90%) and CD99 (70%), especially the fibrous form.[14] Although SFT shares the histological and immunohistochemical characteristics of mammary-type MFB, the cytogenetics of SFT are different from those of mammary-type MFB. The absence of *RB*/13q14 loss in SFTs is the key point for the differential diagnosis.[11,15]

We report these cases due to the rare incidence and diagnostic utility of desmin immunoreactivity. We conclude that, if spindle cell lesions with myofibroblastic differentiation and admixed adipose tissue and mast cells in unusual locations are observed, the diagnosis of mammary-type MFB should be considered as a differential diagnosis, and desmin immunopositivity could be helpful for diagnosis.


http://dx.doi.org/10.4132/jptm.2016.03.26

## Conflicts of Interest

No potential conflict of interest relevant to this article was reported.

## REFERENCES


1. Hameed M, Clarke K, Amer HZ, Mahmet K, Aisner S. Cellular angiofibroma is genetically similar to spindle cell lipoma: a case report. Cancer Genet Cytogenet 2007; 177: 131-4.
2. McMenamin ME, Fletcher CD. Mammary-type myofibroblastoma of soft tissue: a tumor closely related to spindle cell lipoma. Am J Surg Pathol 2001; 25: 1022-9.
3. Mukonoweshuro P, McCormick F, Rachapalli V, Natale S, Smith ME. Paratesticular mammary-type myofibroblastoma. Histopathology 2007; 50: 396-7.
4. Arsenovic N, Abdulla KE, Shamim KS. Mammary-type myofibroblastoma of soft tissue. Indian J Pathol Microbiol 2011; 54: 391-3.
5. Millo NZ, Yee EU, Mortele KJ. Mammary-type myofibroblastoma of the liver: multi-modality imaging features with histopathologic correlation. Abdom Imaging 2014; 39: 482-7.
6. Howitt BE, Fletcher CD. Mammary-type myofibroblastoma: clinicopathologic characterization in a series of 143 cases. Am J Surg Pathol 2016; 40: 361-7.
7. Fletcher CD, Bridge JA, Hogendoorn P, Mertens F. WHO classification of tumours of soft tissue and bone. Lyon: IARC Press, 2013; 61-2.
8. Hox V, Vander Poorten V, Delaere PR, Hermans R, Debiec-Rychter M, Sciot R. Extramammary myofibroblastoma in the head and neck region. Head Neck 2009; 31: 1240-4.
9. Maggiani F, Debiec-Rychter M, Verbeeck G, Sciot R. Extramammary myofibroblastoma is genetically related to spindle cell lipoma. Virchows Arch 2006; 449: 244-7.
10. Flucke U, van Krieken JH, Mentzel T. Cellular angiofibroma: analysis of 25 cases emphasizing its relationship to spindle cell lipoma and mammary-type myofibroblastoma. Mod Pathol 2011; 24: 82-9.
11. Fritchie KJ, Carver P, Sun Y, *et al*. Solitary fibrous tumor: is there a molecular relationship with cellular angiofibroma, spindle cell lipoma, and mammary-type myofibroblastoma? Am J Clin Pathol 2012; 137: 963-70.
12. Magro G, Righi A, Casorzo L, *et al*. Mammary and vaginal myofibroblastomas are genetically related lesions: fluorescence *in situ* hybridization analysis shows deletion of 13q14 region. Hum Pathol 2012; 43: 1887-93.
13. Magro G. Chromosome 13q14 deletion in a mammary-type myofibroblastoma of the big toe: reply. Hum Pathol 2015; 46: 344-5.
14. Gengler C, Guillou L. Solitary fibrous tumour and haemangiopericytoma: evolution of a concept. Histopathology 2006; 48: 63-74.
15. Meguerditchian AN, Malik DA, Hicks DG, Kulkarni S. Solitary fibrous tumor of the breast and mammary myofibroblastoma: the same lesion? Breast J 2008; 14: 287-92.

*Journal of Pathology and Translational Medicine 2016; 50: 390-393*
*http://dx.doi.org/10.4132/jptm.2016.04.18*

■ CASE STUDY ■

# Pulmonary Arteriovenous Fistula: Clinical and Histologic Spectrum of Four Cases

Soomin Ahn · Joungho Han
Hong Kwan Kim[1] · Tae Sung Kim[2]

Departments of Pathology and Translational Genomics, [1]Thoracic Surgery, and [2]Radiology, Samsung Medical Center, Sungkyunkwan University School of Medicine, Seoul, Korea

**Received:** January 6, 2016
**Revised:** March 9, 2016
**Accepted:** April 18, 2016

**Corresponding Author**
Joungho Han, MD
Department of Pathology and Translational genomics, Samsung Medical Center, Sungkyunkwan University School of Medicine, 81 Irwon-ro, Gangnam-gu, Seoul 06351, Korea
Tel: +82-2-3410-2765
Fax: +82-2-3410-0025
E-mail: hanjho@skku.edu

Pulmonary arteriovenous fistula (PAVF) is abnormally dilated vessels that provide a right-to-left shunt between pulmonary artery and pulmonary vein and is clinically divided into simple and complex type. Here, we report four cases of surgically resected sporadic PAVFs presenting various clinical and histologic spectrums. Cases 1 (a 57-old-female) and 2 (a 54-old-female) presented as incidentally identified single aneurysmal fistulas and the lesions were surgically removed without complication. On the other hand, case 3 (an 11-old-male) showed diffuse dilated vascular sacs involving both lungs and caused severe hemodynamic and pulmonary dysfunction. Embolization and surgical resection of the main lesion failed to relieve the symptoms. Case 4 (a 36-old-male) had a localized multiloculated cyst clinically mimicking congenital cystic adenomatoid malformation. Microscopically, the lesion consisted of dilated thick vessels, consistent with the diagnosis of fistulous arteriovenous malformation/hemangioma.

**Key Words:** Lung; Arteriovenous fistula; Arteriovenous malformations

Pulmonary arteriovenous fistula (PAVF) in the lung is unusual. PAVF is described as abnormally dilated vessels that provide a right-to-left shunt between pulmonary artery and pulmonary vein.[1,2] PAVFs are clinically and radiologically divided into simple and complex type and commonly associated with hereditary hemorrhagic telangiectasia (HHT).[1] The treatment option of PAVFs varies depending on the location and severity of the lesion. Here we report four cases of surgically resected sporadic PAVF with different clinical and histologic presentations.

## CASE REPORTS

### Case 1

A 57-year-old woman visited the thoracic surgery department of the Samsung Medical Center, Seoul, for further evaluation of an abnormal finding on lung examination that had been incidentally detected by routine medical check-up. She denied any past medical history, and routine physical exams and laboratory tests were within normal limits. Chest computed tomography (CT) identified a single 4-mm-sized vascular dilation in the anterior segment of left upper lobe (Fig. 1A). There was no abnormality in the rest of lung parenchyma. Under the impression of PAVF, video-assisted thoracoscopic surgery was performed. Cut section of the specimen revealed a 0.5-cm-sized cystic lesion under the pleura. Microscopically, the lesion consisted of irregularly shaped aneurysmal dilation of thick vein (Fig. 1B). Additionally, elastic stain showed hypertrophic arteriopathy of pulmonary arterioles around the main aneurysmal vein (Fig. 1C). The patient was discharged without any post-operative complication.

### Case 2

A 54-year-old woman presented with incidental abnormal finding on chest X-ray. She was on anti-hypertensive medicine due to hypertension. Her routine physical exams and laboratory tests were within normal limits. Chest CT revealed a 38-mm-sized large aneurysmal sac in the right middle lobe (Fig. 1D). Due to the large size, right middle lobectomy was performed. Cut section of the specimen showed a thin-walled cyst with smooth whitish inner surface, measuring 38 mm in diameter





pISSN 2383-7837
eISSN 2383-7845

(Fig. 1E). Elastic stain revealed the lesion to be consisted of aneurysmal dilation of both artery and vein (Fig. 1F). The patient was discharged without any postoperative complication.

### Case 3

An 11-year-old boy visited emergency room due to hemoptysis. He was a known PAVF patient. He has had symptoms of cyanosis and clubbing of fingers since he was 4 years old and diagnosed with PAVF from chest CT work up. He had undergone coil embolization four times, which did not relieve the symptom. He showed general cyanosis and complained of dizziness and general weakness, low extremities in particular. His daily activity was limited and had difficulty in walking for long distance. $SpO_2$ was checked as 70% on average. Despite several coil embolization attempts, cyanosis and signs of chronic heart failure worsened. Chest CT revealed severe vascular engorgement in both lungs (Fig. 1G). Right lower lobectomy was performed to remove the main part of the lesion. Cut section of the specimen showed many engorged vessels with blood clots mainly in the posterobasal segment, measuring approximately 9 cm in extent (Fig. 1H). Microscopically, many dilated veins filled with blood were identified (Fig. 1I). He was discharged with no specific postoperative complication. However, diffuse PAVFs still remained in other lobes. He constantly suffered from general weakness and $SpO_2$ was still checked as 70% on average.

### Case 4

A 36-year-old man was admitted to the thoracic surgery department for scheduled operation. The patient was treated with antibiotics due to lung abscess one month prior. He had had another episode of pneumonia in the right lung 20 years ago. Although his symptom was relieved, post-treatment chest CT still revealed a multi-cystic lesion in the lateral side of right lung showing plump vascular supply through intercostal arteries or pulmonary arteries (Fig. 1J). It showed no segmental or lobar distribution. Under the clinical impression of congenital cystic adenomatoid malformation (CCAM), surgical resection was planned. Right lower lobectomy with en bloc wedge resection of right upper lobe was performed. Cut section of the specimen revealed a multi-lobulated cystic lesion filled with blood, measuring 7 cm in extent (Fig. 1K). Rest of the pulmonary parenchyma showed no abnormality. Microscopic examination revealed that the cystic lining consisted of dilated thick vascular structure (Fig. 1L). Adjacent airway structures were also entrapped and dilated. The final pathologic diagnosis was given as fistulous arteriovenous malformation/hemangioma (AVMH). The patient was discharged without any postoperative complication.

## DISCUSSION

We describe four cases of surgically resected PAVFs exhibiting various clinical and histologic spectrum. PAVF is described as abnormally dilated vessels that provide a right-to-left shunt between pulmonary artery and pulmonary vein and is divided into simple and complex type.[1,2] The literature review showed that abnormal communications between pulmonary arteries and veins have been given various names including PAVF, arteriovenous aneurysm, and arteriovenous hemangioma.[1-3] While PAVFs have been often described as pulmonary arteriovenous malformation in several reports,[1-5] we suggest that pulmonary AVMH should be used preferably to describe tumorous hemangioma lesion and PAVF should be used preferably to describe abnormal vascular communication. PAVFs are divided into simple and complex type, and the former is more common.[1,5] Simple PAVFs are those of a well-defined peripheral nodule and may be rounded or multi-lobulated.[1] Histologically, simple type presents as a single aneurysmal sac and contains a single segmental artery feeding the malformation. Complex PAVFs involve multiple abnormal vessels and consist of one or more lobulated venous sacs of variable size supplied by more than one feeding artery, often arising from adjacent segmental pulmonary artery branches.[1] Complex PAVFs may involve whole lung segments or an entire lobe.[1]

Two patients (cases 1 and 2) presented with solitary aneurysmal vascular lesion, which corresponded to simple PAVF. These incidental lesions did not cause any clinical symptom and surgical removal was successfully performed. On the other hand, case 3 presented with diffuse vascular lesion causing arteriovenous shunt and was consistent with the diagnosis of complex PAVF. Complex PAVFs are supplied by more than one feeding artery.[1] It caused serious respiratory problem and immobility in the patient 3. Lastly, case 4 showed a localized multi-lobular vascular lesion grossly mimicking pulmonary sequestration or CCAM. The histology of case 4 was unusual and also different from cases 1, 2, and 3 in that it had no definite aneurysmal sac or shunt formation. While AVMH is an acquired tumor-like condition characterized by complex thick-walled vessels,[3] it was not certain whether case 4 was a tumorous condition of AVMH or not. However, we concluded that the terminology of AVMH would represent the histologic characteristics of case 4 the best in that there was definite localized overgrowth of thick vessels. Although it did not cause serious hemodynamic or pulmonary

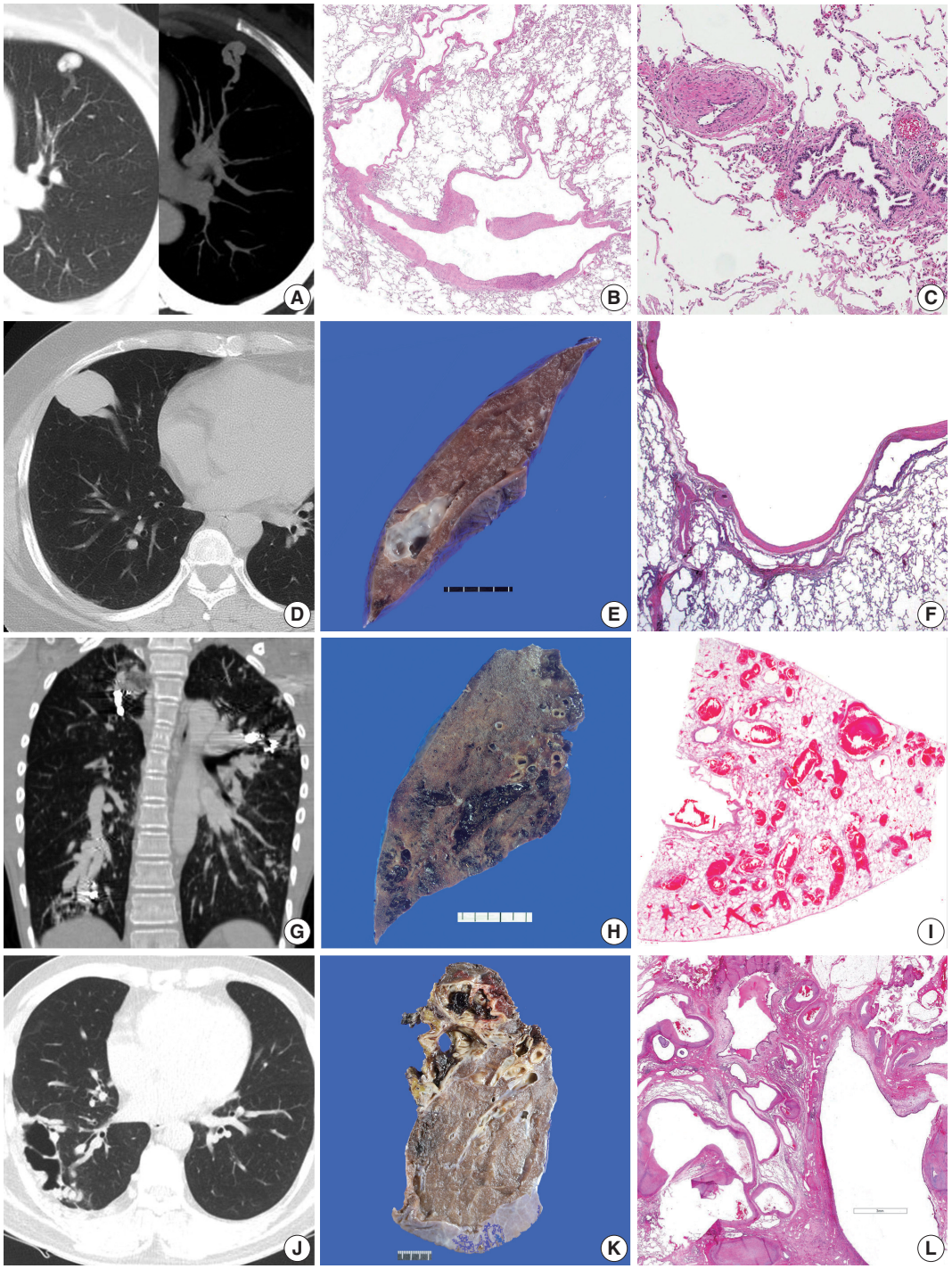


**Fig. 1.** Pulmonary arteriovenous fistula (PAVF). (A–F) Radiologic, gross, and microscopic features of two simple PAVF cases. (A, D) Both incidentally identified lesions are shown as dilated aneurysmal sacs in chest computer tomography (CT). (E) The cut section of case 2 shows a thin-walled cyst with smooth whitish inner surface. Microscopically, they consist of irregularly shaped aneurysmal dilation of thick vein (B, F) and hypertrophic arteriopathy of pulmonary arteriols around the main aneurysmal vein is accompanied in case 1 (C). (G–I) Radiologic, gross, and microscopic features of diffuse PAVF case. (G) Chest CT reveals severe vascular engorgement on both lungs. (H) On the cut section, many engorged vessels with blood clots are shown. (I) Microscopically, many dilated thin veins filled with blood are identified. (J–L) Radiologic, gross, and microscopic features of fistulous arteriovenous malformation/hemangioma. (J) Chest CT shows a multi-cystic lesion in the lateral side of right lung showing vascular supply through the intercostal arteries or pulmonary arteries. (K) The cut section of right lower lobectomy specimen shows a multi-lobulated cystic lesion filled with blood. (L) Microscopically, the cystic lining consists of dilated vascular structure.


http://dx.doi.org/10.4132/jptm.2016.04.18

symptoms, his episodes of pneumonia may probably be related to this lesion.

While most PAVF patients are known to have HHT, patients in our series did not. PAVFs are not easily diagnosed routinely, due to its rarity and its unspecific findings on routine examinations. CT is generally considered the reference standard investigation for diagnosing PAVFs.[1,4] In terms of treatment, embolization is considered first and surgical resection is performed for special indications.[6,7] Therefore, it is rare for pathologists to encounter the histology of PAVFs. The four rare cases of surgically resected PAVFs described herein show various spectrums of clinical and histologic features. They can present as either localized or diffuse, and they can involve either thin or thick blood vessels.

## Conflicts of Interest

No potential conflict of interest relevant to this article was reported.

## REFERENCES

1. Gill SS, Roddie ME, Shovlin CL, Jackson JE. Pulmonary arteriovenous malformations and their mimics. Clin Radiol 2015; 70: 96-110.
2. Gossage JR, Kanj G. Pulmonary arteriovenous malformations: a state of the art review. Am J Respir Crit Care Med 1998; 158: 643-61.
3. Ahn S, Jung S, Cho JH, Kim TS, Han J. A rare case of pulmonary arteriovenous hemangioma presenting as a peribronchial Mass. J Pathol Transl Med 2015 Nov 17 [Epub]. http://dx.doi.org/10.4132/jptm.2015.10.15.
4. Nakayama M, Nawa T, Chonan T, *et al*. Prevalence of pulmonary arteriovenous malformations as estimated by low-dose thoracic CT screening. Intern Med 2012; 51: 1677-81.
5. White RI Jr, Mitchell SE, Barth KH, *et al*. Angioarchitecture of pulmonary arteriovenous malformations: an important consideration before embolotherapy. AJR Am J Roentgenol 1983; 140: 681-6.
6. Terry PB, White RI Jr, Barth KH, Kaufman SL, Mitchell SE. Pulmonary arteriovenous malformations. Physiologic observations and results of therapeutic balloon embolization. N Engl J Med 1983; 308: 1197-200.
7. Gupta P, Mordin C, Curtis J, Hughes JM, Shovlin CL, Jackson JE. Pulmonary arteriovenous malformations: effect of embolization on right-to-left shunt, hypoxemia, and exercise tolerance in 66 patients. AJR Am J Roentgenol 2002; 179: 347-55.

*Journal of Pathology and Translational Medicine 2016; 50: 394-396*
*http://dx.doi.org/10.4132/jptm.2016.03.11*

■ CASE STUDY ■

# Nodular Fasciitis of External Auditory Canal

Jihyun Ahn · Sunyoung Kim
Youngsil Park[1]

Departments of Pathology and [1]Otolaryngology, Dongkang Medical Center, Ulsan, Korea

**Received:** January 28, 2016
**Revised:** March 8, 2016
**Accepted:** March 9, 2016

**Corresponding Author**
Jihyun Ahn, MD
Department of Pathology, Dongkang Medical Center, 239 Taehwa-ro, Jung-gu, Ulsan 44455, Korea
Tel: +82-52-241-1375
Fax: +82-52-241-1366
E-mail: jvcjh@hanmail.net

Nodular fasciitis is a pseudosarcomatous reactive process composed of fibroblasts and myofibroblasts, and it is most common in the upper extremities. Nodular fasciitis of the external auditory canal is rare. To the best of our knowledge, less than 20 cases have been reported to date. We present a case of nodular fasciitis arising in the cartilaginous part of the external auditory canal. A 19-year-old man complained of an auricular mass with pruritus. Computed tomography showed a 1.7 cm sized soft tissue mass in the right external auditory canal, and total excision was performed. Histologic examination revealed spindle or stellate cells proliferation in a fascicular and storiform pattern. Lymphoid cells and erythrocytes were intermixed with tumor cells. The stroma was myxoid to hyalinized with a few microcysts. The tumor cells were immunoreactive for smooth muscle actin, but not for desmin, caldesmon, CD34, S-100, anaplastic lymphoma kinase, and cytokeratin. The patient has been doing well during the 1 year follow-up period.

**Key Words:** Nodular fasciitis; External auditory canal; Ear

Nodular fasciitis is a relatively common benign soft tissue lesion composed of fibroblastic and myofibroblastic proliferation. Since it was first described in 1955 by Konwaler *et al*.,[1] it remains as the most common benign condition that is confused with sarcoma due to rapid growth, high cellularity, and mitotic activity.[2] Clinically, nodular fasciitis presents as a rapidly growing mass or nodule in adults between 20 to 40 years of age. It is sometimes accompanied by previous history of trauma. It can cause tenderness, pain, numbness or paresthesia depending on its location. It most frequently occurs in the upper extremities, especially the flexor forearm. Trunk and head and neck are also common sites for nodular fasciitis.[2-5] However, nodular fasciitis of the auricular region is unusual.[3,4] Here, we present a rare case of nodular fasciitis of external auditory canal.

## CASE REPORT

A 19-year-old man visited our hospital because of an auricular mass. The mass was present for about 4 weeks and it was accompanied by itching sensation. A previous history of trauma was not noted. A computed tomographic examination showed a 1.7 cm sized mass on the posterior wall of the cartilaginous portion of the right external auditory canal (Fig. 1). The mass showed soft tissue density and diffuse enhancement on the contrast image. Destruction of the adjacent bone was not identified. Total mass excision was performed. Grossly, the mass was soft, grayish tan, and relatively myxoid. On light microscopy, the mass was relatively well circumscribed without encapsulation and located in the subcutis and dermis. The mass encircled the cartilage but did not invade it. The mass consisted of spindle to stellate cells with minimal nuclear atypia in myxoid to hyalinized stroma. The tumor cells were arranged in a fascicular or storiform pattern and intermixed with scattered lymphoid cells and red blood cells extravasation (Fig. 2A, B). Microcystic changes were noted in more myxoid areas. Mitotic counts were up to 3 per 10 high power fields. Atypical mitosis was not identified. On immunohistochemistry, the tumor cells were positive for smooth muscle actin, but negative for desmin and caldesmon (Fig. 2C). These findings indicated these cells were fibroblasts or myofibroblasts rather than smooth muscle cells. The tumor cells were also negative for S-100, CD34, anaplastic lymphoma kinase (ALK), and cytokeratin. The tumor cells showed cytoplasmic staining for β-catenin, but nuclear staining was not seen. Based on all these features, we diagnosed this tumor as nodular fasciitis.





pISSN 2383-7837
eISSN 2383-7845

## DISCUSSION

Thompson *et al*.[3] reported the largest number of cases of auricular nodular fasciitis. They described 50 cases of auricular nodular fasciitis and its clinicopathologic characteristics. In their 50 cases, 37 cases (74%) were located in preauricular and postauricular region. Six cases (12%) were located in external auditory canal. Auricular nodular fasciitis accounted for 1.5% of all 3,930 cases of nodular fasciitis in all anatomical sites and for 1.9% of all 2,930 cases of benign and malignant auricular neoplasms and soft tissue reactive condition identified from 1970 to 1990 at their institution. Auricular nodular fasciitis was frequently found in young patients, similar to nodular fasciitis elsewhere. Since it was more superficially and dermally located than the one in the extremity, it may present with ulceration and/or bleeding. One of the 50 cases presented with conductive hearing loss. Lesions in the external auricular canal had smaller size (mean, 1.3 cm) and a shorter duration of symptoms (mean, 1.6 months) than lesions with a mean size of 1.9 cm and a mean duration of symptoms of 5.0 months among the total 50 cases. It seems to be due to the narrow space in the external auricular canal. Thompson *et al*.[3] found that auricular nodular fasciitis had a higher tendency of local recurrence (9.3%) when compared to the recurrence rate of 1%–2% at other sites.[2] They explained that this resulted from increased auricular trauma and difficulty in complete excision due to the anatomical position.

**Fig. 1.** Radiologic finding. An ovoid mass with soft tissue density (arrow) is noted in the right external auditory canal on computed tomography.

Auricular nodular fasciitis has similar findings to those of the lesions arising at other common sites. It is composed of fibroblasts or myofibroblasts arranged in a storiform or fascicular pattern with varying cellularity. Most fibroblastic cells are positive for smooth muscle actin, but negative for desmin and caldesmon. Immunostains for S-100, keratin, CD34, ALK, and p53 are also negative. Cytoplasmic staining for β-catenin can be observed in one-third of the cases.[5]

Nodular fasciitis may be confused with other benign and malignant spindle cell lesions mentioned below.

Inflammatory myofibroblastic tumor shows myofibroblastic proliferation with mixed inflammatory cell infiltrate. Although ALK may be expressed in some cases of inflammatory myofibroblastic tumor, nodular fasciitis does not show ALK expression.[6]

Fibromatosis is usually a large tumor that infiltrates the surrounding soft tissue. Nuclear β-catenin staining is the characteristic finding of fibromatosis.[2,5,7]

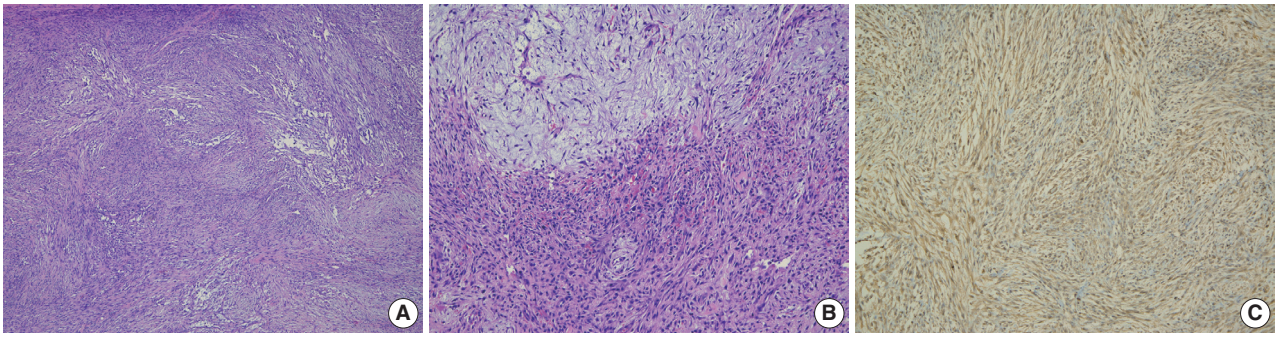


**Fig. 2.** Pathologic findings. (A) Spindle cell proliferation shows a vaguely storiform to fascicular pattern. (B) The bland spindle and stellate cells are set in loose myxoid (upper portion) to hyalinized matrix (lower portion). Extravasated red blood cells and scattered lymphoid cells are identified. (C) The tumor cells are positive for smooth muscle actin.

Benign fibrous histiocytoma is typically located in the dermis and has prominent xanthoma cells and occasional Touton-type giant cells.[8]

Solitary fibrous tumor can also occur in the auricular region. Solitary fibrous tumor consists of oval or spindle cells in a fascicular, whorled or haphazard arrangement. Immunohistochemically, the tumor cells are positive for CD34, Bcl-2, and CD99.[9]

Neurogenic tumor shows characteristic wavy, narrow, and elongated cells with S-100 immunoreactivity. Since nodular fasciitis is usually a small sized lesion and does not show prominent nuclear atypia, necrosis, or atypical mitosis, it can be distinguished from malignant lesions.

Nodular fasciitis has been considered as a reactive process and a self-limiting condition, although it has a rare possibility of recurrence.[10,11] Recently, a few reports reported about the identification of *MYH9-USP6* fusion gene in nodular fasciitis. It provided evidence for clonal neoplastic origin of nodular fasciitis and suggested a new model of "transient neoplasia."[12-14] Also, it showed that the detection of *MYH9-USP6* fusion gene can be used as a diagnostic tool for nodular fasciitis.[13,14] Further investigations related to the molecular analysis of nodular fasciitis are needed.

Here, we presented an unusual case of nodular fasciitis arising in the external auditory canal. Nodular fasciitis must be considered in the differential diagnosis of spindle cell lesions of the external auricular canal. Nodular fasciitis seems to recur more frequently in the auricular region than in the other common sites. Complete excision is likely to be helpful in reducing the recurrence rate.

## Conflicts of Interest

No potential conflict of interest relevant to this article was reported.

## REFERENCES

1. Konwaler BE, Keasbey L, Kaplan L. Subcutaneous pseudosarcomatous fibromatosis (fasciitis). Am J Clin Pathol 1955; 25: 241-52.
2. Weiss SW, Goldblum JR. Enzinger and Weiss's soft tissue tumors. 5th ed. St. Louis: Mosby, 2008.
3. Thompson LD, Fanburg-Smith JC, Wenig BM. Nodular fasciitis of the external ear region: a clinicopathologic study of 50 cases. Ann Diagn Pathol 2001; 5: 191-8.
4. Abdel-Aziz M, Khattab H, El-bosraty H, El-hoshy H, Hesham A, Al-taweel HW. Nodular fasciitis of the external auditory canal in six Egyptian children. Int J Pediatr Otorhinolaryngol 2008; 72: 643-6.
5. Peng WX, Kudo M, Yamamoto T, *et al*. Nodular fasciitis in the parotid gland: a case report and review of the literature. Diagn Cytopathol 2013; 41: 829-33.
6. Jung KH, Kim YW, So YK, Choi SI, Baek MJ. Inflammatory myofibroblastic tumor involving ear lobule. Auris Nasus Larynx 2012; 39: 631-3.
7. Bhattacharya B, Dilworth HP, Iacobuzio-Donahue C, *et al*. Nuclear beta-catenin expression distinguishes deep fibromatosis from other benign and malignant fibroblastic and myofibroblastic lesions. Am J Surg Pathol 2005; 29: 653-9.
8. Morrissey G, Robinson AC, Stirling R. Cellular benign fibrous histiocytoma of the external auditory meatus. J Laryngol Otol 1996; 110: 98-100.
9. Rezk S, Yousef M, Zamansky M, Khan A. Solitary fibrous tumor of the auditory canal. Arch Pathol Lab Med 2004; 128: e169-71.
10. Kim JR, Chi JG. Nodular fasciitis (13 cases analysis). Korean J Pathol 1998; 22: 190-4.
11. Meng GZ, Zhang HY, Zhang Z, Wei B, Bu H. Myofibroblastic sarcoma vs nodular fasciitis: a comparative study of chromosomal imbalances. Am J Clin Pathol 2009; 131: 701-9.
12. Erickson-Johnson MR, Chou MM, Evers BR, *et al*. Nodular fasciitis: a novel model of transient neoplasia induced by *MYH9-USP6* gene fusion. Lab Invest 2011; 91: 1427-33.
13. Amary MF, Ye H, Berisha F, Tirabosco R, Presneau N, Flanagan AM. Detection of *USP6* gene rearrangement in nodular fasciitis: an important diagnostic tool. Virchows Arch 2013; 463: 97-8.
14. Oliveira AM, Chou MM. USP6-induced neoplasms: the biologic spectrum of aneurysmal bone cyst and nodular fasciitis. Hum Pathol 2014; 45: 1-11.

 http://dx.doi.org/10.4132/jptm.2016.03.11

*Journal of Pathology and Translational Medicine 2016; 50: 397-400*
*http://dx.doi.org/10.4132/jptm.2016.01.11*

■ BRIEF CASE REPORT ■

# Pelvic Nodular Histiocytic and Mesothelial Hyperplasia in a Patient with Endometriosis and Uterine Leiomyoma

Yumin Chung · Rehman Abdul · Se Min Jang · Joong Sub Choi[1] · Kiseok Jang

Department of Pathology, [1]Division of Gynecologic Oncology and Gynecologic Minimally Invasive Surgery, Department of Obstetrics and Gynecology, Hanyang University College of Medicine, Seoul, Korea

Nodular histiocytic and mesothelial hyperplasia (NHMH) is a rare and benign proliferative lesion composed of histiocytes with scattered mesothelial cells which was first reported in hernia sac by Rosai and Dehner in 1975.[1] They described NHMH as a "benign reactive condition simulating a neoplastic process."[1] Since then, several cases have been reported in lung, pleura, inguinal region, urinary bladder, and pelvic cavity.[2-9] We report a case of incidentally detected NHMH, presenting as a pelvic nodule during laparoscopic surgery for uterine myoma and endometriosis.

## CASE REPORT

The patient was a 38-year-old woman complaining of abdominal discomfort and infertility without previous pregnancy history. A 8.3×5-cm-sized intramural type myoma was found on gynecologic sonography. There was no medical history of previous abdominal or pelvic surgery. During laparoscopic myomectomy, a left ovarian cyst (2.6×1.6 cm in size), a bladder peritoneal mass (1.6×1 cm in size), and a small nodule in cul-de-sac cavity were incidentally obtained. The pathologic diagnosis of left ovary cyst and bladder peritoneal mass was endometriosis. Gross examination of the mass in cul-de-sac cavity showed a grayish white and solid nodule, measuring 0.8×0.5 cm in size. Microscopically, two populations of cells were identified. The majority of cells showed nodular clusters of round to polygonal cells with moderate amount of pale to pink granular cytoplasm and ovoid or grooved nuclei. The other cell type was low cuboidal cells of stripped arrangement, which were entrapped in nodular clusters (Fig. 1A, B). Immunohistochemically, the round to polygonal cells in nodular lesions showed positivity for the histiocytic marker (CD68) (Fig. 1C), whereas negative for neuroendocrine markers, such as CD56, synaptophysin, and chromogranin. The low cuboidal cells were immunoreactive for pancytokeratin and the mesothelial markers, such as WT-1 and calretinin (Fig. 1D). These histopathologic features are consistent with NHMH.

**Corresponding Author**
Kiseok Jang, MD, PhD
Department of Pathology, Hanyang University College of Medicine, 222-1 Wangsimni-ro, Seongdong-gu, Seoul 04763, Korea
Tel: +82-2-2290-8248, Fax: +82-2-296-7502, E-mail: medartisan@hanyang.ac.kr

**Received:** December 10, 2015 **Revised:** January 6, 2016
**Accepted:** January 11, 2016

## DISCUSSION

NHMH is a benign lesion, which is characterized by non-neoplastic proliferation of histiocytes and mesothelial cells. This lesion is very rare and only 20 cases have been reported in the literature (Table 1). Although patients with these tumors range in age from 2 to 80 years, approximately 70% of the patients are over 40 years old with a mean age of 50.56. This lesion exhibits a slightly higher predilection for female in a ratio of 1.33 to 1. NHMHs are mostly incidental findings and occur at the serosal lining. The lung and pleura are the most frequently affected sites and account for 50% of the NHMH cases. The inguinal region, urinary bladder, and pelvis are less commonly affected sites.

Pathologically, the diagnosis of NHMH is made by identifying nodular proliferation of both histiocytic and mesothelial components supported by immunohistochemistry. The histiocytes are arranged in solid sheets or nests with a mixture of fibrin materials, and they are immunoreactive against CD68. The me-

pISSN 2383-7837
eISSN 2383-7845

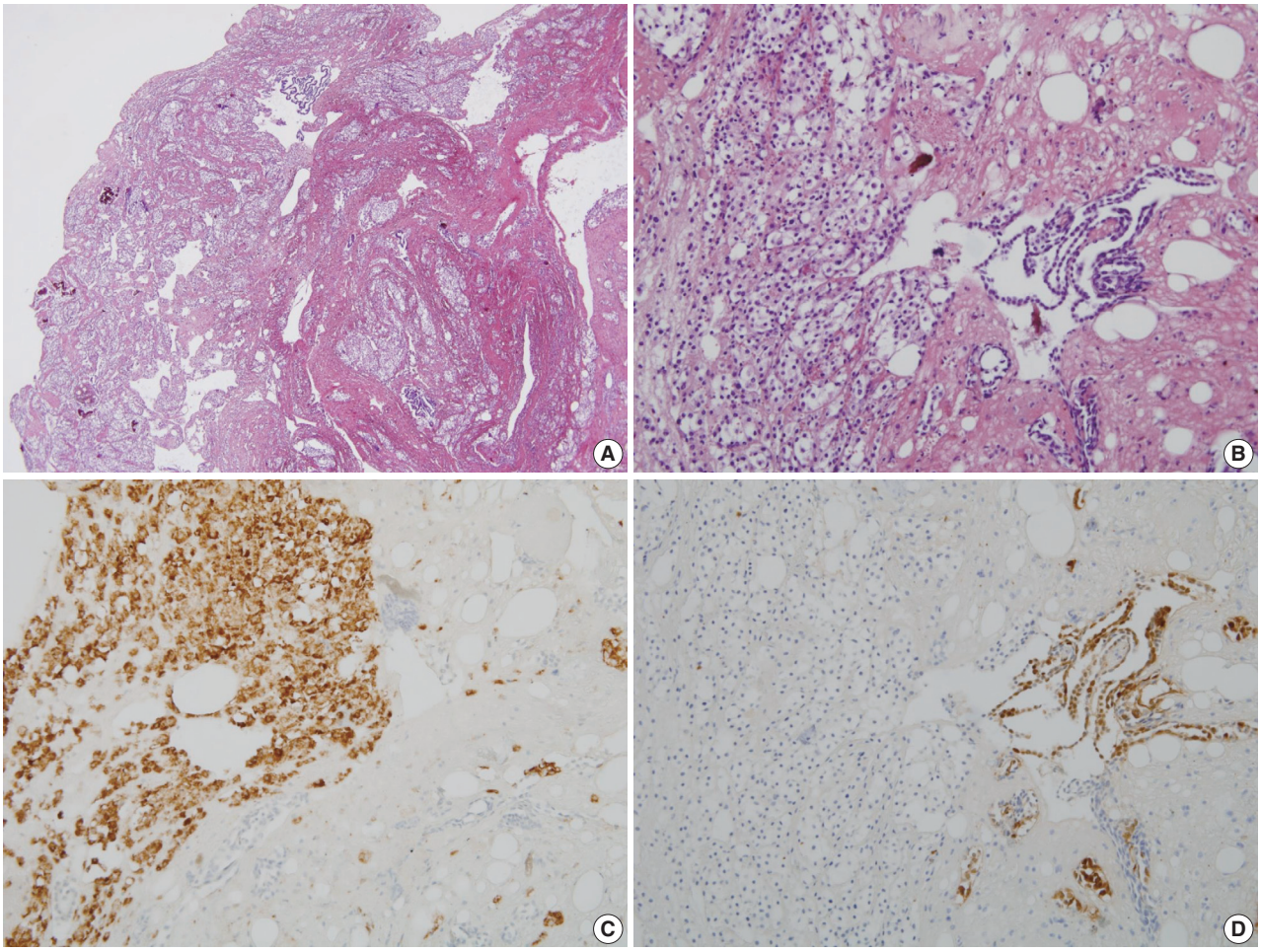


**Fig. 1.** Pathologic findings. (A) Incidentally obtained pelvic nodule reveals a nodular histiocytic and mesothelial hyperplasia, which is a nodular proliferation of two different cell types, histiocytes and mesothelial cells. (B) High power view shows collection of larger histiocytes, which is admixed with fibrin materials, and strips of smaller mesothelial cells. (C) The histiocytes are immunoreactive for CD68. (D) The mesothelial cells are positive for calretinin.

sothelial component, which is arranged in a glandular- or strip-like structure, is positive for mesothelial markers such as calretinin and WT-1. The nuclear atypia is typically absent.

Mesothelial/monocytic incidental cardiac excrescence (MICE), a tumour-like lesion similar to NHMH, is also predominantly composed of histiocytes and scattered mesothelial cells.[10] It can occur incidentally in pericardium, heart chamber and valve, and it has often been found during cardiac valve replacement surgery. MICE are also considered as a reactive condition. Therefore, NHMH and MICE may belong to the same disease entity.

NHMH is considered a reactive lesion which results from irritation by inflammation, mechanical trauma, or adjacent tumors.[2,6] It has been postulated that the nodular aggregation of these reactive cells is mediated by adhesion molecules, such as CD34.[5] Although our case did not have mechanical irritation such as previous surgery or procedure, the patient had a large intramural leiomyoma and endometriosis as accompanying diseases, supporting the above mentioned pathogenesis.

Although benign-looking cytological findings support that the NHMH represents benign reactive proliferation of histiocytes and mesothelial cells, the lesion can be confused with other mesothelial lesions and neoplasms such as low-grade neuroendocrine tumors, mesothelioma, granulosa cell tumor, Langerhans cell histiocytosis, metastatic carcinoma, seminoma and malignant lymphoma. Therefore, immunohistochemical studies as well as histologic examination with proper clinical history provide clues to obtain an accurate diagnosis. In the present case, the solid pattern of histiocytic proliferation with a delicate capillary network (Fig. 1B) was morphologically similar to the histologic finding of a metastatic renal cell carcinoma and paraganglioma, which were excluded by immunohistochemistry.

In conclusion, it is important that pathologists should be aware


http://dx.doi.org/10.4132/jptm.2016.01.11

**Table 1.** Clinical features and pathologicdifferential diagnosis based on previously reported and present cases

| No. | Age (yr)/ Sex | Site | Underlying condition | Differential diagnosis | Reference |
|---|---|---|---|---|---|
| 1 | 57/M | Lung (LLL) | Old TBC lesions | Neuroendocrine neoplasm | Chan *et al*.[2] |
| 2 | 51/F | Lung (RLL) | Weil-Felix agglutination test (+), possible rickettsial pneumonia | Neuroendocrine neoplasm, ectopic meningioma | Chan *et al*.[2] |
| 3 | 23/F | Lleura | Metastatic sarcoma to lung | Metastatic sarcoma | Ordonez *et al*.[3] |
| 4 | 78/F | Pleura | Unknown | Metastatic adenocarcinoma, epithelioid hemangioendothelioma | Ordonez *et al*.[3] |
| 5 | 80/F | Pleura | Unknown | Malignant mesothelioma, metastatic carcinoma, ectopic meningioma, paraganglioma | Choi and Song[4] |
| 6 | Elderly/ M | Pleura | Carcinoma in the lung | Primary or metastatic carcinoma, carcinoid tumor, mesothelioma, histiocytosis X | Chikkamuniyappa *et al*.[6] |
| 7 | 53/F | Pleura | Multiple bilateral lung nodules | Primary or metastatic carcinoma, carcinoid tumor, mesothelioma, histiocytosis X | Chikkamuniyappa *et al*.[6] |
| 8 | 79/M | Lung | Past history of ischemic cardiac disease | Malignancy | Rossi *et al*.[8] |
| 9 | 76/F | Lung (RLL) | Bilateral pneumonia (history of chronic l ymphocytic leukemia) | Non-small cell carcinoma, neuroendocrine tumors, ectopic meningioma | Bejarano *et al*.[7] |
| 10 | 40/F | Lung (LUL) | Consolidation (lung), scleroderma | Non-small cell carcinoma, neuroendocrine tumors, ectopic meningioma | Bejarano *et al*.[7] |
| 11 | 44/F | Lung (RLL) | History of pancreatic carcinoma, history of chemopneumonitis | Non-small cell carcinoma, neuroendocrine tumors, ectopic meningioma | Bejarano *et al*.[7] |
| 12 | 78/F | Lung (LUL) | Lung mass | Non-small cell carcinoma, neuroendocrine tumors, ectopic meningioma | Bejarano *et al*.[7] |
| 13 | 46/M | Lung (LLL) | Bilateral infiltrates (lung) (s/p heart transplant) | Non-small cell carcinoma, neuroendocrine tumors, ectopic meningioma | Bejarano *et al*.[7] |
| 14 | 62/M | Lung (LLL) | Bilateral infiltrates (lung) (s/p heart transplant) | Non-small cell carcinoma, neuroendocrine tumors, ectopic meningioma | Bejarano *et al*.[7] |
| 15 | 2/M | Inguinal | Strangulated hernia | - | Chan *et al*.[2] |
| 16 | 71/M | Inguinal | Relapsed inguinal hernia | - | Suarez-Vilela and Izquierdo-Garcia[5] |
| 17 | 5/M | Inguinal | - | Neuroendocrine tumors, Langerhans cell histiocytosis, seminoma, mesothelioma | Cai *et al*.[9] |
| 18 | 36/F | Pelvis | Infertility | Well-differentiated adenocarcinoma, leukemia/lymphoma | Chikkamuniyappa *et al*.[6] |
| 19 | 37/F | Pelvis | Endometriosis | Well-differentiated adenocarcinoma, leukemia/lymphoma | Chikkamuniyappa *et al*.[6] |
| 20 | 74/M | Bladder | Noninvasive papillary transitional cell carcinoma | Invasive transitional cell carcinoma into the lamina propria | Ordonez *et al*.[3] |
| Present case | 38/F | Pelvis | Uterine leiomyoma endometriosis | Metastatic renal cell carcinoma, paraganglioma | |

M, male; LLL, left lower lobe; TBC, tuberculosis; RLL, right lower lobe; LUL, left upper lobe.

of this entity and correlate clinically, histologically, and immunohistochemically to make a correct diagnosis.

## Conflicts of Interest

No potential conflict of interest relevant to this article was reported.

## REFERENCES


1. Rosai J, Dehner LP. Nodular mesothelial hyperplasia in hernia sacs: a benign reactive condition simulating a neoplastic process. Cancer 1975; 35: 165-75.
2. Chan JK, Loo KT, Yau BK, Lam SY. Nodular histiocytic/mesothelial hyperplasia: a lesion potentially mistaken for a neoplasm in transbronchial biopsy. Am J Surg Pathol 1997; 21: 658-63.
3. Ordonez NG, Ro JY, Ayala AG. Lesions described as nodular mesothelial hyperplasia are primarily composed of histiocytes. Am J Surg Pathol 1998; 22: 285-92.
4. Choi YL, Song SY. Cytologic clue of so-called nodular histiocytic hyperplasia of the pleura. Diagn Cytopathol 2001; 24: 256-9.
5. Suarez-Vilela D, Izquierdo-Garcia FM. Nodular histiocytic/mesothelial hyperplasia: a process mediated by adhesion molecules? Histopathology 2002; 40: 299-300.
6. Chikkamuniyappa S, Herrick J, Jagirdar JS. Nodular histiocytic/mesothelial hyperplasia: a potential pitfall. Ann Diagn Pathol 2004;

8: 115-20.
7. Bejarano PA, Garcia MT, Ganjei-Azar P. Mesothelial cells in transbronchial biopsies: a rare complication with a potential for a diagnostic pitfall. Am J Surg Pathol 2007; 31: 914-8.
8. Rossi G, Cavazza A, Guicciardi N, Marchioni A. Nodular histiocytic/mesothelial hyperplasia on transthoracic biopsy: another source of potential pitfall in a lesion frequently present in spontaneous pneumothorax. Histopathology 2008; 52: 250-2.
9. Cai Z, Xie Q, Wang X, Guo B, Wang X, Wang K. Nodular histiocytic/mesothelial hyperplasia: a clinicopathologic analysis of 7 cases. Zhonghua Bing Li Xue Za Zhi 2014; 43: 256-9.
10. Jiao N, Zhang W, Wang W, *et al*. Mesothelial/monocytic incidental cardiac excrescence: a case report and review of literature. Int J Clin Exp Pathol 2014; 7: 6219-24.


http://dx.doi.org/10.4132/jptm.2016.01.11

*Journal of Pathology and Translational Medicine 2016; 50: 401-403*
*http://dx.doi.org/10.4132/jptm.2016.02.16*

■ BRIEF CASE REPORT ■

# Clear Cell Papulosis: A Case Report

So-Woon Kim · Jin Roh · Chan-Sik Park

Department of Pathology, Asan Medical Center, University of Ulsan College of Medicine, Seoul, Korea

Clear cell papulosis (CCP) is an extremely rare entity, as only about two dozen cases have been reported to date in the English literature.[1] In CCP, white papules arise and cluster bilaterally along the mammary line, usually over the lower abdomen and pubis.[2] There is a predisposition for persons of Asian or Hispanic descents and most cases have been found in healthy children younger than 6 years old.[1,3] Typically, the lesions spontaneously resolve with age.[4] Microscopically, the lesions are composed of aberrant cells derived from sweat gland epithelial cells that grow in a pagetoid pattern in the epidermis.[2] CCP provides evidence for the potential precursor cells for cutaneous Paget's disease.[5] Pathologists should include CCP in the differential diagnosis of whitish maculopapular lesions in the mammary line.

## CASE REPORT

A 2-year-old Korean girl presented with multiple scattered white papules on her lower abdomen and pubic areas, which had gradually increased in size. The lesions were asymptomatic with no pruritus, pain, or sensory impairment. She exhibited no other remarkable medical conditions. A physical examination revealed many sharply demarcated, round-to-oval hypopigmented maculopapules that were predominantly located in the suprapubic area (Fig. 1).

A punch biopsy was obtained from one of the lesions. Microscopically, the lesion showed mild acanthosis and reduced pigmentation of the epidermis (Fig. 2A). A characteristic feature was the presence of benign pagetoid clear cells in the epidermis. The clear cells occurred either in clusters or singly along the basal and suprabasal layers of the epidermis and were less frequent near the surface. There was no involvement of the dermis. The aberrant cells were larger than keratinocytes and had abundant pale eosinophilic to clear cytoplasm without pigmentation (Fig. 2B). Nuclei were round-to-oval without pleomorphism. Nucleoli were not prominent. No mitosis was observed. The abnormal cells were positive for cytokeratin 7 and carcinoembryonic antigen (Fig. 3A, B) by immunohistochemical analyses. By contrast, Melan A and S100 protein stains were negative. Only epidermal melanocytes and dendritic cells showed positive staining for Melan A and S100 protein, respectively (Fig. 3C, D). Epidermal keratinocytes were negative for all stains.

**Corresponding Author**
Chan-Sik Park, MD
Department of Pathology, Asan Medical Center, University of Ulsan College of Medicine, 88 Olympic-ro 43-gil, Songpa-gu, Seoul 05505, Korea
Tel: +82-2-3010-5838, Fax: +82-2-3010-8675, E-mail: csikpark@amc.seoul.kr

**Received:** December 28, 2015 **Revised:** February 2, 2016
**Accepted:** February 16, 2016

## DISCUSSION

We here report a case of CCP, which is an extraordinarily rare condition. CCP is almost always restricted to the skin without systemic symptoms.[4] Lesions can be easily missed without suspicion because the histologic findings are not readily discernible to pathologists who are not familiar with this entity.[1] In such cases, the diagnosis can be confirmed pathologically by immunostaining.[6]

The exact reason for the hypopigmented change remains unknown but may be a consequence of reduced melanization in the epidermis. Additionally, the number of melanocytes is normal or slightly reduced.[7] These findings suggest the dysfunction of melanocytes in lesions, although the role of clear cells in the pathogenesis of this type of melanocytic dysfunction remains to be elucidated.[6]

The differential clinical diagnoses of a hypopigmented lesion include vitiligo, chicken pox scars, idiopathic guttate hypomelanosis, hypomelanotic tinea versicolor, and anetoderma.[7] In a typical clinical setting and with microscopic findings that show no

pISSN 2383-7837
eISSN 2383-7845

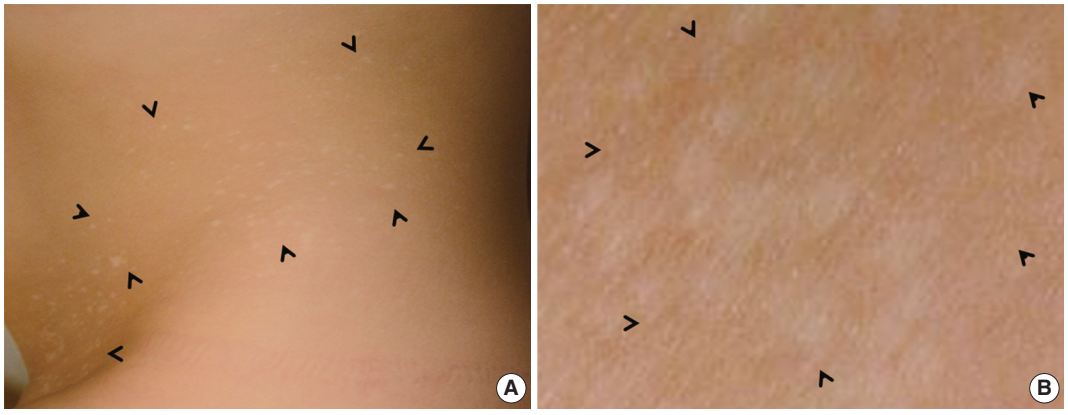

**Fig. 1.** (A) Many small whitish macules are present on the trunk and are particularly numerous in the lower abdomen and pubic area (arrowheads). The milk-line distribution of the lesions is notable. (B) Close-up view of the right pubic areas showing round-to-oval hypopigmented with no scales (arrowheads).

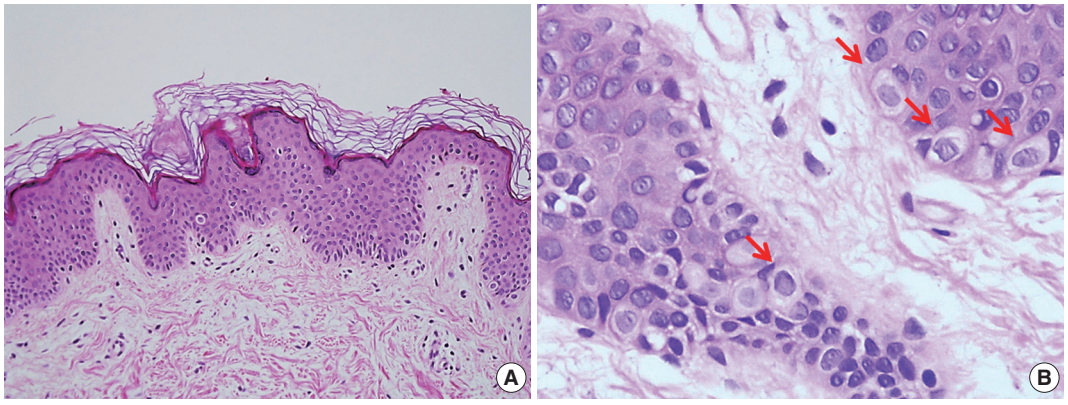

**Fig. 2.** Biopsy of a clear cell papulosis lesion revealing scattered single clear cells in the basal layer with mild acanthosis and no alteration of the keratin layer. (A) There is minimal inflammatory cell infiltration in the dermis. (B) At higher magnification, solitary benign-appearing pagetoid cells with an abundant clear cytoplasm could be observed in the epidermis. No nuclear atypia is noted (arrows, clear cell).

clear cells in basal layer, CCP can usually be differentiated from the aforementioned diseases. Histological differential diagnoses include the early stages of extramammary Paget disease, pagetoid squamous carcinoma, pagetoid melanoma, and sebaceous carcinoma.[7] All of these conditions have malignant cytologic features, whereas the clear cells of CCP clearly appear to be benign.[3] The histological and immunohistochemical staining patterns suggest that the affected cells in CCP are most likely to be of sweat gland epithelial cell origin that are derived from Toker cells.[8,9] However, the natural history of CCP remains unknown. Notably, there is another Toker cell proliferative lesion called Toker cell hyperplasia (TCH), which is usually found nearby extramammary Paget disease. This topographical relation suggested that TCH may be a precursor lesion for extramammary Paget disease.[5] There is no discernible histomorphologic difference between TCH and CCP besides clinical features. Usually, TCH is clinically unremarkable. Her2/neu immunostaining shows faint positivity in some TCH but negativity in CCP. Mucin stains are consistently negative in TCH but variably positive in CCP.

In conclusion, the recognition of hypopigmented lesions in the mammary line is important in clinical practice. CCP should be included in differential diagnoses of both hypopigmented lesions and depigmented extramammary Paget disease. To the best of our knowledge, our current case study represents the first report of CCP in the Korean literature. Awareness and making an accurate diagnosis of CCP may mitigate overly aggressive management.

## Conflicts of Interest

No potential conflict of interest relevant to this article was reported.


http://dx.doi.org/10.4132/jptm.2016.02.16

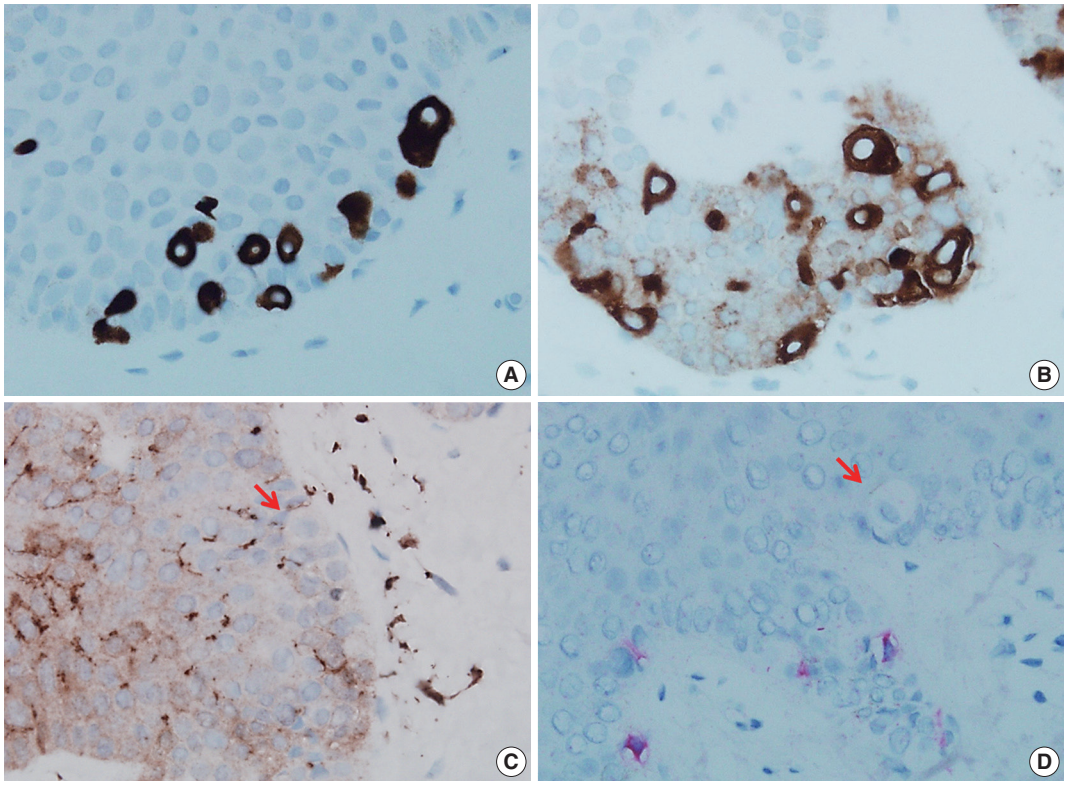


**Fig. 3.** The pagetoid cells strongly express cytokeratin 7 (A) and carcinoembryonic antigen (B) but are negative for either S100 protein (C) or Melan A (D) (arrows, clear cell).

## REFERENCES


1. Silverberg NB. Clear cell papulosis. In: Silver NB, Duran-McKinster C, Tay YK, eds. Pediatric skin of color. New York: Springer, 2015; 229-30.
2. Kuo TT, Chan HL, Hsueh S. Clear cell papulosis of the skin. A new entity with histogenetic implications for cutaneous Paget's disease. Am J Surg Pathol 1987; 11: 827-34.
3. Mohanty SK, Arora R, Kakkar N, Kumar B. Clear cell papulosis of the skin. Ann Diagn Pathol 2002; 6: 385-8.
4. Tseng FW, Kuo TT, Lu PH, Chan HL, Chan MJ, Hui RC. Long-term follow-up study of clear cell papulosis. J Am Acad Dermatol 2010; 63: 266-73.
5. Yu Y, Sukhatme S, Loo DS. Clear cell papulosis: a connection of clear cells to toker cells or paget disease. Arch Dermatol 2009; 145: 1066-8.
6. Wysong A, Sundram U, Benjamin L. Clear-cell papulosis: a rare entity that may be misconstrued pathologically as normal skin. Pediatr Dermatol 2012; 29: 195-8.
7. Chen YH, Wong TW, Lee JY. Depigmented genital extramammary Paget's disease: a possible histogenetic link to Toker's clear cells and clear cell papulosis. J Cutan Pathol 2001; 28: 105-8.
8. Kim YC, Mehregan DA, Bang D. Clear cell papulosis: an immunohistochemical study to determine histogenesis. J Cutan Pathol 2002; 29: 11-4.
9. Di Tommaso L, Franchi G, Destro A, *et al*. Toker cells of the breast: morphological and immunohistochemical characterization of 40 cases. Hum Pathol 2008; 39: 1295-300.